The Role of Interfacial and 'Entropic' Enzymes in Transitory Starch Degradation

A Mathematical Modeling Approach

Dissertation
zur Erlangung des akademischen Grades
doctor rerum naturalium (Dr. rer. nat.)
in der Wissenschaftsdisziplin Bioinformatik/Systembiologie
eingereicht an der
Mathematisch-Naturwissenschaftlichen Fakultät der
Universität Potsdam

von
Herr Dipl.-Biophys. Önder Kartal
aus
Hof/Saale

1. Gutachter: Prof. Dr. J. Selbig
2. Gutachter: Prof. Dr. H.-G. Holzhütter
3. Gutachter: Prof. Dr. S. C. Zeeman

Datum der Einreichung: 2011/02/16
Tag der mündlichen Prüfung: 2011/07/19

Published online at the
Institutional Repository of the University of Potsdam:
URL http://opus.kobv.de/ubp/volltexte/2011/5394/
URN urn:nbn:de:kobv:517-opus-53947
http://nbn-resolving.de/urn:nbn:de:kobv:517-opus-53947

Für Fadime

Danksagung

Diese Arbeit wurde ermöglicht durch das Vertrauen, das mein Gruppenleiter am Max-Planck-Institut für molekulare Pflanzenphysiologie, Oliver Ebenhöh, in mich gesetzt hat. Ich danke ihm für die Unterstützung und seinen unschätzbaren fachlichen Rat. Ich werde seine Begeisterungsfähigkeit und Hilfsbereitschaft immer in guter Erinnerung behalten. Ich danke auch seiner Frau Angelika für die Gastfreundschaft.

Ich danke Joachim Selbig für die Betreuung seitens der Universität Potsdam. Zum Gelingen dieser Arbeit hat das wissenschaftlich anregende Umfeld des Max-Planck-Instituts wesentlich beigetragen. Ich danke Mark Stitt für den fachlichen Zuspruch und den Mitgliedern des Thesis Kommittees, Hermann-Georg Holzhütter, Angelo Valleriani und insbesondere Martin Steup für wichtige Impulse und kritische Hinweise.

Die wissenschaftliche Kooperation mit Martin Steup und unsere Treffen waren mir immer eine Freude. Bei dieser Gelegenheit möchte ich auch Sebastian Mahlow danken, der an diesen Treffen beteiligt war und einen wichtigen Beitrag zum Gelingen dieser Zusammenarbeit zwischen Theoretikern und Experimentatoren geleistet hat.

Ich bin froh, dass ich in der Zeit der Promotion Alexander Skupin kennengelernt habe. Abgesehen von der wissenschaftlich fruchtbaren Zusammenarbeit und der nur vorläufig unter den Teppich gekehrten Frage der biologischen Komplexität, habe ich unser freundschaftliches Verhältnis sehr zu schätzen gelernt.

Mein Dank geht auch an Bernd Binder, sowie an Nils Christian, Georg Basler und Marco Ende für ihre wertvolle Unterstützung in technischen Fragen. Die Mitglieder der *Go*FORSYS Nachwuchsgruppen AG Schroda und AG Nikoloski haben immer ein sehr angenehmes Arbeitsumfeld geschaffen und ich danke ihnen allen für die kritischen Anmerkungen als auch den Zuspruch.

Zu guter letzt möchte ich meiner Familie danken. Meinen Eltern für die beharrliche Unterstützung meiner akademischen Laufbahn, sowie meiner Frau Fadime für ihre Geduld mit mir, ihre Fürsorge und Ermutigung in allen Phasen.

Abstract

Plants and some unicellular algae store carbon in the form of transitory starch on a diurnal basis. The turnover of this glucose polymer is tightly regulated and timely synthesis as well as mobilization is essential to provide energy for heterotrophic growth. Especially for starch degradation, novel enzymes and mechanisms have been proposed recently. However, the catalytic properties of these enzymes and their coordination with metabolic regulation are still to be discovered.

This thesis develops theoretical methods in order to interpret and analyze enzymes and their role in starch degradation. In the first part, a novel description of interfacial enzyme catalysis is proposed. Since the initial steps of starch degradation involve reactions at the starch-stroma interface it is necessary to have a framework which allows the derivation of interfacial enzyme rate laws. A cornerstone of the method is the introduction of the available area function - a concept from surface physics - to describe the adsorption step in the catalytic cycle. The method is applied to derive rate laws for two hydrolases, the β-amylase (BAM3) and the Isoamylase (DBE/ISA3), as well as to the Glucan, water dikinase (GWD) and a Phosphoglucan phosphatase (DSP/SEX4).

The second part uses the interfacial rate laws to formulate a kinetic model of starch degradation. It aims at reproducing the stimulatory effect of reversible phosphorylation by GWD and DSP on the breakdown of the granule. The model can describe the dynamics of interfacial properties during degradation and suggests that interfacial amylopectin side-chains undergo spontaneous helix-coil transitions. Reversible phosphorylation has a synergistic effect on glucan release especially in the early phase dropping off during degradation. Based on the model, the hypothesis is formulated that interfacial phosphorylation is important for the rapid switch from starch synthesis to starch degradation.

The third part takes a broader perspective on carbohydrate-active enzymes (CAZymes) but is motivated by the organization of the downstream pathway of starch breakdown. This comprises α-1,4-glucanotransferases (DPE1 and DPE2) and α-glucan-phosphorylases (Pho or PHS) both in the stroma and in the cytosol. CAZymes accept many different substrates and catalyze numerous reactions and therefore cannot be characterized in classical enzymological

terms. A concise characterization is provided by conceptually linking statistical thermodynamics and polymer biochemistry. Each reactant is interpreted as an energy level, transitions between which are constrained by the enzymatic mechanisms. Combinations of in vitro assays of polymer-active CAZymes essential for carbon metabolism in plants confirmed the dominance of entropic gradients. The principle of entropy maximization provides a generalization of the equilibrium constant. Stochastic simulations confirm the results and suggest that randomization of metabolites in the cytosolic pool of soluble heteroglycans (SHG) may contribute to a robust integration of fluctuating carbon fluxes coming from chloroplasts.

Enzyme kinetics | Enzyme adsorption | Disproportionating Enzyme | Polysaccharides | Statistical Physics

Zusammenfassung

Stärke hat eine herausragende Bedeutung für die menschliche Ernährung. Sie ist ein komplexes, wasserunlösliches Glucosepolymer und dient - als eine der wichtigsten Speicherformen von Kohlenhydraten in Pflanzen - der Aufrechterhaltung des Energiestoffwechsels. Unterschiedliche Organe enthalten Stärke. In Knollen und Samen wird die sogenannte Speicherstärke über lange Zeiträume auf- und abgebaut. Die im Allgemeinen weniger bekannte transitorische Stärke in Blättern und einigen einzelligen Algen wird in einem täglichen Rhythmus umgesetzt: Sie wird während der Photosynthese aufgebaut und in der Nacht abgebaut. Experimentelle Studien haben nachgewiesen, dass die Fähigkeit der Pflanze, den Abbau transitorischer Stärke zu regeln, essentiell ist, um während der Nacht das Wachstum der Pflanze zu gewährleisten. Da die Geschwindigkeit von biochemischen Reaktionen über Enzyme reguliert wird, ist die Aufklärung ihrer Funktion im Stoffwechsel eine notwendige Voraussetzung, um den komplexen Prozess des Wachstums zu erklären.

Die vorliegende Arbeit stellt einen Versuch dar, die Funktion von Enzymen beim Stärkeabbau anhand von mathematischen Modellen und Computersimulationen besser zu verstehen. Dieser Ansatz erlaubt es, Eigenschaften des Systems durch Abstraktion anhand eines idealisierten Abbildes herzuleiten. Die mathematisch notwendigen Folgerungen dienen der Aufstellung von Hypothesen, die wiederum mit experimentellen Resultaten konfrontiert werden können. Stoffwechselsysteme sind komplexe Untersuchungsobjekte, bei denen eine rein qualitative Argumentation schnell an Grenzen gerät, wo mathematische Methoden die Möglichkeit von Aussagen noch zulassen.

Der erste Teil der Arbeit entwickelt einen theoretischen Rahmen, um Gleichungen für die Geschwindigkeit oberflächenaktiver Enzyme herzuleiten. Dies ist notwendig, da die ersten Reaktionen, die dem Stärkeabbau zugeordnet werden, an ihrer Oberfläche stattfinden. Die Methode wird auf vier essentielle Enzyme angewandt: zwei abbauende Enzyme (β-Amylase und Isoamylase) und zwei den Abbau unterstützende Enzyme (α-Glucan,Wasser-Dikinase und Phosphoglucan Phosphatase).

Der zweite Teil entwickelt ein kinetisches Modell des Stärkeabbaus unter Verwendung der hergeleiteten Ratengleichungen. Das Modell bildet die Dynamik des Systems realistisch ab und legt nahe, dass ein spontaner Phasenübergang an der Oberfläche von geordneten zu weniger geordneten Zuständen stattfindet. Ferner wird die Hypothese aufgestellt, dass die reversible Modifikation der Oberfläche durch Enzyme besonders in der Anfangsphase des Abbaus einen synergetischen Effekt hat, d.h. den Abbau enorm beschleunigt. Dies könnte beim schnellen Umschalten von Stärkeaufbau zu Stärkeabbau regulatorisch relevant sein.

Im letzten Teil werden kohlenhydrataktive Enzyme betrachtet, die in der löslichen Phase die Produkte des Stärkeabbaus weiterverarbeiten. Da diese sogenannten Transferasen auch in vielen anderen Organismen und Stoffwechselwegen vorkommen, wird ein allgemeiner Standpunkt eingenommen. Anhand von Methoden aus der statistischen Physik wird theoretisch wie experimentell nachgewiesen, dass diese Enzyme spontan die Entropie innerhalb des Stoffwechselsystems erhöhen. Diese Neigung, «Unordnung» zu schaffen, wird vom Organismus aber paradoxerweise ausgenutzt, um die Weiterverarbeitung von Kohlenhydraten im Stärkestoffwechsel zu stabilisieren. Dieser Mechanismus eröffnet einen neuen Blick auf energie- und entropiegetriebene Prozesse in Zellen.

Enzymkinetik | Enzymadsorption | Disproportionierungsenzym | Polysaccharide | Statistische Physik

Contents

List of Figures

List of Tables

Chapter 1

Introduction

> Darauf kommt es [...] an, in dem Scheine des Zeitlichen und Vorübergehenden die Substanz, die immanent, und das Ewige, das gegenwärtig ist, zu erkennen. Denn das Vernünftige, was synonym ist mit der Idee, indem es in seiner Wirklichkeit zugleich in die äußere Existenz tritt, tritt in einem unendlichen Reichtum von Formen, Erscheinungen und Gestaltungen hervor, und umzieht seinen Kern mit der bunten Rinde, in welcher das Bewußtsein zunächst haust, welche der Begriff erst durchdringt, um den inneren Puls zu finden und ihn ebenso in den äußeren Gestaltungen noch schlagend zu fühlen.
>
> *Grundlinien der Philosophie des Rechts, Vorrede*
>
> G. W. F. Hegel (1770 - 1831)

Since the beginning of the modern age, marked by towering figures like Nicolaus Copernicus (1473–1543), Galileo Galilei (1564–1642) or René Descartes (1596–1650), progress in science is inextricably interwoven with mathematics. Striving for a rigorous foundation of scientific knowledge, mankind has replaced the gods by natural laws which can be expressed in mathematical

form. To assert that the laws of nature are written in the language of mathematics expresses a fundamental conviction into the correspondence between rational human thought and the world we live in. This metaphysical stance is a precondition of doing science as we understand it today.

A central notion of mathematics is quantity. In that sense experimental scientists, much more severely than theorists, accept the reign of mathematics – they measure. The better a system, its internal relations and its motion, can be captured by numbers the more the compelling evidence of order, constancy and reproducibility inflicts upon us the mathematical viewpoint. Hence, no wonder that physics, dealing with less complex non-living matter, has reached a stage where mathematics has become essential. Today, progress in physics even entails progress in mathematics. In sharp contrast to that, the central concepts of biology are of qualitative nature, and the *laws* of living systems still defy a mathematical formalization. SCHWANN and SCHLEIDEN's cell theory, VIRCHOW's *omnis cellula e cellula* or DARWIN's theory of natural selection do not have the form of equations yet. For the time being, we have to limit ourselves to suitable mathematical models of sub-processes of the living, which are analyzed in terms of and with respect to their *physico-chemical* properties. To extract *biological* meaning from this type of analysis, it is necessary to step back again and interpret the results in the light of cellular organization and evolution. This is the basic strategy pursued in this thesis in the context of molecular physiology in general and metabolic systems in particular.

As far as I understand it, there is no reductionist program behind this approach. There *is* a qualitative difference between living and non-living matter. But speaking of matter in both cases, I already admit the continuous aspect of nature. The non-living has produced the living, and the living copes with the non-living, in that it builds and maintains itself with non-living compounds. The interesting question is how the constraints which determine the motion of inanimate subsystems are organized such that they bring about a system which we call a living one.[1]

An important subsystem of organisms is metabolism, the set of enzyme-catalyzed reactions responsible for the transformation of matter. Enzymes,

[1] Polanyi (1968) speaks of "the laws of physics and chemistry which the organism is harnessing."

that is biological catalysts in the broadest sense but usually proteins, enable chemical reactions to take place at a controlled rate. They can themselves be chemically modified in order to alter their activity and thereby control the flux through metabolic pathways. Thus, in its totality metabolism is integrated and orchestrated with other cellular processes like signaling, gene and transcript regulation. However, to assess how a metabolic system *could* react to a 'signal' from another subsystem of the organism, an isolated analysis of the possible behavior of the biochemical reaction system is justified. The intervention by, for example, a post-translational modification can then be seen as a 'signal' which forces the pathway into a certain mode.

Enzymes have long been studied for their mechanisms and kinetic properties (Segel, 1993). However, with the advent of molecular biology and high-throughput techniques the investigation of enzymes has steadily declined (Holzhütter, 2004). The present work is also an attempt to promote the reconsideration of enzymes, since their analysis can still provide unexpected insights into how organisms put the natural laws into work. Of course, this should be integrated with the powerful methods which have come to be known as 'systems biology'.

1.1 Mathematical modeling

The physicist Heinrich Hertz (1857-1894) in his book *Prinzipien der Mechanik* gave a clear definition of modeling:

> *Wir machen uns innere Scheinbilder oder Symbole der äußeren Gegenstände, und zwar machen wir sie von solcher Art, daß die denknotwendigen Folgen der Bilder stets wieder die Bilder seien von den naturnotwendigen Folgen der abgebildeten Gegenstände.* (Hertz, 1894)

Insofar, there is no difference between pictorial and mathematical models. However, mathematics encodes the real world in a special way and can look back to a rich history. Once a mathematical model is formulated, there are powerful rules of inference which can be used and the results can be decoded again. In the words of Heinrich Hertz:

> *Ist es uns einmal geglückt aus der angesammelten bisherigen Erfahrung Bilder von der verlangten Beschaffenheit abzuleiten, so können wir an ihnen, wie an Modellen, in kurzer Zeit die Folgen entwickeln, welche in der äußeren Welt erst in längerer Zeit oder als Folgen unseres eigenen Eingreifens auftreten werden; wir vermögen so den Thatsachen vorauszueilen* [...]. (Hertz, 1894)

In biology, the descriptive rather than the deductive tradition is more prevailing than in physics. From physiologists, especially in the 19$^{\text{th}}$ century, this has been frequently criticized (among them the famous botanist SCHLEIDEN), but this was also a time when biology often fell back into vitalism. In contrast to that, physics has pursued the reactive rather than the functional or teleological paradigm (Rosen, 1985). An outcome of this physical tradition is the mass-action paradigm. Mass-action kinetics provides the basis for the mathematical modeling of many biological systems, from animal populations to biochemical reactions (Heinrich and Schuster, 1996; Murray, 2008; Reich and Sel'kov, 1981; Rosen, 1985).

The modeling of metabolic systems, if we ignore for the moment kinetic studies of enzymes, dates back at least to the 1960s with the investigations of HIGGINS and colleagues (see e.g. Garfinkel et al., 1961). In the 1970s Kacser and Burns (1995) and Heinrich and Rapoport (1974) pioneered metabolic control analysis. In the last twenty years many structural methods have been developed like elementary flux modes and flux balance analysis (Papin et al., 2004).

Together with the advent of high-throughput techniques the focus was more on large-scale analysis rather than on individual enzymes. This is also true for plant science where it is a major aim to find biomarkers or characteristic metabolite profiles to enhance crop yield or other qualitative traits (Sulpice et al., 2009). The starch community though has been more concerned with the biochemistry of their system, since recent discoveries have led to the recognition of novel mechanisms and pathways (Zeeman et al., 2010).

This thesis owes a lot to these studies and is mainly concerned with modeling these newly characterized enzyme-systems and their potential role in metabolism. Details on the modeling approaches will be given in the respective chapters.

1.2 Plant growth and diurnal turnover of transitory starch

A defining feature of plants is that they are autotrophic (Lüttge et al., 2005). They produce complex organic compounds by consuming CO_2, using chemical energy which is derived from the so-called light reactions. Photosynthetic CO_2-assimilation takes place in specialized organelles, the chloroplasts. In higher plants and algae it is supposed that this organelle is a product of primary endosymbiosis with photosynthetically active bacteria. One of the central processes in chloroplasts, starch degradation (Smith et al., 2005), is the main focus of this thesis.

In higher plants, like the model organism *Arabidopsis thaliana*, photosynthetic CO_2-assimilation is localized in leaf cells. Here, the so-called transitory starch is produced which has to be distinguished according to its function and turnover period from reserve starch. The latter accumulates continuously and spatially separated from the site of photosynthesis in plastids of heterotrophic tissues (e.g. in tubers or endosperms). It is turned over relatively slowly: in weeks, occasionally even only once in the whole life cycle. Apparently, its purpose is to support development. The sugars with which the daily energy metabolism is maintained derive from photosynthesis in the leaves. They are transported to sink organs in the form of the disaccharide sucrose. However, during photosynthesis a species-dependent but nevertheless substantial amount of fixed carbon dioxide is not directed towards sucrose synthesis or glycolysis but accumulates as assimilatory (or transitory) starch. Under dark conditions, breakdown of transitory starch becomes the only means for continuous supply of leaf cells and sink organs with reduced carbohydrates. In contrast to reserve starch, transitory starch is turned over on a diurnal basis and its timely synthesis and mobilization is absolutely necessary for maintenance, growth and normal development of the whole organism (Smith and Stitt, 2007; Zeeman et al., 2007).

Remarkably, Graf et al. (2010) have shown that *Arabidopsis* is able to adjust the rate of starch degradation immediately when transferred from light to dark, such that in a normal photo-period starch is exhausted just at the end of the night but not before. Thus, although a long-term genetic or post-

translational control is not excluded, and in fact likely (Kötting et al., 2010), these findings suggest that there is a considerable regulatory potential in the metabolic system itself.

In this respect, biochemical studies in the last decade (see Zeeman et al., 2010, and references therein) clearly show that one can no longer expect to gain an adequate understanding of the overall physiology if the reactions at the starch surface are not taken into account explicitly. The phase transition from a water-insoluble macromolecule to dissolved malto-oligosaccharides involves several interfacial enzymes. In particular, elucidating the role of reversible phosphorylation led to a major shift in the view of starch degradation. It was already known that amylopectin of native starch can contain small amounts of phosphate mono-esters (Blennow et al., 2002), for example 0.1% - 0.5% of the glucose moieties in tuber starch from potato is esterified at C-6 and C-3 positions. The role of phosphorylation in leaves was unclear until a protein known as R1 (Lorberth et al., 1998) has been shown to be responsible for the Arabidopsis *sex1* phenotype, a mutation with starch excess and severe growth reduction (Yu et al., 2001). The prevalent view is that the crystalline order at the surface is "disrupted" by phosphate esters (Blennow and Engelsen, 2010), which supposedly makes the chain ends of amylopectin more susceptible to hydrolytic attack. However, the mechanisms of the associated phase transitions are still unclear.

The degradation of transitory starch in chloroplasts of leaf cells during darkness provides essentially maltose, which is exported to the cytosol in order to support glycolysis as well as sucrose synthesis. Sucrose is the major form in which carbon is transported to sink organs of plants. By exporting maltose, using it as a glucosyl donor, plants can bypass the first reaction of glycolysis (hexokinase) and produce the intermediate glucose-1-phosphate (G1P) via a soluble heteroglycan pool, SHG (Fettke et al., 2009b). G1P is necessary for both the downstream processes of glycolysis and sucrose synthesis. These reactions are catalyzed by carbohydrate-active transferases which have the peculiar property of being relatively unspecific with respect to chain length. Nevertheless, they are very important for the metabolism in both plastid and cytosol, since alterations in their activity lead to a phenotype with reduced growth.

1.3 Synopsis

The exposition follows the degradation pathway, starting with the first committed steps catalyzed by interfacial enzymes and closing with a chapter on downstream metabolism of soluble glycans.

Chapters 2-3 are aimed at developing a kinetic model of starch degradation taking into account the semi-crystalline insoluble nature of starch. **Chapter 2** presents a novel approach to enzymatic processes at interfaces with special emphasis on starch phosphorylation and hydrolysis. To date, interfacial enzyme kinetics is rather poorly covered in computational biochemistry. At first, my objective was to devise a broadly applicable kinetic scheme to obtain the flux through biochemical reactions at interfaces, and to apply this scheme to the major enzymes relevant for starch degradation. This chapter also goes a little bit more into detail regarding the biological aspects and introduces structural aspects of starch.

In terms of the framework of interfacial catalysis, a kinetic model of starch breakdown is formulated in **Chapter 3**. To date, there is no mathematical model of C_3 metabolism which includes processes at the starch granule surface explicitly (Rios-Estepa and Lange, 2007). Rather, in present models (e.g. Nägele et al., 2010; Poolman et al., 2000) starch is treated as an external species. Using data from *in vitro* experiments I demonstrate that interfacial dynamics can be incorporated into a kinetic model which allows to ask questions formerly out of reach.

Finally, the usefulness of a statistical approach to biochemical reaction networks at the macroscopic level is demonstrated.[2] **Chapter 4** is devoted to the metabolism of polysaccharides and carbohydrate-active transferases in general. These enzymes play a crucial role in the metabolism of starch and the turnover of the soluble heteroglycan (SHG) pool in leaf cells. It is shown theoretically and through experimental results, that the associated reaction systems are mainly driven by entropic gradients *within* the metabolite pool.

Notational conventions. Sometimes in modeling it is useful to scale the quantities. This can serve the reduction of parameters without changing the

[2] That is, when the size of the system allows to ignore fluctuations (see e.g. Landau and Lifschitz, 1979).

properties of the model, but moreover it allows to give the numbers obtained a clear meaning. The quantities thus become dimensionless (we will deal with the dimensions length=L, amount=N, mass=M and time=T exclusively). The scale which is attributed to a given quantity, for example time t, is denoted with a diamond superscript, that is $t^\diamond$ in this case. It is common practice then to use greek letters for the corresponding dimensionless variable (Aris, 1994):

$$t \to \tau = \frac{t}{t^\diamond},$$

that is the rescaled time τ is measured in multiplicities of $t^\diamond$, whatever this quantity may be (the choice is not unique). We will follow this recommendation, however, since many physical quantities are denoted with greek letters as well, we will use instead $\underline{x}$ for rescaled quantities whenever this helps in avoiding confusion.

For concentrations in equations, we will consistently use lower-case italic letters. For surface concentrations (and in general quantities which are naturally associated with the surface) we will use an asterisk, for example e^* for the surface concentration of an enzyme.

A stationary state in an open system is called a steady state and denoted by $[x]^{\mathrm{ss}}$. A closed system is not traversed by a net flux and the associated stationary state is a thermodynamic equilibrium, $[x]^{\mathrm{eq}}$. Equilibrium constants will be denoted by q, which may be unusual for biochemists but is common in systems biology or computational biochemistry (Heinrich and Schuster, 1996).

Sometimes a parameter appears in a form, where some factor is omitted or it is time dependent but appears as constants in the equations. These apparent quantities are usually denoted with $\widetilde{x}$.

Other notations are fairly standard and explanations are always given.

The computer algebra system Maxima[3] has been used to solve for nonlinear algebraic equation systems and MATLAB® (R2009a, The MathWorks) for the numerical calculations.

[3]Released under the terms of the GNU General Public License and available at http://maxima.sourceforge.net/.

Chapter 2

Rate laws for interfacial enzymes with application to enzymes acting on starch granules

> For the existence of any science, it is necessary that there exist phenomena which do not stand isolated.
>
> *Cybernetics*
>
> Norbert Wiener (1894 - 1964)

Transitory starch is a complex macromolecule synthesized during photosynthesis in order to sustain central metabolism and sucrose synthesis throughout the night. The mobilization is catalyzed by enzymes acting at the starch-stroma interface. A common problem in metabolic modeling is to correctly include water-insoluble substrates like starch or cellulose. Often these compounds are treated as external metabolites to circumvent the description of the phase boundary, which would entail a distinction between the accessible interface and the inaccessible interior of these compounds. In the case of starch, however, it has become clear that no adequate understanding of its turnover and metabolic regulation is in sight if the enzymatic activity at the interface is ignored (Kötting et al., 2010; Zeeman et al., 2007). In perspective, an integrated view on processes in solution and interfacial kinetics is necessary.

To this end, this chapter develops a simple yet versatile framework to de-

rive mechanistically plausible rate laws for interfacial enzymes which can be readily used in kinetic models of metabolism including interfacial processes. It is shown that the concept of the available area function can be consistently integrated into rate laws with an adsorption step. This allows to treat the sequestration to the interface in a general way. The approach is illustrated for plastidial surface-active enzymes important for starch degradation. The resulting rate laws will be important in modeling starch degradation in Chapter 3. The analysis of the general interfacial analogue of the Michaelis-Menten equation suggests some marked qualitative differences for example the nonlinear dependence on enzyme concentration.

2.1 Introduction

The introductory Section 2.1 presents an overview of interfacial enzymology, gives a brief account of starch structure and degradation, and, based on that, discusses the properties of surface-active enzymes acting on insoluble polysaccharides.

Background. From a basic course or introductory textbook in biochemistry one may get the impression that metabolic reactions take place exclusively in aqueous solutions. Only rarely the novice gets a glimpse on the capability of many enzymes to act at the boundary between two condensed phases, and if so, mostly in the context of intracellular signal transduction where membrane-associated proteins catalyze the synthesis of signaling molecules. A closer inspection reveals, however, that interfacial or heterogeneous reactions abound in living systems and are usually associated with the most common organic compounds on earth. Prominent examples of substrates having interfaces at the meso- to macroscopic scale can be found in all three classes of biomolecules:

- lipid membranes forming the boundary of cells,
- collagen, the most abundant protein in mammals forming fibers in connective tissues,
- cellulose, the most common organic compound on earth being a constituent of plant cell walls and

- glycogen and starch, the major storage carbohydrates in eukaryotes.

The molecular constituents of these substrates form large aggregates, which by their very physical nature have to be distinguished from soluble substrates with respect to enzyme catalysis. This is contrasted in Fig. 2.1, the left panel showing the more common catalysis in soluble phases and the right panel catalysis at an interface. The interaction of an interfacial enzyme with the aggregate precedes the binding of the molecular constituents. This is reflected by the modular organization of surface-active enzymes. Usually separated from the catalytic domain they possess a module specific for the substrate interface. We will consider this in the context of insoluble polysaccharides (see e.g. Boraston et al., 2004).

It seems that the study of surface-active enzymes was at a height in the 70s of the 20$^{\text{th}}$ century, marked especially by the publication of the Verger-DeHaas model regarding lipase (see Verger, 1976, for a review) and thorough investigations on insoluble polysaccharides by Moo-Young and co-workers (Okazaki and Moo-Young, 1978; Suga et al., 1975), which have by now become classic in the biotechnological community. The development of models for starch degradation (e.g. Leloup et al., 1991; Tatsumi and Katano, 2005; Tatsumi et al., 2007) is legging behind owing to the fact that only recently the overriding importance of enzymes at the starch-stroma interface has been revealed (Köt-

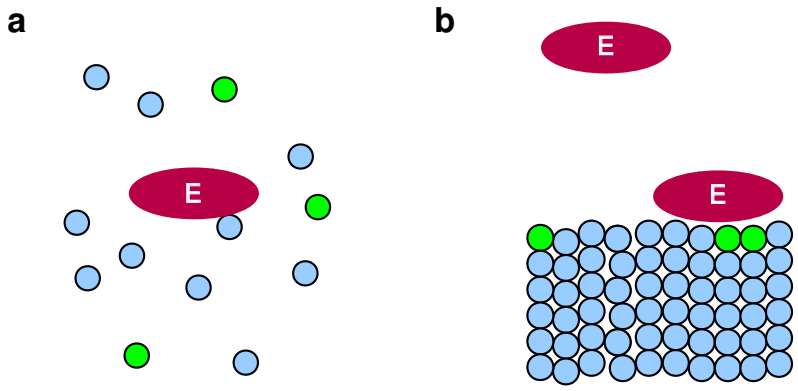

Figure 2.1: **Homogeneous vs. heterogeneous enzyme catalysis**. The blue circles symbolize substrates and the green circles products. **a**, In solution, the enzyme E can readily access and act on substrate molecules which are smaller than its own size. **b**, The surface-active enzyme has to interact with the outer layer of the aggregated substrate.

ting et al., 2009; Zeeman et al., 2010). One gets the impression that there was barely any interaction between communities studying different systems to work out a general framework of interfacial catalysis. Those working on cellulose (Zhang and Lynd, 2004) and, to a certain extent, on starch are more bio-technologically motivated, while the lipid community is more concerned with cell biological aspects. To my knowledge there exists only one textbook on interfacial enzyme kinetics (Berg and Jain, 2002), introducing some general aspects but discussing lipid systems exclusively. A short chapter on interfacial kinetics is contained in the textbook of Marangoni (2003, cf. Chapter 10).

On the experimental side, an important early contribution to heterogeneous reactions with biomolecules is the work of Trurnit (1954) who studied the reaction between chymotrypsin and bovine serum albumin at an interface and introduced the ellipsometer. Recently, Clé et al. (2010) reviewed several techniques useful to monitor the activity of surface-active enzymes, most notably polysaccharide synthesis, using surface plasmon resonance imaging (see also Wegner et al., 2004).

As regards chemists and physicists actively involved in their own field of *surface science*, there seems to have been no overlap of approaches with biochemists except for the recognition of the classical work of Langmuir (1918). The studies on protein adsorption by Ramsden (1993) and Fang and Szleifer (2001) using the random sequential adsorption paradigm (Sec. 2.2 of this thesis and Evans, 1993; Talbot et al., 2000) and a method based on the free energy of the system, respectively, can claim a certain biological relevance. Apart from that, advanced methods have been developed to characterize interfacial phenomena in general including energetic and thermo-mechanical considerations (Rusanov, 2005) and the description of dynamic changes of interfaces by growth, etching or chemical reactions (Kolasinski, 2008; Masel, 1996).

Starch structure and metabolism. Starch is an insoluble polysaccharide composed of the α-D-glucose polymers amylose and amylopectin (Buléon et al., 1998). The relative amounts of both constituents vary with botanical origin and physiological conditions. A common estimate for assimilatory starch in *Arabidopsis* is 15% amylose to 85% amylopectin (Zeeman et al., 2002). Amylose is basically a linear α-1,4-linked glucan, while amylopectin is chemi-

cally comparable to glycogen with glucose residues frequently linked by α-1,6-glucosidic bonds, forming branching points (for further chemical details see Damager et al., 2010). However, the chemical similarity to glycogen does not translate to the structural level. As shown in Fig. 2.2 glycogen is a fairly spherical macromolecule less than 50 nm in diameter and evenly distributed short branches, while amylopectin side-chains do not hinder each other and originate from regions with a peculiar clustering of α-1,6-linkages enabling much larger molecule sizes.

Within starch grains, the side-chains of amylopectin have a mean degree of polymerization (DP) of 14-18 and form double helices which self-assemble into clusters with 9 to 17 side-chains (Gallant et al., 1997). While these highly ordered regions form the crystalline lamellae of starch, the regions made up by the branching points of amylopectin presumably co-localize with amylose and form disordered amorphous lamellae (Kozlov et al., 2007). Crystalline and amorphous lamellae alternate with a periodicity of 9-10 nm, usually forming so-called semi-crystalline growth rings which can have a thickness of 120-400 nm depending on botanical origin (see Corre et al., 2010, and refs. therein). As Fig. 2.3 depicts, these again alternate with amorphous growth rings whose

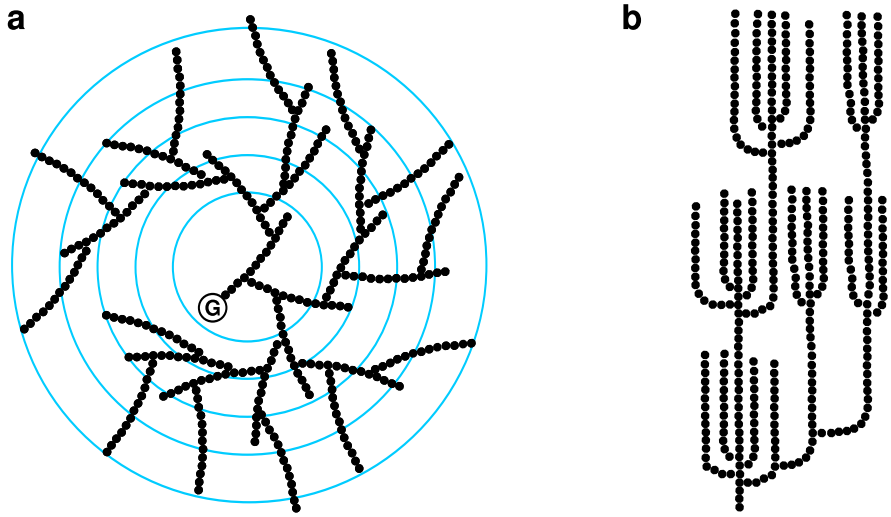

Figure 2.2: **Comparison of glycogen and amylopectin**. **a**, A sketch of the glycogen molecule after Meléndez-Hevia et al. (1993) showing five concentric tiers and the glycogenin protein (G) in the center. **b**, Amylopectin molecule with clustered α-1,6-branchings.

structural properties are, however, unknown.[1] The growth rings are concentric, the polymer chains being oriented perpendicular to them and the surface of the granule (Buléon et al., 1998).

The biosynthesis of transitory starch in chloroplasts of mesophyll cells is known to involve many enzymes with different isoforms. They catalyze elongation, branching and debranching reactions at the starch-stroma interface to trim amylopectin into the right shape and co-synthesize amylose but as to this date it remains unclear how they interact to induce a correct granule assembly (Ball and Morell, 2003).

Certainly, the temporary polymerization of glucose to form a limited number of starch granules allows the plant to store huge amounts of carbohydrates in plastids while high osmotic or colloid-osmotic stresses are avoided. In comparison to the glycogen molecules, starch grains can reach diameters of 50 μm and above and can store much higher amounts of glucose in the semi-crystalline matrix.

Despite this tight packing of glucose polymers in starch, making them almost inert towards hydrolytic degradation, the granules are mobilized immedi-

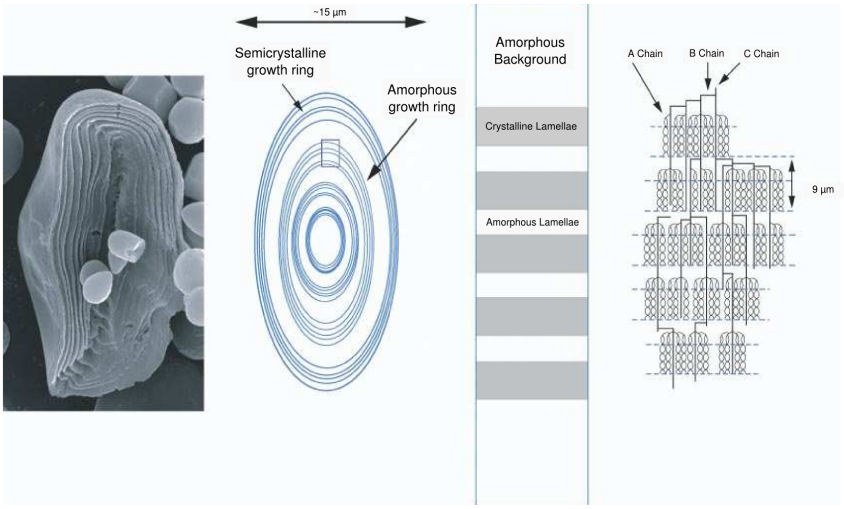

Figure 2.3: **Starch granule organization**. This schematic view is taken from Ball and Morell (2003) and slightly modified to illustrate the hierarchical order of the granule described in the main text.

[1] Zeeman et al. (2002) reports a peculiar exception regarding *Arabidopsis*: in the discoid leaf starch granules of the wild-type no growth rings are visible, but they are present in the spherical granules of the *sex4* mutant.

ately when leaves are transferred from light to dark (Graf et al., 2010). Several studies in the last decade have established the crucial role of reversible phosphorylation (Blennow and Engelsen, 2010; Blennow et al., 2002) of the granule surface in achieving this switch. Most notably, Ritte et al. (2002) characterized a surface-active glucan, water dikinase (GWD) which phosphorylates glucosyl residues, thereby catalyzing an order-disorder transition in crystalline regions of the interface, stimulating hydrolytic breakdown (Edner et al., 2007; Ritte et al., 2004). This led to a significant revision of transitory starch metabolism and the abandonment of the prevailing phosporolytic paradigm for degradation.

Figure 2.4 shows the action mode of the major surface-active enzymes usually sufficient to catalyze the hydrolytic breakdown of starch. Briefly, this so-called hydrolytic pathway suggests that mainly the activity of GWD stimulates a downstream exo-acting β-amylase.[2] After releasing maltose residues from non-reducing glucan ends, the phosphoglucan phosphatase SEX4 (DSP) removes the phosphate esters enabling further degradation by β-amylase and an endo-acting debranching enzyme (DBE) or isoamylase (Delatte et al., 2006). The latter is necessary to remove branching points, releasing short linear oligosaccharides from the starch surface.

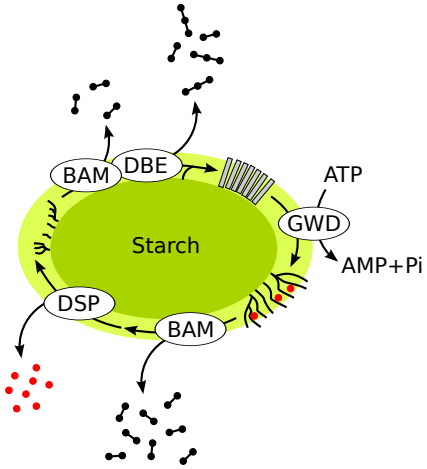

Figure 2.4: **Enzymes acting at the interface during starch degradation**. Rectangles indicate glucan double helices forming the crystalline interface, black dots glucose residues and red dots orthophosphate.

[2]The phosphoglucan, water dikinase (PWD) is not considered here (see Hejazi et al., 2009). The mutant phenotype is less severe and GWD can be considered as a representative of dikinases such that the rate law of PWD is expected to closely resemble that of GWD.

Properties of surface-active CAZymes. Below and in the next chapter, I will go more into detail, but for now it is appropriate to restrict ourselves to the following perspective: What are the structural properties making it possible that the aforementioned surface-active enzymes can attach to the granule? The crucial elements here are carbohydrate-binding modules (CBMs), non-catalytic protein domains which recognize and bind carbohydrates (Boraston et al., 2004; Guillén et al., 2010; Shoseyov et al., 2006). They are currently classified into 61 families, the largest being CBM48 with over 2,700 proteins according to the CAZy database (Cantarel et al., 2009).[3] The CBMs are further discriminated in types according to the topology of their ligand-binding site (Boraston et al., 2004): Type A CBMs are surface-binding CBMs with high affinity towards crystalline polysaccharides and low affinity to soluble polysaccharides. Type B CBMs bind (also insoluble) glycan-chains, which are at the same time substrate of the cognate catalytic module. Finally, lectin-like Type C CBMs are specific for small sugars up to tri-saccharides.

Since our focus is on enzymes acting at the interface of insoluble polysaccharides Type A and B CBMs are of particular interest here. Type A CBMs display a flat hydrophobic surface composed of aromatic amino acids, especially tryptophan and tyrosin, which is responsible for strong Lifshitz-van der Waals interactions with sugar rings. Additionally, polar amino acids can engage in hydrogen bonds with flat surfaces of crystalline polysaccharides. These structural properties make the associated enzymes orders of magnitude more affine for crystalline substrates than amorphous or soluble ones. This is the case for certain starch- and cellulose-binding domains (SBDs and CBDs), respectively, for example in GWD (Mikkelsen et al., 2006). Type B CBMs have a cleft arrangement that makes the enzymes specific for free single chains either in solution or in amorphous insoluble polysaccharides.

In both cases, an important function of CBMs is first to increase the effective concentration of the enzyme at the interface. Second, the active site of the catalytic domain (CD) is positioned in proximity of the polysaccharide chain through CBMs. After the CD has acted the CBM allows the relocation of the enzyme at the surface to start a catalytic cycle anew.

Irreversible binding has been reported for some CBMs but this is still a

[3]Data as of October 22nd, 2010, accessed via http://www.cazy.org

controversial issue. In the literature on interfacial enzymology (Berg and Jain, 2002; Deems, 2000) nearly irreversible binding has been reported for phospholipase A2 acting on small unilammelar vesicles (SUVs). This is referred to as the 'scooting' mode, where the enzyme runs through several catalytic cycles before it eventually dissociates. In contrast to that, if the molecules are rapidly exchanged between vesicles one speaks of the 'hopping' mode.

Coming back to CBMs, apart from substrate recognition they probably can also disrupt the substrate upon binding. Polysaccharide chains in crystalline regions may be disorganized due to polar interactions or weakening of hydrogen bonds which enhances availability of the chains. Interestingly, it has been shown that depending on the molecular order at the substrate binding site, adsorption of CBMs may be enthalpically driven (in non-crystalline regions, Boraston, 2005) or entropically driven (crystalline regions, Creagh et al., 1996).

Motivation and outline. The discussion shows that to describe interfacial enzyme kinetics on insoluble polysaccharides, different physical states at the interface have to be considered. At a typical heterogeneous interface of carbohydrates, certain enzymes will associate with crystalline sites others with amorphous regions of the substrate. This is recognized in the literature on modeling cellulose degradation (Zhang and Lynd, 2004) but has not been developed so far for starch (e.g. Marchal et al., 2003, 2001; Tatsumi and Katano, 2005; Wojciechowski et al., 2001). The present study aims at closing this gap and allows to integrate different interfacial qualities and adsorption models into one framework. Owing to the main theme of the thesis, the presentation is biased towards starch degradation. However, the basic aspects are sufficiently general as to be applicable to other substrates as well. It should be useful in both studying *in vitro* kinetics and introducing interfacial rate laws in models of metabolism. Given the great disparity of existing approaches to interfacial phenomena, in particular regarding interfacial enzymology, an integrated perspective may provide a basis for cross-fertilization.

To quantify the activity of enzymes at the interface, properties of the substrate particles as well as the adsorption of the protein at the substrate interface is considered in Section 2.2. The notions of 'specific surface area' and 'available area function' are introduced and it is discussed how interfacial re-

actants can be included in the framework. In Section 2.3 rate laws for four surface-active enzymes are derived using partial equilibrium mechanisms. The qualitative differences between the Michaelis-Menten-Henri rate law and its generic interfacial analogue is discussed.

2.2 Development of the theoretical approach

2.2.1 The substrate interface

A major factor which determines the partitioning of surface-active enzymes is the bulk interface concentration of the substrate. Thus, we begin with a discussion on how this quantity can be assessed by specifying geometric properties as well as properties of the suspension in which the reactions take place.

Quantifying the interfacial area. In typical experiments with starch from leaf extracts it is rather difficult if not impossible to measure the surface area of the starch granules directly. What can be easily monitored instead is the total mass, M_g, or the mass concentration, $m_\mathrm{g} = M_\mathrm{g}/V$, of granular material in a suspension of volume V. A usual method then is to calculate the corresponding total surface area, A_g, using the formal relationship

$$A_\mathrm{g} = \alpha \cdot M_\mathrm{g} \quad \text{or} \tag{2.1a}$$

$$a_\mathrm{g} = \alpha m_\mathrm{g}, \tag{2.1b}$$

where $a_\mathrm{g} = A_\mathrm{g}/V$ denotes the bulk interface concentration and the parameter α denotes the so-called *specific surface area* characteristic for a substrate suspension. This quantity should encode both the geometry of single granules and the properties of the granule population. The latter is important since distributing a given mass to more but smaller particles increases the surface area and vice versa. Considering the starch population from a certain plant source, the granules are assumed to have different sizes but shape and material density, ρ, are the same. The density is usually measured as specific gravity with reference to water and varies in the range $\rho = 1.4 - 1.5$ g/cm^3 (Buléon et al., 1982; Tatsumi and Katano, 2005). It may be appropriate here to emphasize, that since our model of starch granules assumes a uniform density

there is no internal anisotropy considered. That is, from any point within the granular matrix the bulk properties are invariant in any direction. If it is true, however, that starch can be correctly described by the side-chain liquid-crystalline model (Waigh et al., 2000a,b) and the internal structure becomes decisive for a specific modeling purpose, the approximation of isotropy cannot be uphold anymore. Rather, one would have to include as an additional observable at least the so-called *director*, a unit-vector which can be associated with each coordinate within the liquid-crystal giving the orientation of the molecules (Landau and Lifschitz, 1979).

For uniform particles, it is convenient to use the spheroid as a geometrical model to approximate (and restrict) possible shapes. Following Tatsumi et al. (2007), consider an assay with N_g granules having equatorial and polar diameters of d_i and $h \cdot d_i$, respectively, where $i = 1, \ldots, N_\mathrm{g}$ and h is the polar diameter factor (see Fig. 2.5). The specific surface area reads

$$\alpha = \frac{6z}{\rho} \frac{\sum_i d_i^2}{\sum_i d_i^3}, \tag{2.2}$$

where

$$z = \begin{cases} \{(h/2\epsilon)\ln[(1+\epsilon)/(1-\epsilon)] + 1/h\}/2 & \text{if } h < 1, \\ 1 & \text{if } h = 1, \\ z = [(\arcsin\epsilon')/\epsilon' + 1/h]/2 & \text{if } h > 1, \end{cases} \tag{2.3}$$

is a dimensionless factor encoding the shape in terms of h, the eccentricities being defined by $\epsilon := \sqrt{1-h^2}$ and $\epsilon' := \sqrt{1-h^{-2}}$. Figure 2.5 summarizes the properties of the geometrical model used here and contrasts it with a picture of *Arabidopsis* starch granules. Such images can be evaluated to determine empirical values for h and d to calculate z.

The sums in Eq. (2.2) quantify the influence of the granule size distribution, denoted $\{d_i\}$, where the sum is taken over all granules in an assay. *In vivo*, the number N_g can often be readily estimated. Chloroplasts of *Arabidopsis*, for example, contain about five granules, or even only one in the *ssiv* mutant (Zeeman et al., 2010). The picophytoplanktonic green alga *Ostreococcus tauri* contains only one granule in its single chloroplast (Ral et al., 2004). The number of granules in *in vitro* assays is usually not known exactly, rather a size distribution of a fraction of the whole assay sample is detected. It can be measured using size exclusion chromatography (SEC) as in Witt et al. (2010)

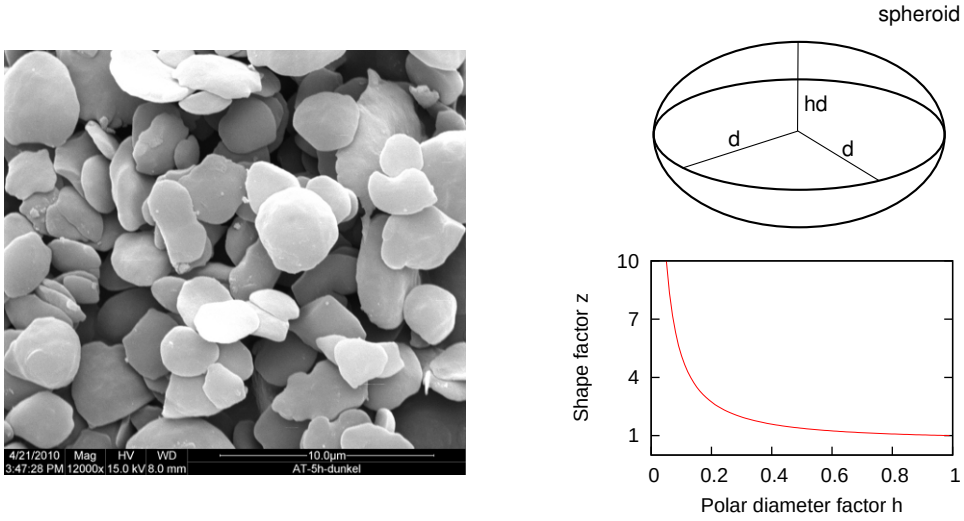

Figure 2.5: **Geometrical model for starch granules**. An electron microscopic picture of *Arabidopsis thaliana* starch shows the flat spheroid-like shape of the granules (kindly provided by AG Steup, University of Potsdam). The shape factor z is plotted against h which quantifies the deviation from a sphere (i.e. $h = 1$).

or an apparatus based on the Coulter principle as in Hejazi et al. (2009) or Tatsumi et al. (2007).[4] Gidley et al. (2010) discuss some of the current issues in reliably measuring starch size distributions.

The data available so far indicate, that the size of granules can be well described by a log-normal distribution, which can be specified by the distribution through mean μ and standard deviation σ. In the case of a continuous readout or a fitted curve, Eq. (2.2) can be reformulated as

$$\alpha = \frac{6z}{\rho} \frac{\langle d^2 \rangle}{\langle d^3 \rangle}, \tag{2.4}$$

where $\langle \cdot \rangle$ denotes the arithmetic mean of the respective variable over the whole assay sample. In fact, these quantities are the second and third (raw) moments of the distribution, respectively (Gnedenko, 2005). Assuming a log-normal distribution, the r^{th} moment of a random variable X is given by $\langle X^r \rangle =$

[4]Examples are flow cytometry (FCM) and scanning ion occlusion spectroscopy (SIOS, Roberts et al., 2010).

$\exp[r\mu + (r^2/2)\sigma]$ and we get[5]

$$\alpha = \frac{6z}{\rho} \mathrm{e}^{-(\mu+(5/2)\sigma)}. \tag{2.5}$$

In their discussion of log-normal distributions Limpert et al. (2001) suggest to use the "back-transformed" parameters $\mu_* = \mathrm{e}^{\mu}$ and $\sigma_* = \mathrm{e}^{\sigma}$ to describe the data. The first is identical to the median and the second is the so-called multiplicative standard deviation describing the shape. In terms of both, the specific surface area reads

$$\alpha = \frac{6z}{\rho \mu_* \sigma_*^{5/2}}, \tag{2.6}$$

which is shown in Fig. 2.6 for two different shapes. On the one hand, it illustrates that for a fixed size distribution given by a pair (μ_*, σ_*) (a point in the plane of Fig. 2.6a and Fig. 2.6b, respectively) the specific surface area is increased for flatter granules. On the other hand, for a given granule and distribution shape (fixed z and σ_*) the specific surface area increases if the granule diameter is decreased, for example during degradation.

Given a size distribution measurement on a representative subset of the sample, the specific surface area can be calculated using the maximum-likelihood estimators of μ_* and σ_* (Limpert et al., 2001).

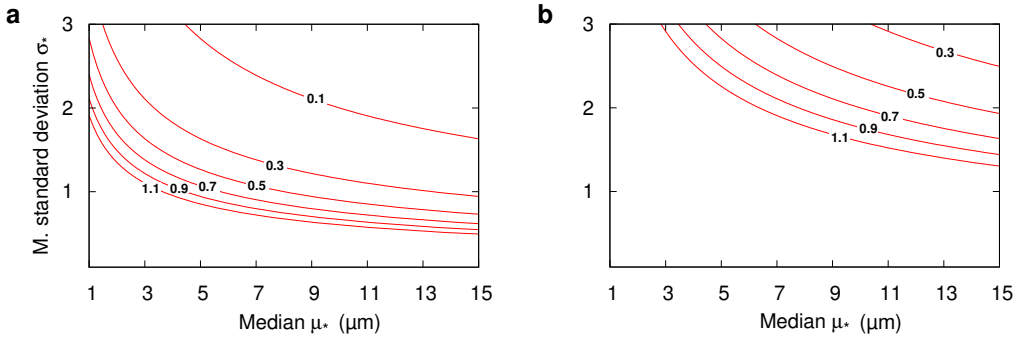

Figure 2.6: **The specific surface area for a log-normal granule size distribution**. Values for specific surface area in the contour plot are to be multiplied by 10^{12} $\mu\mathrm{m}^2/\mathrm{g}$. **a**, Plot for a suspension of spherical granules ($z = 1$). **b**, The same plot for flat spheroids with $z = 7$ (i.e. $h \approx 0.1$). As a typical value for starch density $\rho = 1.5$ g/cm^3 $= 1.5 \cdot 10^{-12}$ g/μm^3 has been used.

[5]Weisstein, Eric W. "Log Normal Distribution." From *MathWorld*–A Wolfram Web Resource. http://mathworld.wolfram.com/LogNormalDistribution.html

Description of interfacial heterogeneity. For the adsorption process, surface chemical heterogeneity can be described by a distribution of *patches*, each type of patch having a characteristic interfacial energy profile (see Ramsden, 2002, and Fig. 2.7 at p. 23 below). This profile, depending on both the considered enzyme and the local interfacial quality, characterizes their interaction. Some regions of the surface may even turn out to be effectively irrelevant for an enzyme.

Given the discussion of the biochemistry of surface-active CAZymes, a model should include at least two types of patches, crystalline and amorphous regions, whose surface fractions are denoted ω^{cr} and ω^{am}, respectively. Although the microscopic realization of each phase can be different, this seems to become relevant only after the enzyme has been adsorbed. In the two-state system it holds $\omega^{\mathrm{cr}} + \omega^{\mathrm{am}} = 1$ and the total surface area simply reads

$$A_{\mathrm{g}} = \omega^{\mathrm{cr}} A_{\mathrm{g}} + \omega^{\mathrm{am}} A_{\mathrm{g}}. \tag{2.7}$$

Whenever necessary, an extension of this phenomenological description to more types of patches is straightforward. In the treatment below we will simply speak of the relevant surface area fraction ω for a single enzyme. In the general case, it will be convenient to introduce an enzyme-patch function, F_j^i, whose values are defined by

$$F_j^i = \begin{cases} 1 & \text{if enzyme } j \text{ binds to patch } i, \\ 0 & \text{otherwise.} \end{cases} \tag{2.8}$$

2.2.2 Adsorption kinetics

In this section we will turn from the properties of the substrates to the kinetics of adsorption of surface-active enzymes. The adsorption, or physisorption to be more precise, of an enzyme (the *adsorbate*) on a substrate's surface (the *adsorbent*) is mainly governed by interfacial energies between the protein, water and the substrate. Contributions of Lifshitz-van der Waals (LW), electrostatic (el) and solvation or electron donor-acceptor (da) forces can be distinguished. Ramsden (2002) reports that LW forces are roughly the same for different proteins but the solvation forces, in aqueous systems usually established by hydrogen bonding, can differ considerably. However, aromatic amino acid

residues (i.e. LW interactions) of CBMs can contribute significantly to the specificity towards interfacial regions, and since both the protein and the substrate interface may carry net charges, electric double layer effects could play an important role in localizing proteins (Goldenberg and Steinberg, 2010).

All interfacial forces contribute to the distance-dependent interaction potential, $U(r)$, where r denotes the protein-surface distance. As depicted in Fig 2.7, its qualitative profile is characterized by the activation energy for adsorption, U_{ads}, the distance r_0, where the energy becomes negative for an incoming particle and the adhesion energy, U_{adh}, at the distance of closest approach r_{adh}. The interaction profile determines the associated rate coefficient of adsorption according to (Ramsden, 2002):

$$k_{\mathrm{a}} = k_{\mathrm{D}} \left[\int_{r_0}^{\infty} \left(\mathrm{e}^{U(r)} - 1 \right) \mathrm{d}r \right]^{-1}, \tag{2.9a}$$

with the dimensions (L=length, T=time) given by

$$\begin{aligned} [k_{\mathrm{a}}] &= \mathsf{L}\mathsf{T}^{-1}, \quad \text{and} \\ [k_{\mathrm{D}}] &= \mathsf{L}^2\mathsf{T}^{-1}. \end{aligned} \tag{2.9b}$$

k_{D} is the diffusion coefficient of the enzyme in the bulk phase given by the Einstein relation (Glaser, 1996)

$$k_{\mathrm{D}} = \mu_{\mathrm{D}} k_{\mathrm{B}} T \tag{2.9c}$$

where μ_{D} denotes the mobility, k_{B} is the Boltzmann constant and T is the temperature.

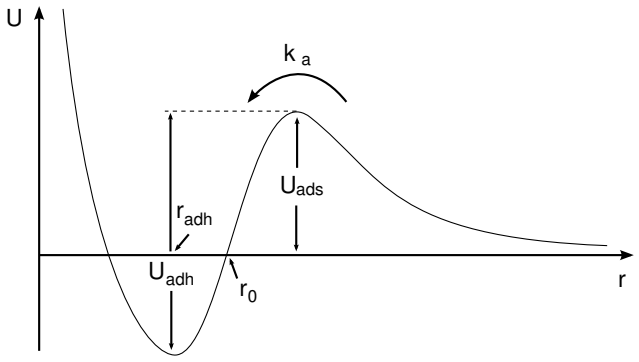

Figure 2.7: **The interaction potential between adsorbate and adsorbent**. These potential energy shapes are often associated with the rates of processes (Hänggi et al., 1990).

In the following, I will derive the kinetic equation for adsorption which also serves in introducing important notions in interfacial kinetics. The aim is to bring to the fore the connections between the more biochemically motivated approach and the physico-chemical concepts as expressed for example in the treatment of Ramsden (2002).

Single enzyme adsorption. Protein adsorption can be considered as a reversible bi-molecular reaction between the enzyme in the soluble phase, E, and a 'relevant ligand' (Deems, 2000) at the interface. As the interface appears effectively as a continuum for the protein in solution (Ramsden, 2002), it is appropriate to interpret 'relevant ligand' as a corresponding adsorption site, S^*_E (Masel, 1996):

$$\mathrm{E} + \mathrm{S}^*_\mathrm{E} \underset{r_\mathrm{d}}{\overset{r_\mathrm{a}}{\rightleftharpoons}} \mathrm{E}^*, \tag{2.10}$$

where the asterisk always denotes an interfacial species and r_a and r_d are the adsorption and desorption rates, respectively. Note, that the adsorption site is a pseudo-species that is used to envision the surface as a lattice which looks different for each adsorbate. Figure 2.8 illustrates this lattice at the substrate surface. The area of an adsorption site for the enzyme E is called the *parking area* A_E occupied upon adsorption. Since we will assume a spherical protein shape with diameter d_E, the parking area is roughly $A_\mathrm{E} \approx d_\mathrm{E}^2$.

At first, we will allude to this classical conception of Langmuir and show

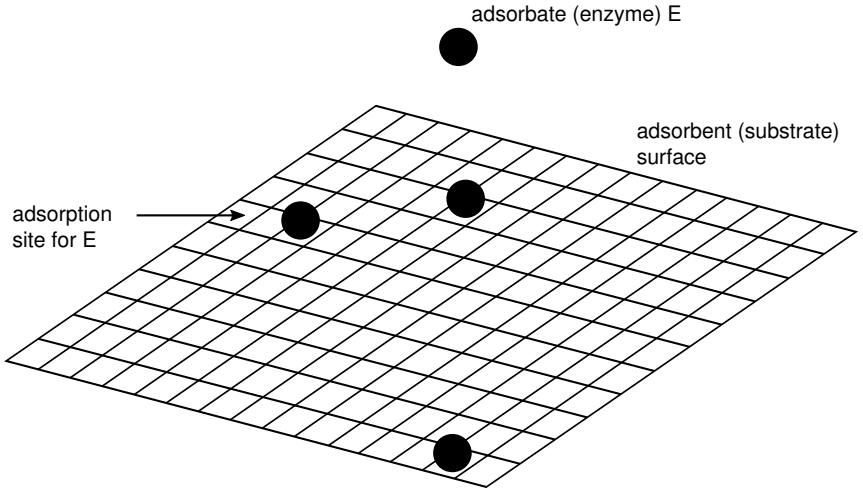

Figure 2.8: **Langmuir's concept of adsorption**.

afterward how the result can be generalized in a straightforward way. In any case, only monolayer adsorption is considered, that is a protein cannot adsorb upon already adsorbed proteins. Multilayer adsorption may play a role if interactions between adsorbed and dissolved proteins target enzymes to the interface.Compared to the usual treatment, I have (a) not excluded the possibility that the surface area may change, and (b) considered surface heterogeneity, as introduced above.

In formulating the ODEs describing reaction (2.10), the rate balance is applied to bulk concentrations (i.e. with respect to the whole reactor). Regarding interfacial species, it is advisable to implicitly use the time derivative of the amounts (dimension N) first. By convention (see Section 1.3) we use lower-case letters for concentrations of species' in their natural environment. Thus, the natural concentration of E is denoted e, having dimension $[e] = \mathsf{NL}^{-3}$, and correspondingly e^* is a surface concentration, $[e^*] = \mathsf{NL}^{-2}$. These quantities change according to

$$\begin{aligned} \frac{\mathrm{d}e}{\mathrm{d}t} &= -r_\mathrm{a} + r_\mathrm{d}, \\ \frac{1}{V}\frac{\mathrm{d}\left(A_\mathrm{g} e^*\right)}{\mathrm{d}t} &= +r_\mathrm{a} - r_\mathrm{d}, \end{aligned} \tag{2.11}$$

where, according to mass action kinetics, the rates for reaction (2.10) are given by

$$r_\mathrm{a} = \widetilde{k}_\mathrm{a} e s_\mathrm{E}^* a_\mathrm{g} \text{ and} \tag{2.12a}$$

$$r_\mathrm{d} = k_\mathrm{d} e^* a_\mathrm{g}. \tag{2.12b}$$

Since the rates have dimension $\mathsf{NL}^{-3}\mathsf{T}^{-1}$, those of the rate constants result in $[k_\mathrm{d}] = \mathsf{T}^{-1}$ and $[\widetilde{k}_\mathrm{a}] = \mathsf{N}^{-1}\mathsf{L}^3\mathsf{T}^{-1}$. By comparison, the latter is not identical to the rate constant given in (2.9b), $\widetilde{k}_\mathrm{a} \neq k_\mathrm{a}$, but the relationship will emerge below. Due to the balance equations the conservation relation

$$e^0 = e + a_\mathrm{g} e^* \tag{2.13}$$

holds and algebraically determines one of the variables in terms of the other via the initial bulk concentration of enzyme e^0. In the following, we will concentrate on the ODE for the interfacial species. Applying the rule for differentiating products and rearranging terms yields

$$\frac{\mathrm{d}e^*}{\mathrm{d}t} = \widetilde{k}_\mathrm{a} e s_\mathrm{E}^* - \left(k_\mathrm{d} + r_\mathrm{g}\right) e^*, \tag{2.14}$$

where the *growth rate* of the interfacial reaction space

$$r_{\mathrm{g}} := \frac{1}{A_{\mathrm{g}}} \frac{\mathrm{d}A_{\mathrm{g}}}{\mathrm{d}t}, \ [r_{\mathrm{g}}] = \mathsf{T}^{-1}, \tag{2.15}$$

has been introduced.[6] Next, the concentration of adsorption sites s^*_{E} has to be determined. We first introduce the *maximum enzyme concentration* per unit area

$$e^{*\max} = 1/\left(N_{\mathrm{A}} A_{\mathrm{E}}\right), \tag{2.16}$$

which depends solely on the enzyme's parking area, A_{E}, and the Avogadro constant N_{A}. In terms of this quantity, the concentration of free adsorption sites can be written as

$$s^*_{\mathrm{E}} = \frac{A^{\mathrm{av}}_{\mathrm{g}}}{A_{\mathrm{g}}} e^{*\max}, \tag{2.17}$$

where the *available surface area*, $A^{\mathrm{av}}_{\mathrm{g}} \leqslant A_{\mathrm{g}}$, depends on the fraction of the surface relevant for adsorption and the *excluded surface area*, $A^{\mathrm{ex}}_{\mathrm{g}}$, due to already occupied sites:

$$A^{\mathrm{av}}_{\mathrm{g}} = \omega A_{\mathrm{g}} - A^{\mathrm{ex}}_{\mathrm{g}}. \tag{2.18}$$

In the LANGMUIR model, the excluded surface area is proportional to the number of adsorbed enzymes with the parking area being the proportionality constant,

$$\begin{aligned} A^{\mathrm{ex}}_{\mathrm{g}} &= A_{\mathrm{E}} \cdot n^*_{\mathrm{E}} \\ &= A_{\mathrm{E}} \cdot \left(e^* A_{\mathrm{g}} N_{\mathrm{A}}\right), \\ &= \theta_{\mathrm{E}} A_{\mathrm{g}}. \end{aligned} \tag{2.19}$$

In the last transformation, (2.16) has been used to introduce the dimensionless *fractional surface coverage* defined by (Marangoni, 2003)

$$\theta_{\mathrm{E}} := \frac{e^*}{e^{*\max}}, \ \theta_{\mathrm{E}} \in [0, 1]. \tag{2.20}$$

With (2.18) and (2.19) the adsorption site concentration (2.17) can be written as

$$s^*_{\mathrm{E}} = \left(\omega - \theta_{\mathrm{E}}\right) e^{*\max}, \tag{2.21}$$

[6] Kacser and Burns (1995) and Heinrich and Schuster (1996) define the growth rate analogously for a changing three-dimensional reaction space.

and the balance equation (2.14) for the interfacial species reads

$$\frac{\mathrm{d}e^*}{\mathrm{d}t} = \widetilde{k}_\mathrm{a} e^{*\max} e\,(\omega - \theta_\mathrm{E}) - (k_\mathrm{d} + r_\mathrm{g})\, e^*. \tag{2.22}$$

Replacing (2.21) in the adsorption rate (2.12a) establishes, by comparing dimensions, the link to (2.9a),

$$k_\mathrm{a} = \widetilde{k}_\mathrm{a} e^{*\max}. \tag{2.23}$$

To simulate the temporal behavior it is advised to nondimensionalize the system, so that the numbers are not arbitrary but have a clear intrinsic meaning. We will introduce the association constant of adsorption $K_\mathrm{a} = k_\mathrm{a}/k_\mathrm{d}$ with $[K_\mathrm{a}] = \mathsf{L}$ (sometimes the inverse dissociation constant, K_d, is more convenient to use). With the scaling in Table 2.1 the dynamic system (2.11) can be recast in the form,

$$\frac{\mathrm{d}\theta_\mathrm{E}}{\mathrm{d}\tau} = \left(\underline{e}^0 - \underline{a}_\mathrm{g}\theta_\mathrm{E}\right)(\omega - \theta_\mathrm{E}) - (1 + \varrho_\mathrm{g})\,\theta_\mathrm{E}, \tag{2.24}$$

Up to the initial conditions θ_E^0 and $\underline{e}^0$, the quantities ω and $\underline{a}_\mathrm{g}$ uniquely determine all solution trajectories. Here, these quantities figure as parameters, but if we were to simulate the dynamics with a changing substrate area, additional ODEs for them would be required. We set $\mathrm{d}_\tau\theta_\mathrm{E} = 0$ to see what the limiting behavior would look like. The quasi-steady state coverage reads then:

$$\theta_\mathrm{E}^\mathrm{ss} = \frac{\omega\underline{e}^\mathrm{ss}}{1 + \underline{e}^\mathrm{ss} + \varrho_\mathrm{g}}. \tag{2.25}$$

Without change in surface heterogeneity, this quasi-steady state is time-independent only if the surface area grows or shrinks exponentially, $\mathrm{d}_t A_\mathrm{g} \propto A_\mathrm{g}$, since then $\varrho_\mathrm{g} = \text{const.}$ holds according to (2.15). In the case of a constant surface area ($\varrho_\mathrm{g} = 0$), or if the growth rate is assumed to be very slow compared

Table 2.1: Scaling for the dynamic system of a single adsorbed enzyme.

Dimensional quantity	**Scale**	**Non-dimensional quantity**
Time t	$t^\diamond = 1/k_\mathrm{d}$	$\tau = tk_\mathrm{d}$
Surface concentration e^*	$e^{*\diamond} = e^{*\max}$	$\theta_\mathrm{e} = e^*/e^{*\max}$
Bulk concentration e	$e^\diamond = e^{*\max}/K_\mathrm{a}$	$\underline{e} = eK_\mathrm{a}/e^{*\max}$
Interface concentration a_g	$a_\mathrm{g}^\diamond = 1/K_\mathrm{a}$	$\underline{a}_\mathrm{g} = a_\mathrm{g}K_\mathrm{a}$
Growth rate r_g	$r_\mathrm{g}^\diamond = k_\mathrm{d}$	$\varrho_\mathrm{g} = r_\mathrm{g}/k_\mathrm{d}$

to the desorption rate constant of the enzyme (hence $\varrho_\mathrm{g} \approx 0$) the system approaches the equilibrium state

$$\theta_\mathrm{E}^\mathrm{eq} = \frac{\omega \underline{e}^\mathrm{eq}}{1 + \underline{e}^\mathrm{eq}}, \tag{2.26}$$

with saturation coverage $\theta_\infty = \omega$. Here the *relevant* surface area is half covered if $\underline{e}^\mathrm{eq} = 1$, that is $e^\mathrm{eq} = e^{*\,\mathrm{max}}/K_\mathrm{a}$. As expected, equation (2.26) reduces to the classical *Langmuir adsorption isotherm* for $\omega = 1$:

$$\theta^\mathrm{eq} = \frac{e^\mathrm{eq} K_\mathrm{a}}{e^{*\,\mathrm{max}} + e^\mathrm{eq} K_\mathrm{a}}. \tag{2.27}$$

The adsorption dynamics for a single particle is illustrated in Fig. 2.9. It shows that the relaxation time and the equilibrium coverage are altered by higher enzyme loadings while the saturation coverage is determined by ω.

The available area function. What makes the adsorption rate discussed so far specifically LANGMUIRian is in fact the functional dependence on the coverage. It is advised here to express the rate in the general form

$$r_\mathrm{a} = k_\mathrm{a} e \phi a_\mathrm{g}. \tag{2.28}$$

We see that the LANGMUIRian model is simply realized by setting $\phi = \omega - \theta_\mathrm{E}$. As indicated above (see Eq. 2.19), the critical assumption leading to this result

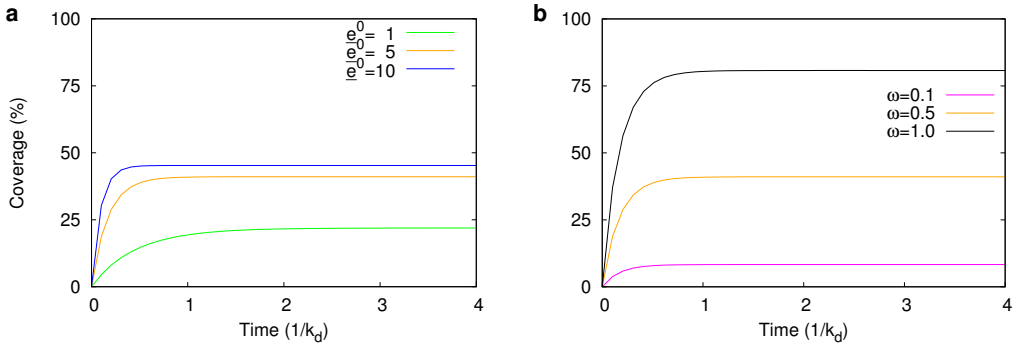

Figure 2.9: **Adsorption dynamics and equilibrium for a single particle due to LANGMUIR**. The simulations were performed according to Eq. (2.24). **a**, Dynamics for fixed relevant surface fraction, $\omega = 0.5$, but different initial values for enzyme loading $\underline{e}^0$ showing the higher coverage in equilibrium with higher enzyme loading. **b**, A fixed loading of $\underline{e}^0 = 5$ has been chosen and different available surface fractions ω showing the change in the saturation coverage. In all simulations $\varrho_\mathrm{g} = 0$ and $\underline{a}_\mathrm{g} = 1$ hold.

is that the excluded surface area depends linearly on the surface coverage. This is strictly valid only if the adsorption sites are independent and the adsorbed molecules do not interact with each other. In physics the quantity ϕ is known as the *available area (surface) function* (Ramsden, 2002; Talbot et al., 2000) or the *sticking probability* (Evans, 1993). Like the coverage, its value varies in the range $[0, \omega]$, however, it is always complementary to the coverage and gives the probability of finding an empty site upon impingement. The advantage of using the kinetic scheme (2.28) lies in the easy adaptation to more complicated adsorption models by formally replacing the corresponding available area function.

For example, a physically more realistic model of monolayer adsorption is *random sequential adsorption* (RSA, see e.g. Evans, 1993). It is not presupposed that the proteins adsorb onto well-defined neighboring sites to arrange perfectly, but the surface is treated as a continuum. As indicated, for proteins this is indeed the case regardless of the nature of the surface (Ramsden, 2002). RSA can describe the realistic phenomenon that the surface may be 'jammed' although it is not fully covered. The saturation coverage for RSA is $\theta_\infty \approx 0.547$ (Talbot et al., 2000), considerably lower than in LANGMUIR's model where $\theta_\infty = 1$. For RSA a further increase is not possible since any free space at the surface is individually too small to accommodate an additional molecule.[7] In the 1D case, known as the car-parking problem, the model has been solved for ϕ exactly, but only approximate solutions are known in the 2D case (Talbot et al., 2000). Basically, in contrast to LANGMUIRian adsorption the excluded surface does not depend linearly on the coverage but is expanded in powers of θ. For disks of a defined size adsorbing on a plane surface the available area function results in (Schaaf and Talbot, 1989)

$$\phi = 1 - 4\theta + \frac{6\sqrt{3}}{\pi}\theta^2 + \left(\frac{40}{\sqrt{3}\pi} - \frac{176}{3\pi^2}\right)\theta^3 + O\left(\theta^4\right), \tag{2.29}$$

where O is the Landau symbol.[8] RSA can be generalized to treat polydisperse mixtures (Olson and Talbot, 2000), cooperative effects and conformational

[7] Interestingly, the saturation coverage of particles following RSA approaches that of LANGMUIR-type adsorption if the proteins cluster to form a tight-packed crystalline layer at the surface (Ramsden, 2002).

[8] $O(\theta^4)$ means that this term is growing at most in the order of four around $\theta = 0$ (Amann and Escher, 1998, Chapter 4).

changes upon adsorption (Talbot et al., 2000), aspects which may be relevant for proteins.

Competitive adsorption. An important generalization of the model which can be conveniently implemented using the available area function is *competitive adsorption*. This is a most relevant setting for interfacial enzyme kinetics, since in many cases the activity of several enzymes is relevant to catalyze reactions on insoluble substrates. Consider a mixture of, say, m interfacial enzymes. The corresponding dynamic system is a straightforward generalization in the case of a homogeneous interface. For $j = 1, \ldots, m$ we have

$$\begin{aligned} \frac{\mathrm{d}e_j}{\mathrm{d}t} &= a_\mathrm{g} \left[-\frac{\mathrm{d}e_j^*}{\mathrm{d}t} \right], \\ \frac{\mathrm{d}e_j^*}{\mathrm{d}t} &= k_{\mathrm{a},j} e_j \phi - \left(k_{\mathrm{d},j} + r_\mathrm{g} \right) e_j^*, \end{aligned} \tag{2.30}$$

where the available area function mediates the dynamic competition for adsorption sites by coupling the ODEs. Within the classical LANGMUIRian framework, the adsorption sites are independent and A_g^ex is linear in the coverage of each interfacial species, resulting in

$$\phi = 1 - \sum_{j=1}^{m} \theta_j. \tag{2.31}$$

Generalizing competitive adsorption to heterogeneous interfaces can be achieved using the enzyme-patch function (2.8). Competition for adsorption sites is now confined to those enzymes which bind to the same type of patch, respectively. If an enzyme binds to more than one type of patch one has to introduce corresponding interfacial concentration variables for each patch, which slightly complicates the dynamic equations. We will write e_j^{*i} or θ_j^i, respectively, for an enzyme j adsorbing to patch i. The available area function is now defined for each patch type, $i \in \{1, \ldots, p\}$, separately:

$$\phi^i = \omega^i - \sum_{j=1}^{m} F_j^i \theta_j^i, \tag{2.32a}$$

or in matrix notation

$$\boldsymbol{\phi} = \boldsymbol{\omega} - \left(\mathbf{F} \circ \boldsymbol{\theta} \right) \mathbf{1}_{(m \times 1)}, \tag{2.32b}$$

where $\boldsymbol{\phi}$ and $\boldsymbol{\omega}$ are $(p \times 1)$ matrices, $\mathbf{F}$ and $\boldsymbol{\theta}$ are $(p \times m)$ matrices and $\mathbf{1}$ is a vector with m rows and only ones as entries. The Hadamard product, $A \circ B$, is defined for matrices of the same dimensionality and is simply the entrywise ordinary product, that is $A \circ B = \{a_{ij} \cdot b_{ij}\}$ (Horn and Johnson, 1985). The dynamic system (2.30) now including surface heterogeneity reads

$$\begin{aligned} \frac{\mathrm{d}e_j}{\mathrm{d}t} &= a_\mathrm{g} \left[-\sum_{i=1}^{p} \frac{\mathrm{d}e_j^{*i}}{\mathrm{d}t} \right], \\ \frac{\mathrm{d}e_j^{*i}}{\mathrm{d}t} &= F_j^i \left[k_{\mathrm{a},j}^i e_j \phi^i - \left(k_{\mathrm{d},j}^i + r_\mathrm{g} \right) e_j^{*i} \right], \end{aligned} \tag{2.33a}$$

and can be written as a single equation for the $(p \times m)$ matrix of surface concentrations together with the conservation relation,

$$\begin{aligned} \frac{\mathrm{d}\mathbf{e}^*}{\mathrm{d}t} &= \mathbf{F} \circ \left[(\mathrm{dg}\boldsymbol{\phi})\, \mathbf{k}_\mathrm{a}\, (\mathrm{dg}\mathbf{e}) - \left(\mathbf{k}_\mathrm{d} + r_\mathrm{g} \mathbf{1}_{(p \times m)} \right) \circ \mathbf{e}^* \right], \\ \mathbf{e} &= \mathbf{e}^\mathbf{0} - a_\mathrm{g} \left(\mathbf{1}_{(1 \times p)} \mathbf{e}^* \right)^T. \end{aligned} \tag{2.33b}$$

Here, $(\mathrm{dg}\boldsymbol{\phi})$ and $(\mathrm{dg}\mathbf{e})$ denote square diagonal matrices with the entries given by the vectors $\boldsymbol{\phi}$ and $\mathbf{e}$, respectively. As done before, it is appropriate to express this result in terms of coverages by choosing $e_j^{*i\diamond} = e_j^{*\max}$ for a given enzyme j and $i = 1, \ldots, p$.

Note, that in analogy to the non-competitive case the equilibrium coverages can be given by the condition

$$[\theta_j^i]^\mathrm{eq} = \frac{\phi^i}{K_{\mathrm{d},j}^i e_j^{*\,\max}} [e_j]^\mathrm{eq} = \frac{\phi^i}{\widetilde{K}_{\mathrm{d},j}^i} [e_j]^\mathrm{eq}. \tag{2.34}$$

For simulations, a choice for the time scale $t^\diamond$ is reasonable the better it ensures the approximation $\varrho_\mathrm{g} \approx 0$. We take the largest desorption rate constant in the system, setting $t^\diamond = 1/\max_{ij}\{k_{\mathrm{d},j}^i\}$ which results in relative desorption constants $\kappa_{\mathrm{d},j}^i = k_{\mathrm{d},j}^i / \max_{ij}\{k_{\mathrm{d},j}^i\}$ satisfying $\kappa_{\mathrm{d},j}^i \leq 1$. Concerning the bulk enzyme concentrations, $e_j \to \underline{e}_j$, in analyzing competitive adsorption one may normalize to the total enzyme loading given by

$$e_\mathrm{t} = \sum_{j=1}^{m} e_j^0. \tag{2.35}$$

After some elementary calculations (see Appendix A) we arrive at

$$\begin{aligned} \frac{\mathrm{d}\boldsymbol{\theta}}{\mathrm{d}\tau} &= \mathbf{F} \circ \left[(\mathrm{dg}\boldsymbol{\phi})\, \boldsymbol{\Lambda}_\mathrm{a}\, (\mathrm{dg}\underline{\mathbf{e}}) - \boldsymbol{\theta} \right] \circ \boldsymbol{\kappa}_\mathbf{d}, \\ \underline{\mathbf{e}} &= \underline{\mathbf{e}}^\mathbf{0} - \underline{a}_\mathrm{g}\, (\mathrm{dg}\underline{\mathbf{e}}^{*\,\max}) \left(\mathbf{1}_{(1 \times p)} \boldsymbol{\theta} \right)^T, \end{aligned} \tag{2.36}$$

where all scalings are summarized in Table 2.2.

Equation (2.36) shows that the values in $\boldsymbol{\kappa}_\mathbf{d}$ solely determine the relaxation time, whereas the parameters appearing in the bracket, that is $\boldsymbol{\Lambda}_\mathrm{a}$ and (implicitly) ω^i, determine the equilibria. Figure 2.10 illustrates the relaxation to equilibrium of a system with three enzymes adsorbing on a substrate with two different interface qualities. Enzyme 1 binds to patch type 1 ($\theta_1^1 \neq 0$) and enzyme 2 to patch type 2 ($\theta_2^2 \neq 0$), whereas the third enzyme adsorbs onto both patches ($\theta_3^1 \neq 0$ and $\theta_3^2 \neq 0$) but with different affinities ($\Lambda_{\mathrm{a},3}^1 > \Lambda_{\mathrm{a},3}^2$). An interesting aspect of the temporal profile is that the slow adsorption of enzyme 2 on patch 2 ($\kappa_{\mathrm{d},2}^2 = 0.1$) leads to a temporary overshoot in the adsorption of the fast enzyme 3 on the same patch. Such dynamic behavior resulting from separation of characteristic times of the adsorption process may have a physiological significance if enzymes have to act sequentially at the substrate interface. It is more efficient then if they do not hinder each other

Table 2.2: Scaling for the dynamic system describing competitive adsorption.

Dimensional quantity	**Scale**	**Non-dimensional quantity**
Time t	$t^\diamond = 1/\max_{ij}\{k_{\mathrm{d},j}^i\}$	$\tau = t \cdot \max_{ij}\{k_{\mathrm{d},j}^i\}$
Surface concentrations e_j^{*i}	$e_j^{*\diamond} = e_j^{*\max}$	$\theta_j^i = e_j^{*i}/e_j^{*\max}$
Bulk concentrations e_j, e_j^0	$e_j^\diamond = e_\mathrm{t}$	$\underline{e} = eK_\mathrm{a}/e^{*\max}$
Interface concentration a_g	$a_\mathrm{g}^\diamond = e_\mathrm{t}/\max_j\{e_j^{*\max}\}$	$\underline{a}_\mathrm{g} = a_\mathrm{g}\max_j\{e_j^{*\max}\}/e_\mathrm{t}$
Growth rate r_g	$r_\mathrm{g}^\diamond = \max_{ij}\{k_{\mathrm{d},j}^i\}$	$\varrho_\mathrm{g} = r_\mathrm{g}/\max_{ij}\{k_{\mathrm{d},j}^i\}$
$K_{\mathrm{a},j}^i = k_{\mathrm{a},j}^i/k_{\mathrm{d},j}^i$	$[K_{\mathrm{a},j}^i]^\diamond = e_j^{*\max}/e_\mathrm{t}$	$\Lambda_{\mathrm{a},j}^i = K_{\mathrm{a},j}^i e_\mathrm{t}/e_j^{*\max}$
$e_j^{*\max}$	$[e_j^{*\max}]^\diamond = \max_j\{e_j^{*\max}\}$	$\underline{e}_j^{*\max} = e_j^{*\max}/\max_j\{e_j^{*\max}\}$

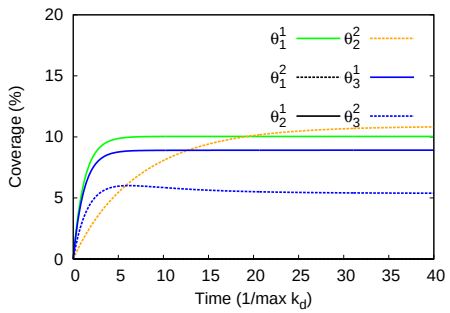

Figure 2.10: **Competitive Langmuirian adsorption**. The enzymes are distinguished by color, whereas solid lines indicate adsorption to patch 1 and dashed lines indicate adsorption to patch 2. Parameter: Relative surface area is $\underline{a}_\mathrm{g} = 0.1$, relevant fractions are $\omega_1 = \omega_2 = 0.5$, and enzyme loading is $\underline{e}^0 = 1/3$ each.

and competition for adsorption sites is minimized.

2.2.3 Concentration of interfacial reactants

Description of the complete catalytic cycle of an interfacial enzyme requires a thermodynamically consistent but at the same time convenient choice for the concentration units of interfacial reactants. Two features should be emphasized here. First, the encounter of enzyme and reactant takes place in a two-dimensional reaction space, hence the rate is determined by surface concentrations. Secondly, the reactants interact and constitute a condensed phase, so they probably behave non-ideally.

Most models (Burns et al., 1982; Eaton and Dennis, 1976; Holtzapple et al., 1984; Tatsumi and Katano, 2005; Verger, 1976) of interfacial enzyme catalysis use the surface number density (or surface concentration, i.e. moles per area) for interfacial reactants. This complicates the description if heterogeneous reactions lead to a significant erosion of the substrate. In this case, the interface is moving which entails virtual replenishment fluxes (Chu and Bazant, 2007; Gan et al., 2003) due to the mass balance

$$M^* = M^{\mathrm{tot}} - M^{\mathrm{int}} - M^{\mathrm{aq}}, \tag{2.37}$$

where M^{tot} is the total substrate mass, M^{aq} is the dissolved mass, and M^{int} is the undissolved mass not in contact with the aqueous phase. M^* is called the excess mass contained in the dividing surface (a mathematical concept introduced by Gibbs, reviewed in section 3.1 in Rusanov, 2005) remaining if the mass of the two bulk phases is subtracted. Consider Fig. 2.11**a**, which exemplifies the situation for a single granule. Two bulk phases can be distinguished, the aqueous phase (aq) and the solid (s) granule phase, divided by a moving interface.

If replenishment of the interface from the bulk phase is overlooked (as in (Converse and Optekar, 1993)) the model in fact only describes the reactants at the outermost monolayer but not those which are 'digged out' during degradation. This may be approximately valid for initial rate assays but it is not realistic for longer time scales which are usually also considered in metabolic models.

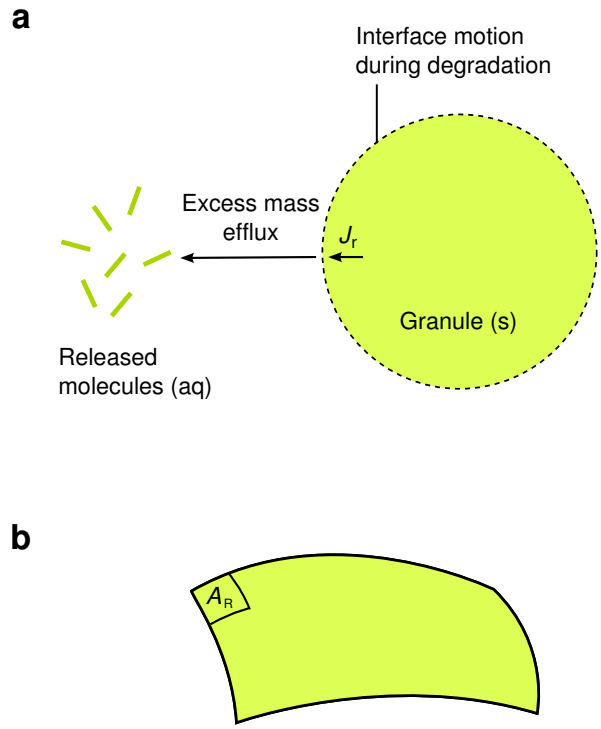

Figure 2.11: **On the choice of interfacial reactant concentration units**. **a**, Motion of the dividing surface at the interface separating the aqueous phase (aq) from the solid (s) granule phase. Degradation leads to a decreasing excess mass (i.e. of the mass confined to the dividing surface) which has to be accounted for by introducing an appropriate replenishment flux J_r. **b**, When using mole fractions, instantaneous replenishment is assumed and the area A_R occupied by any interfacial reactant is the same and independent of the total interface area.

The complication introduced by replenishment fluxes can be circumvented if the total surface number density of reactants $c^{*\,\max}$ remains constant throughout the process, that is

$$c^{*\,\max} = \sum_k c_k^* = \text{const.} \tag{2.38}$$

This is a good approximation if each reactant is assumed to occupy the same effective area A_R at the dividing surface, see Fig. 2.11**b**, for then the total number density is given by

$$c^{*\,\max} = (N_A A_R)^{-1}\,. \tag{2.39}$$

Observe the formal similarity to the calculation of $e^{*\max}$, Eq. (2.16). Thus, the independence of $c^{*\max}$ on changes in the total interface area allows to scale the number particle densities to introduce mole fractions:

$$\chi_k^* = \frac{c_k^*}{c^{*\max}}. \tag{2.40}$$

Hence, we will use mole fractions for the concentration of interfacial reactants which amounts to assuming that replenishment occurs instantaneously.

In their discussion (see Theory Box 3.2 in Berg and Jain, 2002), Berg and Jain point out that interfacial reactants occupying different areas can be handled by area correction factors to introduce activity coefficients. These account for nonidealities to first order in the mole fractions.

2.3 Rate laws

General considerations. A biochemical rate law describes the flux through an enzymatic reaction in terms of reactants, effectors and the amount of enzyme present. The functional relation between these quantities are derived from detailed mechanisms in the form of elementary reaction steps endowed with mass action kinetics. Using additional assumptions regarding the time scales of these steps it is possible to eliminate the enzyme intermediates. This can either be achieved by the rapid-equilibrium approximation (REA) or the quasi-steady state assumption (QSSA). Both are satisfied under certain conditions, however, never throughout the whole reaction progress (Beard and Qian, 2008). Expressions for the rates of enzyme-catalyzed reactions for a variety of mechanisms and the techniques to derive them are discussed in depth in standard textbooks on enzyme kinetics, for example Segel (1993). They usually have the form of a fraction with polynomials in numerator, N, and denominator, D:

$$v = \frac{N}{D}. \tag{2.41}$$

In general, it is a good advice to derive rate laws using the REA first: the resulting expressions have sometimes less terms than those derived with the QSSA, and most parameters can be interpreted as equilibrium constants, which are often readily accessible experimentally (Alberty, 2008). If these rate laws consistently fail to reproduce experimental data they can be replaced by QSSA

rate laws. An approach increasingly used to simplify the modeling of large metabolic networks is to assume generic or convenient rate equations for enzymes, whose mechanistic details are missing or supposedly unimportant for the question at hand (Bulik et al., 2009; Liebermeister and Klipp, 2006).

Starch-degrading enzymes. In the following, rate laws for the most important surface-active enzymes in transitory starch degradation will be derived. Since adsorption does not involve the cleavage or formation of chemical bonds it is reasonable to assume a fast turnover of enzymes between the aqueous and insoluble phase such that this subsystem may be considered close to equilibrium and is only adiabatically perturbed by the slower catalytic steps. Moreover, an interesting aspect of using the REA rather than the QSSA is that the absolute amounts on both the interface and the aqueous phase can still change. The intermediary enzyme complexes not involved in adsorption will be assumed to be in a QSS.[9] An appropriate scheme to derive these hybrid rate laws has been devised by Cha (1968). Care must be taken, since the catalytic cycle of interfacial enzymes involves reaction spaces of different dimensionality.

All enzymes discussed here act on polymeric substrates. Due to the more or less random attack many reactants with different degrees of polymerization (DP) and phosphate ester positions would have to be distinguished. In order to avoid a zoo of variables and to highlight the basic structure of the rate laws I restricted myself to certain substrate groups, members of which are assumed to have the same specificity towards their enzyme. According to the action mode depicted in Fig 2.4 (p. 15)and more precisely in Fig. 2.12 we may distinguish the following interfacial substrate groups:

- native maltodextrin chains, either in helical (Gh^*) or random coil (Gc^*) conformation
- (singly) phosphorylated maltodextrin chain (pG^*)
- partially degraded phosphodextrin (pGx^*)

[9] In computational biochemistry this is called the *standard* QSSA, sQSSA. Schnell and Maini (2003) give a very useful overview of different QSSAs and compare their range of validity.

- partially degraded dextrin (Gx*) and
- β-limit dextrin-like stubs (Gb*) of DP2 and DP3

The rate laws are derived in the order of the complexity of the mechanism, starting with the endo-acting debranching enzyme (isoamylase), followed by the dual-specificity phosphatase SEX4 which acts on interfacial as well as soluble phosphodextrins. Both are assumed to bind to amorphous patches only, whereas the mechanism of the exo-acting β-amylase allows for adsorption to both amorphous and crystalline regions. Finally, the glucan, water dikinase exemplifies a catalytic cycle where two of the enzyme intermediates are partitioned between interface and solution.

2.3.1 Debranching Enzyme (DBE)

Background. Plants have two types of debranching enzymes, limit-dextrinase (LDA, EC 3.2.1.142) and isoamylase (EC 3.2.1.68, glycoside hydrolase family 13, GH13) of which three isoforms exist. During the night, LDA and the isoform ISA3 are active on β-limit dextrin-like substrates. ISA3 has been shown to be localized at the granule interface (Delatte et al., 2006) and acts

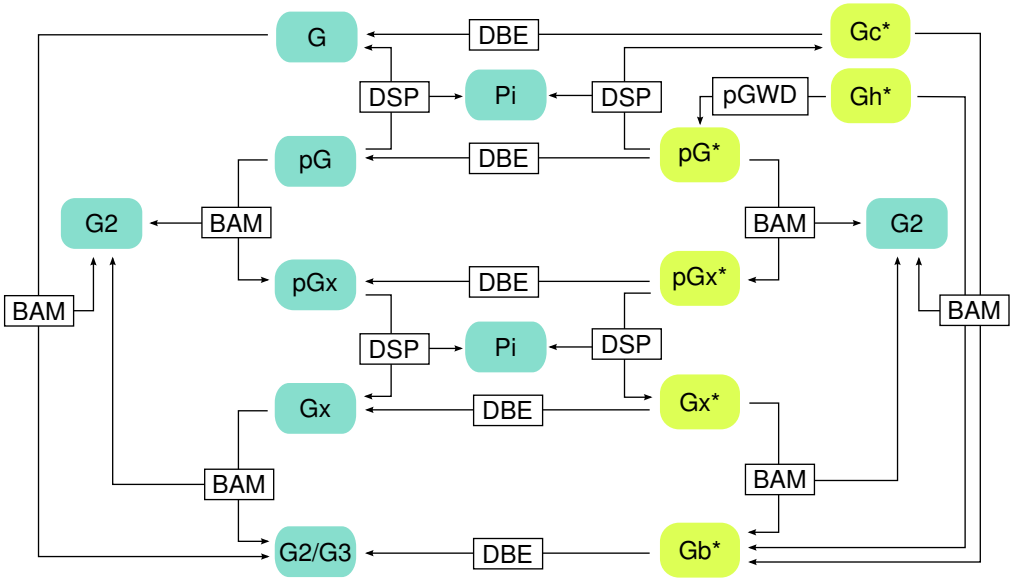

Figure 2.12: **Reactions of interfacial and dissolved reactants catalyzed by surface-active enzymes**. Interfacial species and species in solution are highlighted by a green and blue background, respectively.

on Gb* as indicated in Fig. 2.12. These short side-chains are products of the hydrolytic activity on the α-1,4-bonds of amylopectin branches, whereas DBEs are necessary to remove the branches by hydrolyzing α-1,6-bonds. This makes further bonds in a deeper layer accessible for continued starch degradation. Most likely, maltosyl and maltotriosyl residues are released by ISA3 (Zeeman et al., 2010).

Probably, a CBM48 is present in ISA3 as it is in most isoamylases from archaea and bacteria according to the CAZy database (Cantarel et al., 2009). The preferred adsorption region for this CBM is amorphous, since the enzyme acts in branched regions of amylopectin unable to form double helices.

Mechanism and rate law. The mechanism of the surface-active DBE, ISA3, is sketched in Fig. 2.13a. Reaction 1 is the adsorption step. Since the DBE acts on all interfacial substrates except for the helical glucans, Gh, S_i^* is used as a short-hand to avoid blowing up the scheme. Reaction 2 is the association with the interfacial substrate and reaction 3 the irreversible release of the product. Thus, the interfacial cycle resembles a classical irreversible uni-uni reaction, which becomes more obvious in the corresponding partial equilibrium mechanism depicted in Fig. 2.13b. This diagram is the first step in deriving rate laws for partial equilibrium mechanisms according to Cha (1968). The *rapid equilibrium segment*, E$\rightleftharpoons$E*, is condensed into a single node, X. This pseudo-species has the concentration $x = e + a_\mathrm{g} e^*$ and, as can be seen, the arrow ensuing from this intermediate is weighted by a *fractional concentration factor* f_E^*. Together with the complementary factor f_E and taking E as the reference species, these factors read

$$f_\mathrm{E} = \frac{e}{e + a_\mathrm{g} e^*} = \frac{1}{1 + a_\mathrm{g} e^*/e} = \frac{1}{1 + K_\mathrm{a} \phi^\mathrm{am} a_\mathrm{g}}, \tag{2.42a}$$

$$f_\mathrm{E}^* = \frac{a_\mathrm{g} e^*}{e + a_\mathrm{g} e^*} = \frac{a_\mathrm{g} e^*/e}{1 + a_\mathrm{g} e^*/e} = \frac{K_\mathrm{a} \phi^\mathrm{am} a_\mathrm{g}}{1 + K_\mathrm{a} \phi^\mathrm{am} a_\mathrm{g}}, \tag{2.42b}$$

where in the last transformation the equilibrium relation for adsorption,

$$\left[\frac{e^*}{e}\right]^\mathrm{eq} = K_\mathrm{a} \phi^\mathrm{am}, \tag{2.43}$$

has been exploited (see previous section). Of course, the fractions making up the whole equilibrium segment have to sum up to unity, $f_\mathrm{E} + f_\mathrm{E}^* = 1$.

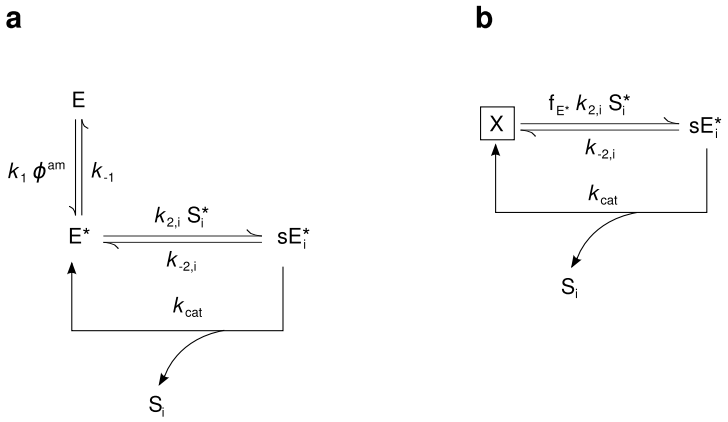

Figure 2.13: **Catalytic mechanism of the surface-active debranching enzyme (DBE)**. Diagrams are applied to each interfacial substrate S_i^*. **a**, The full mechanism with adsorption ($k_{\pm 1}$) and interfacial uni-uni reaction ($k_{\pm 2}$, k_{cat}^*). **b**, The condensed mechanism, where the enzyme forms E and E^* are part of a rapid equilibrium segment, X, and f_{E}^* is the relevant fractional concentration factor.

Next, the QSSA is applied to the condensed diagram. Here and in the following sections, the concentration of enzyme intermediates, for example the complex sE_i^*, is always denoted as $c_{\mathrm{sE}_i^*}$. Since the rate laws, $v_{(\mathrm{DBE}|\mathrm{S}_i)}$, are given by the net flux through the rate-limiting catalytic step,

$$v_{(\mathrm{DBE}|\mathrm{S}_i)} = k_{\mathrm{cat}} a_{\mathrm{g}} [c_{\mathrm{sE}_i^*}]^{\mathrm{ss}}, \tag{2.44}$$

we need to determine the steady state concentration of the interfacial complexes denoted by the superscript ss.[10] This is done by setting the corresponding balance equations to zero,

$$\frac{\mathrm{d}c_{\mathrm{sE}_i^*}}{\mathrm{d}t} = 0, \tag{2.45}$$

leading to

$$0 = k_{2,i} \chi_{\mathrm{S}_i^*} f_{\mathrm{E}}^* \frac{x}{a_{\mathrm{g}}} - \left(k_{-2,i} + k_{\mathrm{cat}}\right) c_{\mathrm{sE}_i^*} - r_{\mathrm{g}} c_{\mathrm{sE}_i^*}. \tag{2.46}$$

This is solved for $[c_{\mathrm{sE}_i^*}]^{\mathrm{ss}}$ and $[x]^{\mathrm{ss}}$, additionally using the equation expressing the conservation of enzyme concentration,

$$e^0 = x + a_{\mathrm{g}} \sum_i c_{\mathrm{sE}_i^*}. \tag{2.47}$$

[10] Note, that the rate is defined for the whole reactor, that is per unit volume.

The computer algebra system Maxima[11] was used to carry out the algebraic calculations. Assuming again that the interfacial growth rate, r_g, is slow with respect to both the enzyme desorption rate constant, k_{-1}, and the two-dimensional association rate constant k_2 and replacing the fractional concentration factor f_E^* in the solution yields the rate law

$$v_{(\mathrm{DBE}|\mathrm{S}_i)} = \frac{k_\mathrm{cat}^* e^0 \cdot \frac{\phi^\mathrm{am} a_\mathrm{g}}{K_\mathrm{d}} \frac{\chi_{\mathrm{S}_i^*}}{K_{\mathrm{S}_i^*}}}{1 + \frac{\phi^\mathrm{am} a_\mathrm{g}}{K_\mathrm{d}} \left(1 + \sum_i \frac{\chi_{\mathrm{S}_i^*}}{K_{\mathrm{S}_i^*}}\right)}. \tag{2.48}$$

The phenomenological half-saturation concentrations (Michaelis constants),

$$K_{\mathrm{S}_i^*} = \left(k_{-2,i} + k_\mathrm{cat}^*\right) / k_{2,i}, \tag{2.49}$$

are dimensionless corresponding with the use of mole fractions and $[k_\mathrm{cat}^*] = \mathsf{T}^{-1}$.

The rate law has a particularly simple and reasonable form, the interfacial reactants appearing in a term analogous to soluble rate laws $(1 + \ldots)$ but multiplied with the concentration of the available interface, $\phi^\mathrm{am} a_\mathrm{g}$, relative to the dissociation constant K_d. As shown in Section 2.2.2, the available area function depends on the enzyme loading. This is setting the interfacial rate laws apart from standard rate laws, and the associated effects on the catalytic turnover will be discussed below after the remaining rate laws are presented.

2.3.2 Phosphoglucan phosphatase (DSP or SEX4)

Background. SEX4 (EC 3.1.3.48) is a protein of approximately 45 kDa with a catalytic dual-specificity phosphatase (DSP) domain at its amino terminus and a CBM48 at the carboxy terminus (Kooi et al., 2010; Niittylä et al., 2006). Until very recently the DSP motif was thought to be responsible for hydrolyzing phosphotyrosine and phosphoserine/-threonine substrates only. It came as a surprise when repeatedly it was demonstrated that nonproteinaceous molecules such as phosphoglucans (see e.g. Tagliabracci et al., 2007; Worby et al., 2006) may be targeted as well. These findings show that the DSP domain is rather unspecific with respect to the nature of the esterified molecule and that the CBM determines the preferred target of SEX4. A CBM is also present in a functionally similar vertebrate enzyme called laforin, which essentially makes

[11] http://maxima.sourceforge.net/

these the only phosphatases known to date to be active on carbohydrates.[12] Hejazi et al. (2010) have shown that SEX4 is not inhibited by crystalline but soluble maltodextrins indicating that the preferential binding site at the starch interface are amorphous regions. This is consistent with ISA3 which also has a CBM48 and targets amorphous regions as well.

Mechanism and rate law. SEX4 is active on interfacial (pG* and pGx*) as well as dissolved (pG and pGx) phosphoglucans. Hence, four catalytic cycles have to be considered resulting in the same number of rate equations. Considering the catalytic cycles in the soluble and the insoluble phase ensures the correct denominator polynome, D, which both fluxes must have in common. As emphasized before, I restricted myself to the generic case of singly-phosphorylated phosphoglucans. In experiments with crystalline maltodextrins as substrates, these make up approximately 90% of the phosphoglucans, the rest being at most triply-phosphorylated (Hejazi et al., 2009). The analysis of *sex4* mutants suggests (Kötting et al., 2009), that this dominance of singly-phosphorylated phosphoglucans may also be expected *in vivo*. Moreover, we do not distinguish between C6- and C3-phosphate esters both of which can be hydrolyzed by SEX4 (Hejazi et al., 2010). In the same publication it has been shown that glucans above a certain DP, especially maltoheptaose, can inhibit SEX4 activity. In Fig. 2.14a, showing the assumed mechanism of SEX4, this effect is considered. The rate-limiting and irreversible hydrolysis of the phosphoester bond is assumed to proceed with the same rate constant, k_{cat} and k^*_{cat}, respectively, regardless of the DP. Hydrolysis at the interface is deemed irreversible also because the inorganic phosphate, Pi, is immediately released into the aqueous phase and thus virtually inaccessible to E*.

[12]For the sake of completeness, I refer to Gentry et al. (2007) who shows that laforin has a CBM20 and orthologues are also found in protists. These findings suggest that since very early in evolution the metabolism of complex carbohydrates in general and the cyclic turnover of insoluble carbohydrates in particular are tied to phosphorylation.

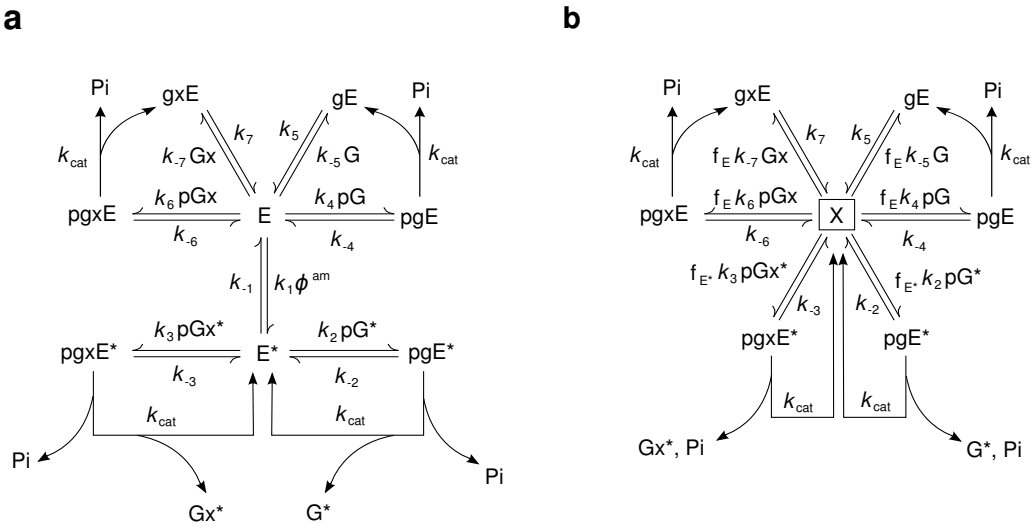

Figure 2.14: **Catalytic mechanism of the carbohydrate-active dual-specificity phosphatase SEX4**. **a**, The mechanism comprises four enzyme-phosphoglucan complexes, pgE* and pgxE* in the interface and pgE and pgxE in the aqueous phase. Accordingly, two inhibitory complexes, gE and gxE, with unphosphorylated glucans are included. **b**, The associated partial rapid equilibrium mechanism with one rapid equilibrium segment comprising the adsorption step.

To calculate the net fluxes

$$v_{(\mathrm{DSP|pG^*})} = k_{\mathrm{cat}} a_{\mathrm{g}} [c_{\mathrm{pgE^*}}]^{\mathrm{ss}}, \tag{2.50}$$

$$v_{(\mathrm{DSP|pGx^*})} = k_{\mathrm{cat}} a_{\mathrm{g}} [c_{\mathrm{pgxE^*}}]^{\mathrm{ss}}, \tag{2.51}$$

$$v_{(\mathrm{DSP|pG})} = k_{\mathrm{cat}} [c_{\mathrm{pgE}}]^{\mathrm{ss}}, \tag{2.52}$$

$$v_{(\mathrm{DSP|pGx})} = k_{\mathrm{cat}} [c_{\mathrm{pgxE}}]^{\mathrm{ss}}, \tag{2.53}$$

six balance equations and the conservation relation given in Table 2.3 have to be solved for the QSS concentrations of the intermediates in Fig. 2.14b. The rate and phenomenological constants appearing in the equations are summarized in Table 2.4.

The fractional concentration factors are formally the same as in (2.42a), but both of them appear now in the partial rapid equilibrium mechanism. The algebraic calculation yields the following denominator polynome which all

Table 2.3: Balance equations for the QSS and conservation relation of SEX4/DSP. The superscript (ss) is omitted as well as the growth rate term, assuming $\varrho_g \approx 0$.

Species	**Equation**
c_{pgE^*}	$0 = \chi_{\mathrm{pG}^*} f_{\mathrm{E}}^* x/a_{\mathrm{g}} - K_{\mathrm{pG}^*} c_{\mathrm{pgE}^*}$
c_{pgxE^*}	$0 = \chi_{\mathrm{pGx}^*} f_{\mathrm{E}}^* x/a_{\mathrm{g}} - K_{\mathrm{pGx}^*} c_{\mathrm{pgxE}^*}$
c_{pgE}	$0 = pg\ f_{\mathrm{E}} x - K_{\mathrm{pG}} c_{\mathrm{pgE}}$
c_{pgxE}	$0 = pgx\ f_{\mathrm{E}} x - K_{\mathrm{pGx}} c_{\mathrm{pgxE}^*}$
c_{gE}	$0 = K_{\mathrm{i,G}} c_{\mathrm{pgE}} - c_{\mathrm{gE}} + g/q_{\mathrm{G}}\ f_{\mathrm{E}} x$
c_{gxE}	$0 = K_{\mathrm{i,Gx}} c_{\mathrm{pgxE}} - c_{\mathrm{gxE}} + gx/q_{\mathrm{Gx}}\ f_{\mathrm{E}} x$
All	$e^0 = x + a_{\mathrm{g}} \left(c_{\mathrm{pgE}^*} + c_{\mathrm{pgxE}^*}\right) + c_{\mathrm{pgE}} + c_{\mathrm{pgxE}} + c_{\mathrm{gE}} + c_{\mathrm{gxE}},$

Table 2.4: Elementary rate and phenomenological constants for SEX4/DSP.

Parameter	**Dimension**[†]
$k_{\pm 2}, k_{\pm 3}, k_{\pm 4}, k_{\pm 6}, k_5, k_7$	T^{-1}
k_{-5}, k_{-7}	$\mathsf{N}^{-1}\mathsf{L}^3\mathsf{T}^{-1}$
$k_{\mathrm{cat}}^*, k_{\mathrm{cat}}$	T^{-1}
$K_{\mathrm{pG}^*} = \left(k_{-2} + k_{\mathrm{cat}}^*\right)/k_2$	1
$K_{\mathrm{pGx}^*} = \left(k_{-3} + k_{\mathrm{cat}}^*\right)/k_3$	1
$K_{\mathrm{pG}} = \left(k_{-4} + k_{\mathrm{cat}}\right)/k_4$	NL^{-3}
$K_{\mathrm{pGx}} = \left(k_{-6} + k_{\mathrm{cat}}\right)/k_6$	NL^{-3}
$K_{\mathrm{i,G}} = k_{\mathrm{cat}}/k_5$	1
$K_{\mathrm{i,Gx}} = k_{\mathrm{cat}}/k_7$	1
$q_{\mathrm{G}} = k_5/k_{-5}$	NL^{-3}
$q_{\mathrm{Gx}} = k_7/k_{-7}$	NL^{-3}

[†] N=amount, L=length, T=time

rates have in common:

$$D_{\mathrm{DSP}} = 1 + \frac{g}{q_{\mathrm{G}}} + \frac{gx}{q_{\mathrm{Gx}}} + (K_{\mathrm{i,G}} + 1)\frac{pg}{K_{\mathrm{pG}}} + (K_{\mathrm{i,Gx}} + 1)\frac{pgx}{K_{\mathrm{pGx}}} + \frac{\phi^{\mathrm{am}} a_{\mathrm{g}}}{K_{\mathrm{d}}}\left(1 + \frac{\chi_{\mathrm{pG}^*}}{K_{\mathrm{pG}^*}} + \frac{\chi_{\mathrm{pGx}^*}}{K_{\mathrm{pGx}^*}}\right) \tag{2.54a}$$

The numerators for the different catalytic cycles read

$$N_{(\mathrm{DSP}|\mathrm{pG}^*)} = k^*_{\mathrm{cat}} e^0 \cdot \frac{\phi^{\mathrm{am}} a_{\mathrm{g}}}{K_{\mathrm{d}}} \frac{\chi_{\mathrm{pG}^*}}{K_{\mathrm{pG}^*}}, \tag{2.54b}$$

$$N_{(\mathrm{DSP}|\mathrm{pGx}^*)} = k^*_{\mathrm{cat}} e^0 \cdot \frac{\phi^{\mathrm{am}} a_{\mathrm{g}}}{K_{\mathrm{d}}} \frac{\chi_{\mathrm{pGx}^*}}{K_{\mathrm{pGx}^*}}, \tag{2.54c}$$

$$N_{(\mathrm{DSP}|\mathrm{pG})} = k_{\mathrm{cat}} e^0 \cdot \frac{pg}{K_{\mathrm{pG}}}, \tag{2.54d}$$

$$N_{(\mathrm{DSP}|\mathrm{pGx})} = k_{\mathrm{cat}} e^0 \cdot \frac{pgx}{K_{\mathrm{pGx}}}. \tag{2.54e}$$

2.3.3 β-amylase (BAM)

Background. BAM (EC 3.2.1.2, GH14) occurs in *Arabidopsis* in a total of at least nine isoforms, which seem to have versatile functions, in metabolism as well as in sugar signalling (Fulton et al., 2008). The catalytically active isoforms bind to the non-reducing end of malto-oligosaccharides and cleave off maltose residues, that is BAMs are exo-acting amylases. Experimental studies (Ishikawa et al., 2007) and computational approaches (Hanson, 1962; Nakatani, 1997) suggest that the enzyme releases maltose residues repetitively before it dissociates. The processivity may depend on the degree of polymerization but as well on chemical modifications of the substrate. Of particular relevance is the position of phosphate esters. The enzyme cannot work past the phosphate and dissociates before the full glucan can be hydrolized. This is where the DSP activity becomes so important to remove the phosphate enabling further hydrolytic degradation.

In *Arabidopsis*, the dominant isoform localized at the starch-stroma interface is a 61 kDa protein called BAM3. It is not clear if a CBM is present in plant BAMs but according to the CAZy database possible candidates are CBM20 and CBM25, both of which have been demonstrated in BAMs from other sources to have the capacity to bind starch. As the *in vitro* activity of BAM3 on soluble glucans is much higher compared to granules it seems that BAM3 preferably localizes in amorphous regions of the interface. However, Edner et al. (2007) have shown that BAM3 is able to release a limited amount of maltose from native unphosphorylated granules which are practically inert for the endo-acting isoamylase. This hints at the accessibility of non-reducing chain ends even in crystalline regions. Thus, BAM3 may be a surface-active enzyme with a disorganizing effect upon adsorption and consequently adsorption

to crystalline regions will not be excluded in the rate law.

Mechanism and rate law. According to Fig. 2.12 BAM3 is assumed to act on three distinct substrates upon adsorption, native chains in helical (Gh*) or coil (Gc*) state, respectively, partially degraded chains (Gx*) and undigested but phosphorylated chains (pG*). We will assume that BAM3 does not dissociate from the substrate unless it has degraded the substrate to Gb and pGx, respectively. The DP of these products and the number of released maltose residues of course depends on the initial DP and the position of the phosphate. The study of Hanson (1962) suggests how this model can be further refined if necessary, however, it seems that if it is desired to treat such polymeric systems in depth to cover all potential species it is rather appropriate to take full advantage of probabilistic (e.g. as done in Wojciechowski et al., 2001, or Chapter 4 of this thesis) or rule-based deterministic approaches (Feret et al., 2009; Harmer et al., 2010).

As the mechanism in Fig. 2.15 shows, maltose (G2) is considered as a relevant competitive end-product inhibitor of BAM in solution ($K_\mathrm{i} = 11.5 - 11.7$ mM, Damme et al., 2001; Lizotte et al., 1990), while the phosphodextrin and maltodextrin stubs are potential inhibitors at the interface. We ommit the soluble substrates (G, pG and Gx) of BAM in order not to distract from the main approximation made. Of course, they will appear in the rate law together with the corresponding Michaelis constants. The rates for cleavage of the different substrates in the amorphous region are given by

$$v_{(\mathrm{BAM|Gc^*})} = k_3 a_\mathrm{g} [c_{\mathrm{gcE^*}}]^{\mathrm{ss}}, \tag{2.55a}$$

$$v_{(\mathrm{BAM|Gx^*})} = k_6 a_\mathrm{g} [c_{\mathrm{gxE^*}}]^{\mathrm{ss}}, \tag{2.55b}$$

$$v_{(\mathrm{BAM|pG^*})} = k_8 a_\mathrm{g} [c_{\mathrm{pgE^*}}]^{\mathrm{ss}}, \tag{2.55c}$$

and for helical glucans by

$$v_{(\mathrm{BAM|Gh^*})} = k_{12} a_\mathrm{g} [c_{\mathrm{ghE^*}}]^{\mathrm{ss}}. \tag{2.55d}$$

The balance equations to be solved are given in Table 2.5 and the associated parameter are explained in Table 2.6. As the rapid equilibrium segment now comprises three species,

$$x = e + a_\mathrm{g} \left(e^{*\mathrm{am}} + e^{*\mathrm{cr}} \right), \tag{2.56}$$

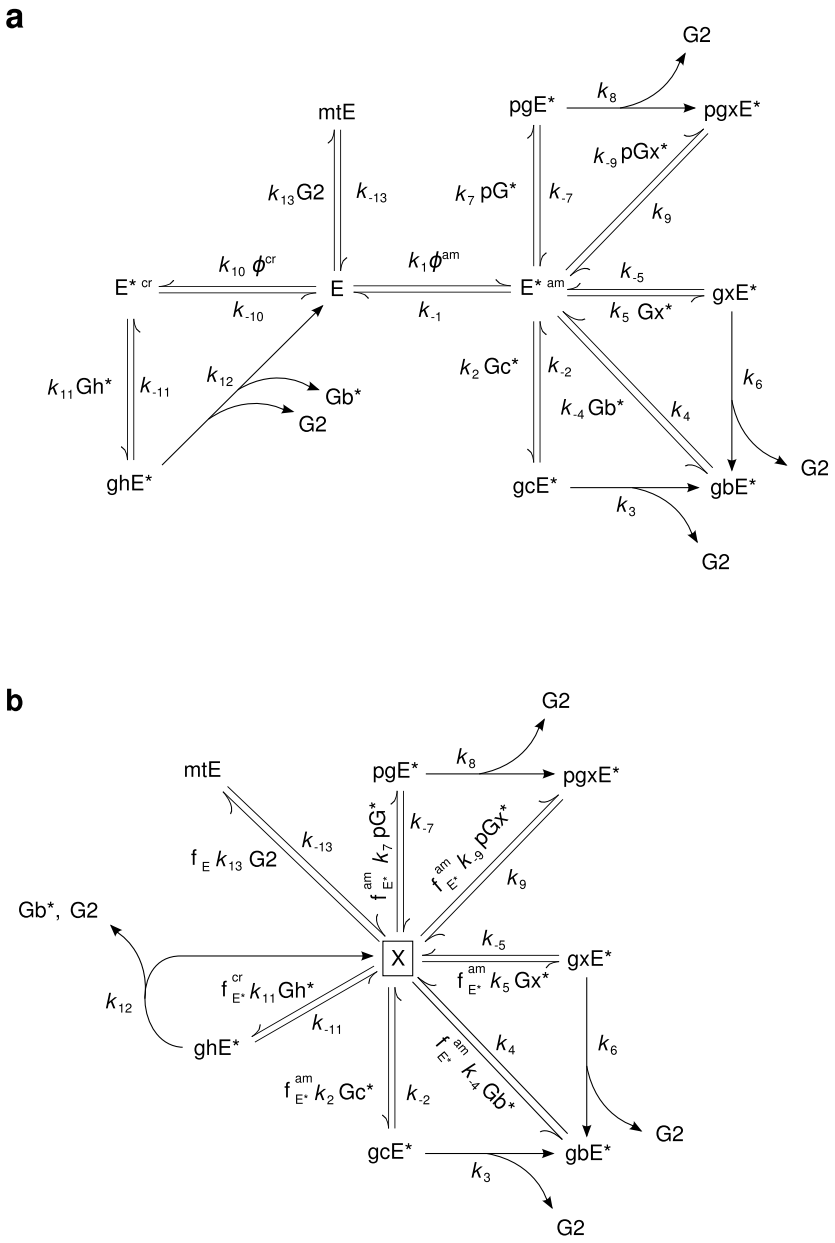

Figure 2.15: **Catalytic mechanism of β-amylase (BAM)**. **a**, The catalytic cycles comprise interfacial substrates only and two adsorption steps ($k_{\pm 1}$ and $k_{\pm 10}$). **b**, The associated partial rapid equilibrium mechanism with one rapid equilibrium segment comprising both adsorption steps.

the fractional concentration factors are given by

$$f_{\mathrm{E}} = \frac{1}{1 + K_{\mathrm{a}}^{\mathrm{am}}\phi^{\mathrm{am}}a_{\mathrm{g}} + K_{\mathrm{a}}^{\mathrm{cr}}\phi^{\mathrm{cr}}a_{\mathrm{g}}}, \tag{2.57a}$$

$$f_{\mathrm{E}}^{\mathrm{am}} = \frac{K_{\mathrm{a}}^{\mathrm{am}}\phi^{\mathrm{am}}a_{\mathrm{g}}}{1 + K_{\mathrm{a}}^{\mathrm{am}}\phi^{\mathrm{am}}a_{\mathrm{g}} + K_{\mathrm{a}}^{\mathrm{cr}}\phi^{\mathrm{cr}}a_{\mathrm{g}}}, \tag{2.57b}$$

$$f_{\mathrm{E}}^{\mathrm{cr}} = \frac{K_{\mathrm{a}}^{\mathrm{cr}}\phi^{\mathrm{cr}}a_{\mathrm{g}}}{1 + K_{\mathrm{a}}^{\mathrm{am}}\phi^{\mathrm{am}}a_{\mathrm{g}} + K_{\mathrm{a}}^{\mathrm{cr}}\phi^{\mathrm{cr}}a_{\mathrm{g}}}. \tag{2.57c}$$

The result is a somewhat long but structurally straightforward expression for the denominator which all rates have in common:

$$\begin{aligned} D_{\mathrm{BAM}} = 1 &+ \frac{g_2}{q_{\mathrm{mt}}} + \frac{g}{K_{\mathrm{G}}} + \frac{gx}{K_{\mathrm{Gx}}} + \frac{pg}{K_{\mathrm{pG}}} + \frac{\phi^{\mathrm{am}} a_{\mathrm{g}}}{K_{\mathrm{d}}^{\mathrm{am}}} \Bigg[1 + \frac{\chi_{\mathrm{Gb}^*}}{q_{\mathrm{Gb}^*}} + \frac{\chi_{\mathrm{pGx}^*}}{q_{\mathrm{pGx}^*}} \\ &+ (K_{\mathrm{i1,Gb}^*} + 1) \frac{\chi_{\mathrm{Gc}^*}}{K_{\mathrm{Gc}^*}} + (K_{\mathrm{i2,Gb}^*} + 1) \frac{\chi_{\mathrm{Gx}^*}}{K_{\mathrm{Gx}^*}} + (K_{\mathrm{i,pGx}^*} + 1) \frac{\chi_{\mathrm{pG}^*}}{K_{\mathrm{pG}^*}} \Bigg] \\ &+ \frac{\phi^{\mathrm{cr}} a_{\mathrm{g}}}{K_{\mathrm{d}}^{\mathrm{cr}}} \left(1 + \frac{\chi_{\mathrm{Gh}^*}}{K_{\mathrm{Gh}^*}} \right). \end{aligned} \tag{2.58}$$

The numerators for the interfacial activities are

$$\begin{aligned} N_{(\mathrm{BAM|Gc}^*)} &= k_{\mathrm{cat,Gc}^*}^* e^0 \cdot \frac{\phi^{\mathrm{am}} a_{\mathrm{g}}}{K_{\mathrm{d}}^{\mathrm{am}}} \frac{\chi_{\mathrm{Gc}^*}}{K_{\mathrm{Gc}^*}}, \\ N_{(\mathrm{BAM|Gx}^*)} &= k_{\mathrm{cat,Gx}^*}^* e^0 \cdot \frac{\phi^{\mathrm{am}} a_{\mathrm{g}}}{K_{\mathrm{d}}^{\mathrm{am}}} \frac{\chi_{\mathrm{Gx}^*}}{K_{\mathrm{Gx}^*}}, \\ N_{(\mathrm{BAM|pG}^*)} &= k_{\mathrm{cat,pG}^*}^* e^0 \cdot \frac{\phi^{\mathrm{am}} a_{\mathrm{g}}}{K_{\mathrm{d}}^{\mathrm{am}}} \frac{\chi_{\mathrm{pG}^*}}{K_{\mathrm{pG}^*}}, \\ N_{(\mathrm{BAM|Gh}^*)} &= k_{\mathrm{cat,Gh}^*}^* e^0 \cdot \frac{\phi^{\mathrm{cr}} a_{\mathrm{g}}}{K_{\mathrm{d}}^{\mathrm{cr}}} \frac{\chi_{\mathrm{Gh}^*}}{K_{\mathrm{Gh}^*}}. \end{aligned} \tag{2.59}$$

For the hydrolysis in solution we have

$$\begin{aligned} N_{(\mathrm{BAM|G})} &= k_{\mathrm{cat,G}} e^0 \cdot \frac{g}{K_{\mathrm{G}}}, \\ N_{(\mathrm{BAM|Gx})} &= k_{\mathrm{cat,Gx}} e^0 \cdot \frac{gx}{K_{\mathrm{Gx}}}, \\ N_{(\mathrm{BAM|pG})} &= k_{\mathrm{cat,pG}} e^0 \cdot \frac{pg}{K_{\mathrm{pG}}}. \end{aligned} \tag{2.60}$$

2.3.4 Glucan, water dikinase (GWD)

Background. In contrast to the enzymes discussed above, the catalytic cycle of GWD is partitioned between both the aqueous phase and the interface. The enzyme binds to starch in a catalytically active, phosphorylated form and has to desorb after esterification of an interfacial glucan to activate itself again in the soluble phase by using ATP. GWD does not act on glucans in solution and it seems necessary that the substrate is present in an aggregated form with a certain degree of molecular order. Hence, stable association with crystalline regions precedes glucan phosphorylation. The starch-binding domain (SBD), identified as a family 20 CBM (Christiansen et al., 2009; Mikkelsen et al., 2006) is responsible for the interfacial localization.

Table 2.5: Balance equations for the QSSs of intermediates in the catalytic cycle of BAM. The superscript (ss) is omitted as well as the growth rate term, assuming $\varrho_g \approx 0$.

Species	**Equation**
$c_{\mathrm{gcE^*}}$	$0 = \chi_{\mathrm{Gc^*}} f^{\mathrm{am}}_{\mathrm{E^*}} x/a_{\mathrm{g}} - K_{\mathrm{Gc^*}} c_{\mathrm{gcE^*}}$
$c_{\mathrm{gxE^*}}$	$0 = \chi_{\mathrm{Gx^*}} f^{\mathrm{am}}_{\mathrm{E^*}} x/a_{\mathrm{g}} - K_{\mathrm{Gx^*}} c_{\mathrm{gxE^*}}$
$c_{\mathrm{pgE^*}}$	$0 = \chi_{\mathrm{pG^*}} f^{\mathrm{am}}_{\mathrm{E^*}} x/a_{\mathrm{g}} - K_{\mathrm{pG^*}} c_{\mathrm{pgE^*}}$
$c_{\mathrm{pgxE^*}}$	$0 = K_{\mathrm{i,pGx^*}} c_{\mathrm{pgE^*}} - c_{\mathrm{pgxE^*}} + \frac{\chi_{\mathrm{pGx^*}}}{q_{\mathrm{pGx^*}}} f^{\mathrm{am}}_{\mathrm{E^*}} x/a_{\mathrm{g}}$
$c_{\mathrm{gbE^*}}$	$0 = K_{\mathrm{i1,Gb^*}} c_{\mathrm{gcE^*}} - c_{\mathrm{gbE^*}} + \frac{\chi_{\mathrm{Gb^*}}}{q_{\mathrm{Gb^*}}} f^{\mathrm{am}}_{\mathrm{E^*}} x/a_{\mathrm{g}} + K_{\mathrm{i2,Gb^*}} c_{\mathrm{gxE^*}}$
$c_{\mathrm{ghE^*}}$	$0 = \chi_{\mathrm{Gh^*}} f^{\mathrm{cr}}_{\mathrm{E^*}} x/a_{\mathrm{g}} - K_{\mathrm{Gh^*}} c_{\mathrm{ghE^*}}$
c_{mtE}	$0 = g_2 f_{\mathrm{E}} x - q_{\mathrm{mt}} c_{\mathrm{mtE}}$
All	$e^0 = x + c_{\mathrm{gE}} + c_{\mathrm{gxE}} + c_{\mathrm{pgE}} + c_{\mathrm{mtE}} + a_{\mathrm{g}} (c_{\mathrm{gcE^*}} + c_{\mathrm{gxE^*}} + c_{\mathrm{pgE^*}} + c_{\mathrm{pgxE^*}} + c_{\mathrm{gbE^*}} + c_{\mathrm{ghE^*}})$

Mechanism and rate law. Figure 2.16 shows the supposed mechanism of GWD and the partial equilibrium counterpart. In the soluble phase the autophosphorylation of GWD takes place by transfer of the β-phosphate of ATP and release of AMP and the γ-phosphate (Ritte et al., 2002). The resulting phosphohistidine intermediate is the only form able to catalyze the phosphotransfer to interfacial glucans. However, it is acid- and heat-labile and can dissociate into free enzyme and orthophosphate. This creates a 'leak' of phosphate, which has been shown to result in waste of ATP if no carbohydrate acceptor is present (Hejazi et al., 2010, and M. Steup, pers. comm.). This flux is included as an essentially irreversible loss of phosphate by the reaction step with the rate constant k_7 in Fig. 2.16. The exact mechanism of GWD is not known, but a free pyrophosphoryl enzyme intermediate could not be detected to date. Therefore, I basically adopted a mechanism which has been proposed for a very similar enzyme, the phosphoenolpyruvate synthetase (Berman and Cohn, 1970a,b; Mikkelsen et al., 2004). It is simplified here in that interconversions of enzyme complexes in the soluble phase are not considered explicitly if no reactant is released. Such intermediates usually do not have any effect on the kinetic form of the rate laws, although the phenomenological constants are then composed of distinct microscopic constants.

The net flux through the reaction is determined by both the rate of auto-

Table 2.6: Elementary rate and phenomenological constants for BAM.

Parameter	**Dimension**[†]
$k_{\pm 2}, k_{\pm 4}, k_{\pm 5}, k_{\pm 7}, k_{\pm 9}, k_{\pm 11}, k_{-13}$	T^{-1}
k_{13}	$\mathsf{N}^{-1}\mathsf{L}^{3}\mathsf{T}^{-1}$
$k_{\mathrm{cat,Gc^*}} = k_3$	T^{-1}
$k_{\mathrm{cat,Gx^*}} = k_6$	T^{-1}
$k_{\mathrm{cat,pG^*}} = k_8$	T^{-1}
$k_{\mathrm{cat,Gh^*}} = k_{12}$	T^{-1}
$K_{\mathrm{Gc^*}} = (k_{-2} + k_3)/k_2$	1
$K_{\mathrm{Gx^*}} = (k_{-5} + k_6)/k_5$	1
$K_{\mathrm{pG^*}} = (k_{-7} + k_8)/k_7$	1
$K_{\mathrm{Gh^*}} = (k_{-11} + k_{12})/k_1 1$	1
$K_{\mathrm{i,pGx^*}} = k_8/k_9$	1
$K_{\mathrm{i1,Gb^*}} = k_3/k_4$	1
$K_{\mathrm{i2,Gb^*}} = k_6/k_4$	1
$q_{\mathrm{pGx^*}} = k_9/k_{-9}$	1
$q_{\mathrm{Gb^*}} = k_4/k_{-4}$	1
$q_{\mathrm{mt}} = k_{-13}/k_{13}$	NL^{-3}
K_{G}	NL^{-3}
K_{Gx}	NL^{-3}
K_{pG}	NL^{-3}

[†] N=amount, L=length, T=time

catalytic phosphorylation and glucan phosphorylation

$$v_{\mathrm{GWD}} = k_2[c_{\mathrm{atpE}}]^{\mathrm{ss}} + a_{\mathrm{g}} k_5 [c_{\mathrm{gpE^*}}]^{\mathrm{ss}}. \tag{2.61}$$

Table 2.7 summarizes the relevant balance equations for the quasi-steady state intermediates, where the concentration of the rapid equilibrium segments are given by

$$x = e + a_{\mathrm{g}} e^* \qquad \text{and} \tag{2.62}$$

$$x' = c_{\mathrm{pE}} + a_{\mathrm{g}} c_{\mathrm{pE^*}}, \tag{2.63}$$

respectively, and the associated fractional concentration factors with the solu-

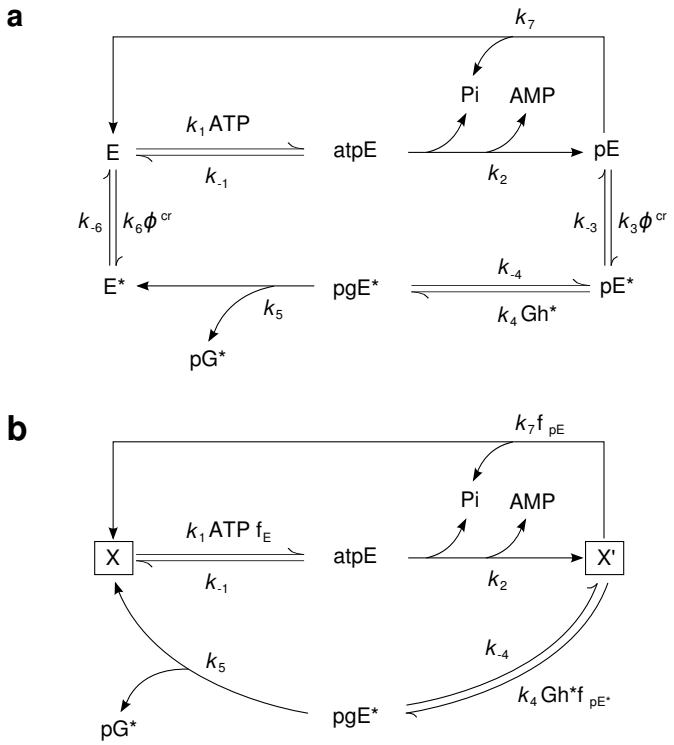

Figure 2.16: **Catalytic mechanism of glucan, water dikinase (GWD)**.**a**, The catalytic cycle involves soluble and interfacial intermediates. ATP is hydrolyzed to AMP and orthophosphate Pi to generate the autophosphorylated enzyme pE. After phosphorylation of a helical interfacial glucan Gh* the unphosphorylated enzyme E* desorbs which completes the cycle. **b**, The associated partial rapid equilibrium mechanism has two rapid equilibrium segments, X and X′.

ble enzyme intermediate being the reference species read

$$f_{\mathrm{E}} = \frac{1}{1 + K_{\mathrm{a,E}}\phi^{\mathrm{cr}}a_{\mathrm{g}}}, \tag{2.64a}$$

$$f^*_{\mathrm{E}} = \frac{K_{\mathrm{a,E}}\phi^{\mathrm{cr}}a_{\mathrm{g}}}{1 + K_{\mathrm{a,E}}\phi^{\mathrm{cr}}a_{\mathrm{g}}}, \tag{2.64b}$$

$$f_{\mathrm{pE}} = \frac{1}{1 + K_{\mathrm{a,pE}}\phi^{\mathrm{cr}}a_{\mathrm{g}}}, \tag{2.64c}$$

$$f^*_{\mathrm{pE}} = \frac{K_{\mathrm{a,pE}}\phi^{\mathrm{cr}}a_{\mathrm{g}}}{1 + K_{\mathrm{a,pE}}\phi^{\mathrm{cr}}a_{\mathrm{g}}}. \tag{2.64d}$$

The associated rate constants relevant for the partial equilibrium mechanism are explained in Table 2.8.

Defining phenomenological constants as given in Table 2.8 we obtain the

Table 2.7: Balance equations for the QSSs of intermediates in the catalytic cycle of GWD. The superscript (ss) is omitted as well as the growth rate term, assuming $\varrho_g \approx 0$.

Species	**Equation**[†]
c_{atpE}	$0 = a_3 \left(1 - f^*_{\mathrm{E}}\right) x - K_{\mathrm{atp}} c_{\mathrm{atpE}}$
c_{pgE^*}	$0 = \chi^*_{\mathrm{Gh}} f^*_{\mathrm{pE}} x' / a_{\mathrm{g}} - K^*_{\mathrm{Gh}} c_{\mathrm{pgE}^*}$
x'	$0 = \dfrac{\widetilde{k}_{\mathrm{aut}}}{K^*_{\mathrm{Gh}} - \widetilde{k}^*_{\mathrm{cat}}} c_{\mathrm{atpE}} + a_{\mathrm{g}} c_{\mathrm{pgE}^*} - \dfrac{x'}{K^*_{\mathrm{Gh}} - \widetilde{k}^*_{\mathrm{cat}}} \left[\left(\chi^*_{\mathrm{Gh}} - \widetilde{k}_{\mathrm{leak}}\right) f^*_{\mathrm{pE}} + \widetilde{k}_{\mathrm{leak}}\right]$
All	$e^0 = x + x' + c_{\mathrm{atpE}} + a_{\mathrm{g}} c_{\mathrm{gpE}^*}$

[†] Phenomenological constants as given in Table 2.8 and for legibility $\widetilde{k}_{\mathrm{aut}} = k_{\mathrm{aut}}/k_4$, $\widetilde{k}_{\mathrm{leak}} = k_{\mathrm{leak}}/k_4$, etc. are used.

following numerator and denominator for the GWD rate law:

$$
\begin{aligned}
N_{\mathrm{GWD}} &= e^0 k_{\mathrm{aut}} \frac{a_3}{K_{\mathrm{atp}}} \left(1 + 2 \frac{k^*_{\mathrm{cat}}}{k_{\mathrm{leak}}} \frac{\phi^{\mathrm{cr}} a_{\mathrm{g}}}{K_{\mathrm{d,pE}}} \frac{\chi^*_{\mathrm{Gh}}}{K^*_{\mathrm{Gh}}}\right), \\
D_{\mathrm{GWD}} &= 1 + \frac{a_3}{K_{\mathrm{atp}}} \left(1 + \frac{k_{\mathrm{aut}}}{k_{\mathrm{leak}}}\right) + \frac{\left(\phi^{\mathrm{cr}} a_{\mathrm{g}}\right)^2}{K_{\mathrm{d,E}} K_{\mathrm{d,pE}}} \frac{\chi^*_{\mathrm{Gh}}}{K^*_{\mathrm{Gh}}} \frac{k^*_{\mathrm{cat}}}{k_{\mathrm{leak}}} \\
&\quad + \frac{\phi^{\mathrm{cr}} a_{\mathrm{g}}}{K_{\mathrm{d,pE}}} \left[\frac{a_3}{K_{\mathrm{atp}}} \frac{\chi^*_{\mathrm{Gh}}}{K^*_{\mathrm{Gh}}} \left(\frac{k_{\mathrm{aut}}}{k_{\mathrm{leak}}} + \frac{k^*_{\mathrm{cat}}}{k_{\mathrm{leak}}}\right) + \frac{a_3}{K_{\mathrm{atp}}} \frac{k_{\mathrm{aut}}}{k_{\mathrm{leak}}} + \frac{\chi^*_{\mathrm{Gh}}}{K^*_{\mathrm{Gh}}} \frac{k^*_{\mathrm{cat}}}{k_{\mathrm{leak}}}\right] \\
&\quad + \frac{\phi^{\mathrm{cr}} a_{\mathrm{g}}}{K_{\mathrm{d,E}}}.
\end{aligned}
\tag{2.65}
$$

Table 2.8: Elementary rate and phenomenological constants for GWD.

Parameter	**Dimension**[†]
k_1	$\mathsf{N}^{-1}\mathsf{L}^3\mathsf{T}^{-1}$
k_{-1}, k_4, k_{-4}	T^{-1}
$k_{\mathrm{aut}} = k_2$	T^{-1}
$k^*_{\mathrm{cat}} = k_5$	T^{-1}
$k_{\mathrm{leak}} = k_7$	T^{-1}
$K_{\mathrm{atp}} = \left(k_{-1} + k_2\right)/k_1$	NL^{-3}
$K^*_{\mathrm{Gh}} = \left(k_{-4} + k_5\right)/k_4$	1

[†] N=amount, L=length, T=time

2.3.5 The interfacial analogue of the Michaelis-Menten equation

As indicated above, the most interesting aspect of the interfacial rate laws is the occurence of the available area function. To study its role within the framework developed here we may formulate an interfacial analogue of the Michaelis-Menten-Henri (MMH) equation (Segel, 1993) with a rapid adsorption pre-equilibrium in the form of a specific activity as

$$\frac{v}{e^0} = \frac{k^*_{\mathrm{cat}} \phi a_{\mathrm{g}} \chi^*}{K_{\mathrm{d}} K^*_{\mathrm{m}} + \phi a_{\mathrm{g}} \left(K^*_{\mathrm{m}} + \chi^*\right)}, \tag{2.66}$$

or in terms of mass concentration of the substrate

$$\frac{v}{e^0} = \frac{k^*_{\mathrm{cat}} \phi \alpha m_{\mathrm{g}} \chi^*}{K_{\mathrm{d}} K^*_{\mathrm{m}} + \phi \alpha m_{\mathrm{g}} \left(K^*_{\mathrm{m}} + \chi^*\right)}. \tag{2.67}$$

In this rate law the interface enters via its concentration, a_{g}, the interfacial reactant mole fraction, and the fraction of relevant unoccupied surface area, ϕ. The latter quantity renders the saturation term dependent on the enzyme concentration. Thus, while in soluble kinetics the active site of the enzyme becomes saturated but the rate increases linearly with enzyme concentration according to $v_{\max}$, we may here also observe the opposite phenomenon of saturation of the substrate interface. Remember, that the coverage for which $\phi \to 0$ can be well below unity as for example the RSA model indicates (Sec. 2.2.2). In general, Fig. 2.9 suggests, that surface 'jamming' may happen if the binding of the enzyme to the interface is too tight or the enzyme loading is too high.

To analyze this further, it is necessary to elucidate how ϕ depends on the system parameters during catalysis. This can fortunately be done exactly in the case of a single enzyme and LANGMUIRian adsorption, using the four relations given in Table 2.9. They were solved simultaneously for $\underline{e}^{\mathrm{eq}}$, which is the enzyme concentration relative to the interface concentration, for the coverages of the free interfacial enzyme, θ^{eq}_E, and the interfacial enzyme-substrate complex, $\theta^{\mathrm{eq}}_{ES}$, and ϕ. Even for this most basic example, the result is a rather complicated looking equation, where the arguments enter the function in a

nonlinear fashion. Introducing polynomes in ω we get

$$\begin{aligned}
&\phi(\underline{e}^0, \Lambda_\mathrm{d}, \omega, \chi^*, K_\mathrm{m}^*) \\
&\quad = \frac{1}{2}\left[\sqrt{\omega^2 + 2\left(\frac{K_\mathrm{m}^*\Lambda_\mathrm{d}}{(K_\mathrm{m}^* + \chi^*)} - \underline{e}^0\right)\omega + \left(\frac{K_\mathrm{m}^*\Lambda_\mathrm{d}}{(K_\mathrm{m}^* + \chi^*)} + \underline{e}^0\right)^2}\right. \\
&\qquad \left. + \omega - \left(\frac{K_\mathrm{m}^*\Lambda_\mathrm{d}}{(K_\mathrm{m}^* + \chi^*)} + \underline{e}^0\right)\right],
\end{aligned} \tag{2.68}$$

nevertheless, it is not easy to immediately infer the effect on the available area. It is expected that during catalysis the value of ϕ may drift, since it depends on quantities which may change in time, either because of the activity of the enzyme directly (changing χ^*) or due to secondary effects which change the interface concentration (due to degradation) or the relevant surface fraction ω (e.g. through phase transitions between the crystalline and amorphous state). The dynamics of these factors will be discussed in the next chapter. For now, setting $\omega = 1$ allows to consider the available area as a function of two variables and one parameter, the interfacial Michaelis constant K_m^*. The two-variable dependency can be conveniently analyzed graphically. Figure 2.17 shows the results for $K_\mathrm{m}^* = 1.0$ and $K_\mathrm{m}^* = 0.1$. As expected, a decrease is observed for higher loadings and tighter adsorption and the decrease is more steep for lower Michaelis constants, that is for higher affinity towards the interfacial reactant.

Apart from the graphical analysis, it is useful to derive some exact results about the qualitative properties. Using Maxima one can validate that

$$\lim_{\underline{e}^0 \to \infty} \phi = 0, \tag{2.69}$$

Table 2.9: Algebraic relations to determine the available area function.

Equation[†]	**Description**
$\theta_\mathrm{E}^\mathrm{eq} = \underline{e}^\mathrm{eq}\phi/\Lambda_\mathrm{d}$	Adsorption equilibrium
$\phi = \omega - \theta_\mathrm{E}^\mathrm{eq} - \theta_\mathrm{ES}^\mathrm{ss}$	LANGMUIRian available area function
$\underline{e}^0 = \underline{e}^\mathrm{eq} + \theta_\mathrm{E}^\mathrm{eq} + \theta_\mathrm{ES}^\mathrm{ss}$	Enzyme conservation
$0 = \chi^*\theta_\mathrm{E}^\mathrm{eq} - K_\mathrm{m}^*\theta_\mathrm{ES}^\mathrm{ss}$	QSS for interfacial complex ES*

[†] Scalings: $e^{(0)\diamond} = a_\mathrm{g} e^{*\,\max}$, $K_\mathrm{d}^\diamond = a_\mathrm{g}$

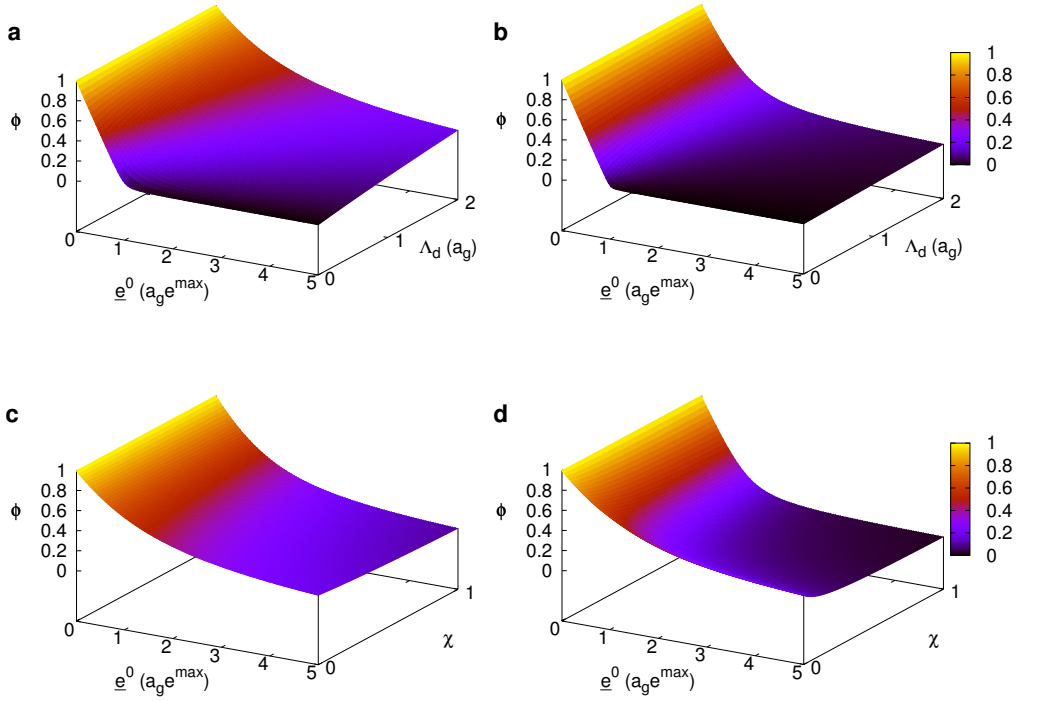

Figure 2.17: **Available area function in the generic interfacial rate law**. All plots are done setting $\omega = 1$. **a**, $\phi = \phi(\underline{e}^0, \Lambda_\mathrm{d})$ with fixed $K^*_\mathrm{m} = 1$ and $\chi^* = 1$. **b**, $\phi = \phi(\underline{e}^0, \Lambda_\mathrm{d})$ with fixed $K^*_\mathrm{m} = 0.1$ and $\chi^* = 1$. **c**, $\phi = \phi(\underline{e}^0, \chi^*)$ with fixed $K^*_\mathrm{m} = 1$, $\Lambda_\mathrm{d} = 1$. **d**, $\phi = \phi(\underline{e}^0, \chi^*)$ with fixed $K^*_\mathrm{m} = 0.1$, $\Lambda_\mathrm{d} = 1$. Michaelis constant of $K^*_\mathrm{m} = 0.1$ results in a sharper decrease in approaching $\phi = 0$.

for any value of the remaining parameters. As $\underline{e}^0$ is a scaled quantity relative to a_g the result applies to both $e^0 \to \infty$ and $a_\mathrm{g} \to 0$. Vice versa, when no enzyme is present or $a_\mathrm{g} \to \infty$ we get

$$\phi(\underline{e}^0 = 0) = \omega. \tag{2.70}$$

Moreover, as expected the available area vanishes if $\omega = 0$,

$$\phi(\omega = 0) = 0. \tag{2.71}$$

A biologically interesting limiting case is that of irreversible adsorption. This can be calculated by setting the desorption constant to zero which yields

$$\phi(\Lambda_\mathrm{d} = 0) = \omega - \underline{e}^0, \tag{2.72}$$

showing that the available area only depends on the relevant surface fraction and the enzyme loading in this case.

The question is how this limiting behaviors interfere with the other quantities in the generic rate law (2.66). A significant difference to the MMH rate equation can be derived for the maximum velocity, since

$$\begin{aligned} v_{\max} = \lim_{a_\mathrm{g}\to\infty} v &= \frac{k^*_\mathrm{cat}\chi^* \cdot \lim_{a_\mathrm{g}\to\infty}\phi}{\lim_{a_\mathrm{g}\to\infty}\left(K_\mathrm{d}K^*_\mathrm{m}/a_\mathrm{g} + \phi\left(K^*_\mathrm{m}+\chi^*\right)\right)} \cdot e^0 \\ &= \frac{k^*_\mathrm{cat}\chi^*}{\left(K^*_\mathrm{m}+\chi^*\right)} \cdot e^0 \\ &= \widetilde{k}^*_\mathrm{cat} \cdot e^0. \end{aligned} \tag{2.73}$$

Thus, the apparent catalytic rate constant, $\widetilde{k}^*_\mathrm{cat}$, turns out to be reduced and can even change during the course of reaction due to its dependence on the interfacial reactant mole fraction. In the same vain, we may look at the rate as e^0 is increased. Taking the corresponding limit of (2.66), using (2.69) and L'Hospital's rule to resolve the indetermined product $(\infty \cdot 0)$ shows that

$$\begin{aligned} \lim_{e^0\to\infty} v &= \frac{k^*_\mathrm{cat}a_\mathrm{g}\chi^*}{K_\mathrm{d}K^*_\mathrm{m}} \lim_{e^0\to\infty}\left(e^0\cdot\phi\right) \\ &= \frac{k^*_\mathrm{cat}a_\mathrm{g}\chi^*}{K_\mathrm{d}K^*_\mathrm{m}}\left(\infty\cdot 0\right) \\ &= \frac{k^*_\mathrm{cat}a_\mathrm{g}\chi^*}{K_\mathrm{d}K^*_\mathrm{m}} \lim_{e^0\to\infty}\frac{(e^0)'}{(1/\phi)'} \\ &= \frac{k^*_\mathrm{cat}a_\mathrm{g}\chi^*}{K_\mathrm{d}K^*_\mathrm{m}}\frac{1}{0} \\ &= \infty, \end{aligned} \tag{2.74}$$

where the prime indicates the derivative with respect to e^0.

Thus, although the surface may become saturated the rate is unbounded for increased enzyme loading as for the MMH rate law. However, it should be emphasized that due to ϕ the increase of the rate with e^0 cannot be expected as linear anymore. To further analyze this and other qualitative properties, it is interesting to look at the elasticities of the interfacial rate equation and compare them with those of the MMH equation. Scaled elasticities of an enzymatic reaction rate, v, are defined as (see Heinrich and Schuster, 1996)

$$\varepsilon\text{-elasticity:} \qquad \varepsilon^v_x = \frac{x}{v}\frac{\partial v}{\partial x}, \tag{2.75}$$

with respect to the concentration, x, of a metabolite and as

$$\pi\text{-elasticity:} \qquad \pi^v_p = \frac{p}{v}\frac{\partial v}{\partial p}, \tag{2.76}$$

with respect to a parameter p. They quantify the local effect of the respective quantities on the reaction rate, the ε-elasticities in particular being interpreted as apparent kinetic orders of the rate with respect to metabolites (Fell, 1992). Table 2.10 summarizes the results and compares them to the elasticities of the MMH rate law wherever this makes sense.

Note, that the elasticity towards the available area function is strictly positive similar to the enzyme loading observed for the classical MMH velocity equation. With respect to the latter, observe that $\pi^v_{e^0} \approx 1$ if the associated elasticity of the available area function $\pi^\phi_{e^0}$ approaches zero, that is if ϕ becomes insensitive towards e^0. Fig. 2.17 suggests, however, that ϕ becomes rather independent from enzyme loading only for very high loadings.

2.4 Discussion

Summary. This chapter develops a framework to derive interfacial rate laws. Section 2.2.1 introduces the interface concentration as a substrate observable. This is augmented by a phenomenological description of surface heterogene-

Table 2.10: Elasticities for MMH and interfacial rate law.

v	**Enzyme in solution** $= \dfrac{k_{\mathrm{cat}} e^0 s}{K_{\mathrm{m}} + s}$	**Surface-active Enzyme**[†] $= \dfrac{k^*_{\mathrm{cat}} e^0 \phi a_{\mathrm{s}} \chi^*}{K_{\mathrm{d}} K^*_{\mathrm{m}} + \phi a_{\mathrm{s}} (K^*_{\mathrm{m}} + \chi^*)}$
$\varepsilon^v_{s,a_{\mathrm{s}}}$	$\dfrac{K_{\mathrm{m}}}{K_{\mathrm{m}} + s}$	$(\varepsilon^\phi_{a_{\mathrm{s}}} + 1)\Gamma$
$\varepsilon^v_{\chi^*}$	not defined	$(\varepsilon^\phi_{\chi^*} + 1 + \dfrac{\phi a_{\mathrm{s}}}{K_{\mathrm{d}}})\Gamma$
ε^v_ϕ	not defined	1
$\pi^v_{e^0}$	1	$\pi^\phi_{e^0}\Gamma + 1$
$\pi^v_{K_{\mathrm{m}},K^*_{\mathrm{m}}}$	$-\dfrac{K_{\mathrm{m}}}{K_{\mathrm{m}} + s}$	$(\pi^\phi_{K_{\mathrm{m}^*}} - 1 - \dfrac{\phi a_{\mathrm{s}}}{K_{\mathrm{d}}})\Gamma$
$\pi^v_{K_{\mathrm{d}}}$	not defined	$\left[\pi^\phi_{K_{\mathrm{d}}} - 1 - \pi^\phi_{K_{\mathrm{d}}} \dfrac{\phi a_{\mathrm{s}}}{K_{\mathrm{d}}} (K_{\mathrm{d}} - 1)(K^*_{\mathrm{m}} + \chi^*)\right]\Gamma$

[†] $\Gamma = \frac{K_{\mathrm{d}} K^*_{\mathrm{m}}}{K_{\mathrm{d}} K^*_{\mathrm{m}} + \phi a_{\mathrm{s}} (K^*_{\mathrm{m}} + \chi^*)}$

ity, enabling a distinction between amorphous and crystalline patches. Section 2.2.2 develops the framework of competitive adsorption of enzymes using the concept of the available area function. Section 2.2.3 argues for the mole fraction as the appropriate variable for interfacial reactants. In Section 2.3 rate laws for the most important starch-degrading enzymes are derived. This is followed by a discussion of the qualitative properties of the interfacial analogue to the classical Michaelis-Menten-Henri velocity equation.

The kinetic modeling of enzymatic reactions on soluble substrates is a topic very well developed. It has a rich history of more than a hundred years in which many different mechanisms have been studied and sophisticated mathematical treatments have been presented. As the metabolic maps found in databases like KEGG (Ogata et al., 1999) or the different BioCyc databases (Caspi et al., 2007) become more and more complete the role of enzymes will come into focus again, since it is not enough to know which reactions occur in a cell but at which rate, and when and how they can be regulated. Thus, a proper understanding of biological systems requires capturing the dynamic aspects and enzymes are the major players here.

In this respect, what frequently causes trouble when trying to translate a map in the databases into a mathematical model, are those reactions associated with macromolecules. For example in KEGG one may find

```
Starch <=> 1,4-alpha-D-Glucan + Maltose
```
(2.77)

for the β-amylase. The difficulty in assigning a meaningful stoichiometry to this reaction is apparent, not to speak of a suitable free energy of reaction and rate law. If one cannot simply ignore these reactions and wants to surpass a purely phenomenological non-mechanistic description, it is important to clarify the concentration measures relevant for such reactions. Since the macromolecules are usually much larger than proteins, the associated catalysts are surface-active enzymes and the concentration of the interface in the bulk reaction space becomes decisive.

In this chapter, I have shown a straightforward approach to derive interfacial rate laws for enzymatic mechanisms of any complexity including the possibility of heterogeneous interfaces. This was achieved by

(a) introducing the available area function into enzyme kinetics to capture

different adsorption models in one framework,

(b) modifying the available area function to include the relevant surface fractions ω for the LANGMUIRian case,

(c) describing the interfacial reactants through their molar fractions assuming a uniform density at the dividing surface, and

(d) applying the method of Cha (1968), assuming partial equilibrium mechanisms.

The rate laws have a particularly straightforward form. This property is useful when building larger metabolic models, where the interaction of the enzyme with effectors or different substrates has to be considered. The rate laws can be easily adapted much like the usual rate laws derived with the rapid equilibrium assumption (Segel, 1993).

The new approach to interfacial catalysis has been applied to enzymes involved in starch degradation to derive rate laws which will be used in the next chapter. To my knowledge, this is the first time that rate laws have been derived for the glucan, water dikinase and phosphoglucan phosphatase SEX4 consistent with the fact that they catalyze interfacial reactions.[13]

On the one hand, enzyme adsorption has been studied using the LANGMUIR model in many kinetic studies. For example, it was used for lipases (Burns et al., 1982), cellulases (Medve et al., 1994; Zhang and Lynd, 2004), α-amylases (Leloup et al., 1991) and glucosidases (Tatsumi and Katano, 2005). Converse and Optekar (1993) use the LANGMUIR approach implicitly in their study of competitive adsorption. Medve et al. (1997) and Medve et al. (1998) have applied a combined Langmuir-Freundlich isotherm which is analogous to a Hill equation used to describe cooperative adsorption. Also the binding domains were studied, for example starch binding domains (SBDs) in Guillén et al. (2007); Mikkelsen et al. (2006) and Wayllace et al. (2010).

However, none of these studies has used the concept of the available area function. I believe that the introduction of this framework to derive rate

[13] A model of GWD kinetics was published earlier in Kartal and Ebenhöh (2008). However, I decided not to reproduce it here, since it was very simplified, less mechanistic treatment. As a preliminary stage which is implicit in the more appropriate and detailed account given in this thesis it may be considered obsolete.

laws is an aid in unifying different approaches to surface-active enzymes. The proposed rate laws have the desirable property that the effects of different assumptions on adsorption can be readily tested without changing the form of the equations. Recently, Levine et al. (2010) have applied RSA in a model of cellulose hydrolysis but no rate laws have been derived and the temporal evolution was studied with a large set of kinetic equations and additional stochastic simulations. The approach presented here is sufficiently abstract such that it does not suffer from being tailored to a specific enzyme-substrate system. Of course, as we have seen no exact solution may be available for ϕ in a complicated system and what remains to be done in the future is to develop applicable approximation schemes which can also be tested for experimentally.

Originally developed for a description of gas particles adsorbing onto well defined solid surfaces it is clear that the underlying assumptions of LANGMUIR's approach cannot capture all the complexities of proteins interacting with a complex and possibly eroding substrate interface (see e.g. Tzafriri et al., 2002). Nevertheless, as a landmark in the study of interfacial reactions it is widely acknowledged as being a reasonable first approximation. An additional virtue of this approach is that it allows to derive exact formulae expressing qualitative properties of the interfacial rate law.

The analogue of the MMH rate law as derived here can be confronted with interfacial rate laws found in the literature. Most notably, the rate laws used for lipases (Deems, 2000) and for pretreated biomass (cellulose), for example the HCH-1 model (see Brown and Holtzapple, 1990; Holtzapple et al., 1984) are suitable for a comparison to Eq. (2.66) (see Table 2.11).

Table 2.11: Comparison of generic rate laws for surface-active enzymes.

Reference	**Specific activity** (v/e^0)	**Approximation**
This work	$\dfrac{k^*_{\mathrm{cat}}\phi a_{\mathrm{g}}\chi^*}{K_{\mathrm{d}}K^*_{\mathrm{m}} + \phi a_{\mathrm{g}}\left(K^*_{\mathrm{m}} + \chi^*\right)}$	REA and QSSA
Deems (2000)	$\dfrac{k_{\mathrm{cat}}c_{\mathrm{L}}\chi^*}{K_{\mathrm{L}}K^*_{\mathrm{m}} + c_{\mathrm{L}}\left(K^*_{\mathrm{m}} + \chi^*\right)}$	QSSA
Brown and Holtzapple (1990)	$\dfrac{ks}{K + \varphi s + \varepsilon e^0}$	QSSA

The velocity equation discussed in Deems (2000) is formally similar the equation derived in this work with the sole but significant difference that the bulk concentration of the 'relevant ligand' c_{L} replaces the term ϕa_{g}. As DEEMS points out, "the bulk concentration of anything that holds the enzyme to the surface must be included in this term, whether it be a discrete molecular species or a general surface term." This term could be difficult to specify and more importantly it does not involve any inhibitory effect of the enzyme concentration as it is the case when ϕ is used (see Fig. 2.17). Indeed, adsorption is here merely an ordinary ligand interaction necessarily taking place upstream of the true catalytic step. Upon binding the ligand, the interfacial substrate concentration χ^* is altered. Thus, this is not a true adsorption model.

In this respect, the HCH-1 rate law is more appropriate. The inhibitory effect of higher enzyme loadings is indeed captured in the HCH-1 model by the term εe^0, where ε denotes the number of cellulose sites occupied by an adsorbed or complexed enzyme. This is introduced because the authors count the total substrate basically as (in our nomenclature) $s = s^{\mathrm{f}} + \varepsilon(ae^* + ac^*_{\mathrm{sE}})$, where s^{f} is the concentration of free sites. The term φ which they define as the ratio of free to total adsorption sites is *not* identical to the available area function. It has been derived for the particular mechanism used by Holtzapple et al. (1984) and cannot be adapted to, for example, RSA. Moreover, without modifactions the HCH-1 model cannot be applied when different interfacial qualities are present. This is also the case if different interfacial reactants have to be considered, since there is no distinction made between the interface and interfacial reactants.

Some aspects (e.g. interfacial heterogeneity) which are not captured by the rate laws compared here are sometimes treated in kinetic models where the intermediary steps of the catalytic cycle are incorporated explicitly (cf. the review from Zhang and Lynd, 2004). This has the obvious drawback of generating a model with many parameters and variables and the enzyme rate is 'hidden' in the differential equations. Consequently, many of these models are tailored towards biotechnological applications in reactors and are of little use if one aims at constructing kinetic models of metabolism.

In view of these considerations, the existing rate laws are unsatisfactory and too rigid for the purpose of modeling starch-degrading enzymes. In contrast,

the consequent use of the available area function allows to develop models in which the different elements, adsorption and interfacial catalysis, can be elaborated individually making extensions and hypothesis-testing easier in the future.

From an applied viewpoint, a remaining task is to develop a (maybe graphical) scheme enabling experimentalists to readily extract information on parameters in the interfacial rate law. Regarding the mathematical analysis, it could be well worth to analyze further in which cases certain approximations are justified, for example the combined adsorption equilibrium and QSS assumptions. This requires the application of more sophisticated tools like singular perturbation techniques (Murray, 2008).

Chapter 3

Modeling leaf starch degradation by surface-active enzymes: the role of interfacial phase transitions and reversible phosphorylation

> Almost any plausible proposed relation among aspects of nature is likely to be true in the sense that it occurs (although rarely and slightly). Yet all models leave out a lot and are in that sense false, incomplete, inadequate. The validation of a model is not that it is "true" but that it generates good testable hypotheses relevant to important problems. A model may be discarded in favor of a more powerful one, but it usually is simply outgrown when the live issues are not any longer those for which it was designed.
>
> *The strategy of model building in population biology*
>
> Richard Levins, 1966

In the last decade, interfacial enzymes have been shown to be essential for

the breakdown pathway of leaf starch. This led to the establishment of a novel hydrolytic pathway which dominates the carbon flux from starch during the night. However, the hydrolytic enzymes alone are insufficient to provide the mobilization at an extent necessary to sustain normal growth rates. Reversible phosphorylation supposedly triggers phase transitions at the interface stimulating hydrolytic attack. Currently, there exists no dynamic model of these processes and it is difficult to assess how the complicated physical processes could interfere with metabolic regulation.

Building on the framework and the rate laws for interfacial catalysis derived in the previous chapter, a kinetic model of leaf starch degradation is formulated and analyzed. I restrict myself to the *in vitro* case, since the focus is on the basic mechanistic questions here and the most reliable data on that is from these experiments.

First, the model suggests that spontaneous helix-coil transitions of nonphosphorylated interfacial glucans take place. These transitions are supported by phosphorylation. The decreasing crystallinity leads to a sequestration of hydrolytic enzymes at the surface, hence degradation is stimulated. The extent of this stimulation is quantified by the degree of synergy in a multi-enzyme system. It is shown that the stimulatory effect is time-dependent. Interestingly, the positive effect of reversible phosphorylation on hydrolysis is more pronounced in early phases of degradation. This hints at the regulatory role of phosphorylation in early phases of degradation and suggests that its main function is in supporting rapid transition from starch synthesis to degradation.

3.1 Introduction

Leaf starch degradation has proved to be a formidable example of how biochemical and physical processes are entangled (Blennow and Engelsen, 2010). The activity of enzymes at the starch-stroma interface forces us to go beyond the paradigm of enzymes acting in solution. The last chapter has developed a reformulation of interfacial catalysis by enzymes, elaborating a clear distinction between phenomena linked to adsorption alone and to catalysis at the interface. Here, we will show how these rate laws are incorporated into a kinetic model of starch degradation. The model aims at simulating how enzymatic

catalysis changes physical properties of bulk matter, the starch grain interface. Thus, we will study a macroscopic effect of biochemical reactions which goes beyond the mere alteration of concentrations.

Background. The enzymes which have been explained in the last chapter are also those most thoroughly investigated in experiments. In particular, the following investigation aims at reproducing *in silico* the stimulatory effect observed when the enzymes act in concert. We quantify this by introducing the *degree of synergy* Ξ, defined for a set of enzymes $Z = \{E_1, \ldots, E_{|Z|}\}$, where $|Z|$ denotes the number of enzymes. Basically, it relates the amount of glucose equivalents released if all enzymes in Z are present to the sum released by certain subsets of Z. We only require that the subsets do not overlap and that the union of the subsets covers the whole set Z. Formally, we can use the concept of the power set $\mathscr{P}(Z)$, which comprises *all* possible subsets of Z as elements, denoted Z_1, Z_2, etc. Now, in accordance with the informal definition above, we may define a subset of $\mathscr{P}(Z)$ by

$$W \subset \mathscr{P}(Z) : \bigcup_i W_i = Z \wedge \bigcap_i W_i = \emptyset, \tag{3.1}$$

where $W_i \in W$. Furthermore, let $n(A)$ denote the amount of glucose equivalents released by a set of enzymes A. Then the degree of synergy of an enzyme set Z relative to a set W can be compactly written as

$$\Xi(Z; W) = \frac{n_{\mathrm{Z}}}{\sum_i n(W_i)}. \tag{3.2}$$

This quantity can also be time-dependent which is considered in the simulations in Section 3.3.

In experiments (Edner et al., 2007; Kötting et al., 2009), the glucose equivalents are quantified after certain time periods to see if the concerted activity of dikinases, phosphatases and amylases yields more product. To illustrate this, the experimental degrees of synergy after 90 min from Edner et al. (2007, see Figure 3.1a, data kindly provided by M. Steup) relative to individual enzymes

read

$$\begin{aligned} \Xi(\{\text{GWD, BAM}\};\ \{\{\text{GWD}\},\{\text{BAM}\}\}) &= 2.3 \\ \Xi(\{\text{GWD, ISA}\};\ \{\{\text{GWD}\},\{\text{ISA}\}\}) &= 0.8 \\ \Xi(\{\text{BAM, ISA}\};\ \{\{\text{BAM}\},\{\text{ISA}\}\}) &= 2.7 \\ \Xi(\{\text{BAM, ISA,GWD}\};\ \{\{\text{BAM}\},\{\text{ISA}\},\{\text{GWD}\}\}) &= 5.2 \end{aligned} \tag{3.3}$$

The stimulatory effect ($\Xi > 1$) when endo- and exo-acting enzymes co-operate is apparent, being even more pronounced when phosphorylation by GWD takes place. Interestingly, the released amounts can become even higher if dephosphorylation by SEX4 takes place simultaneously, see Fig. 3.1b which depicts results from Kötting et al. (2009). That is, the degree of synergy increases if turnover of interfacial phosphate is increased. These experiments, amongst others, have established the crucial role of reversible phosphorylation for starch degradation.

Using a very basic model it will be analyzed if spontaneous helix-coil transitions are present at the interface and if these are possibly triggered by phosphorylation. In Section 2.1 on starch structure some remarks were already made on the disorganizing effect of phosphorylation. Native glucans at the interface form double helices, which are stabilized by hydrogen bonding. This is reflected by certain dihedral angles between the α-1,4-glucosidic bonds compatible with helix formation. There are findings (Blennow and Engelsen, 2010; Hansen et al., 2009) indicating that phosphorylation of a glucosyl residue induces strain in a vicinal α-1,4-glucosidic linkage. By presumably making the helical state energetically unfavorable this increases the transition probability into the random coil state. There seems to be a difference depending on which of the C-atoms is phosphorylated, however, this was inferred by using an isolated maltose molecule as a model (Hansen et al., 2009). Thus, these findings cannot really preclude that phosphate esters at both C-3 and C-6 position affect the order in crystalline lamellae. We will include helix-coil transitions as part of a kinetic model of the biochemical system.

Kinetic modeling paradigm. In a system where chemical reactions take place the amounts of species change but not in an arbitrary fashion. It was one of the path-breaking findings of Antoine Lavoisier (1743–1794) that

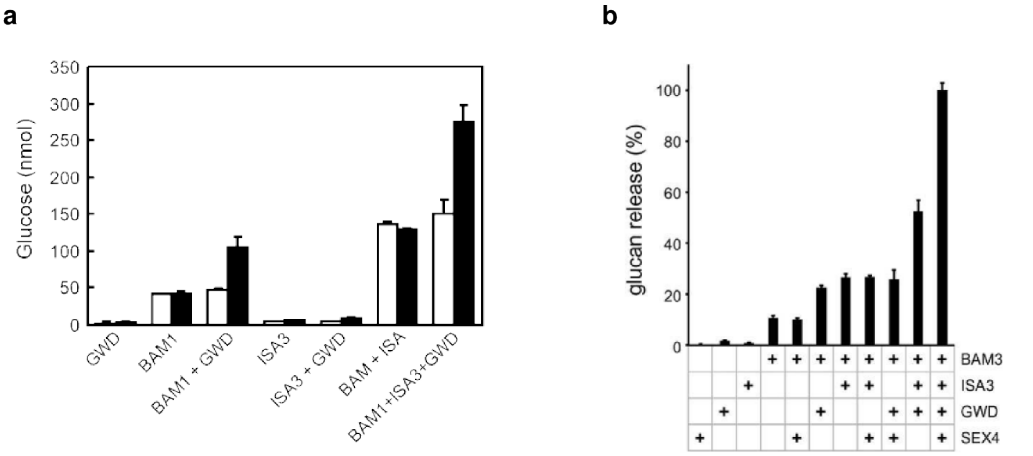

Figure 3.1: ***In vitro* experiments from literature on the stimulation of starch degradation by GWD and SEX4**. **a**, Figure from Edner et al. (2007) showing the release of glucans after 90 min for different combinations of surface-active enzymes. The released amount is counted in glucose equivalents. White bars are controls without ATP, black bars are measurements with 0.25 mM ATP. **b**, A similar experiment from Kötting et al. (2009) confirming the additional stimulation of degradation by simultaneous dephosphorylation via SEX4/DSP. Active enzymes are highlighted by a cross. Measurements are normalized to the highest value of glucose measured in the supernatant after 60 min.

the produced amounts are stoichiometrically coupled. The stoichiometry in a biochemical reaction network with m metabolites and r reactions is compactly encoded in a stoichiometric matrix $\mathbf{N}$ of dimension $m \times r$ (Heinrich and Schuster, 1996). Each entry of the matrix, ν_{ij}, gives the stoichiometric coefficient of the i^{th} reactant in the j^{th} reaction.

The stoichiometric matrix is important in describing the temporal change in metabolite concentrations $\mathbf{c} = (c_1, \ldots, c_m)^T$ in terms of a *kinetic model*, since at any instance of time it maps the vector of fluxes or reaction rates,

$$\mathbf{v}(\mathbf{c}, \mathbf{k}) = (v_1, v_2, \ldots, v_r)^T,$$

where $\mathbf{k}$ denotes the vector of parameters, onto the rates of change of metabolite concentrations,

$$\frac{\mathrm{d}}{\mathrm{d}t}\mathbf{c} = (\frac{\mathrm{d}}{\mathrm{d}t}c_1, \frac{\mathrm{d}}{\mathrm{d}t}c_2, \ldots, \frac{\mathrm{d}}{\mathrm{d}t}c_m)^T.$$

The corresponding *balance equations* for the m metabolites can be written as a single matrix equation,

$$(\mathrm{dg}\mathbf{P})\,\frac{\mathrm{d}\mathbf{c}}{\mathrm{d}t} = \mathbf{N}\mathbf{v}(\mathbf{c},\mathbf{k}). \tag{3.4}$$

Here, (dg$\mathbf{P}$) is a diagonal matrix with $\mathbf{P} = (P_1, \ldots, P_m)$ being the *partition coefficients*. Given a reference volume, V_0, $P_i := V_i/V_0$ denotes the relative volume of the compartment in which the i^{th} metabolite resides (Beard and Qian, 2008, p. 235).

Since the reaction rates depend on the concentrations, the kinetic model (3.4) is an ordinary differential equation system for the concentrations. Solving this model means deriving the set of global trajectories $c_1(t), \ldots, c_m(t)$, characterizing the dynamics of the system. The changing state can also be envisioned as a point moving in the m-dimensional state space of the system.

Due to nonlinearities in the rate equations, finding analytic solutions is a hopeless endeavor for realistic metabolic systems.[1] A valid strategy then is to simulate a limited set of trajectories in order to identify how qualitative properties depend on model parameters. An important qualitative property is the existence of stable attractors, that is regions (or submanifolds) of the state space to which the dynamical system eventually relaxes after a transient period (Aris, 1994; Heinrich and Schuster, 1996). Most notably, it is of interest to analyze *stationary states*, determined by setting $\mathrm{d}_t\mathbf{c} = \mathbf{0}$, for stability. This has been done in numerous computational studies of metabolism (see e.g. Heinrich and Schuster, 1996; Rapoport et al., 1976; Reich and Sel'kov, 1981) and can be applied also to an experimentally given stationary state by combining kinetic and structural methods (Grimbs et al., 2007).

However, if the time scale of interest is the diurnal carbon balance in plants no steady state is approached which is especially true for the amount of starch in chloroplasts. The decrease in granule mass is accompanied by a transient change in metabolite levels (Fulton et al., 2008; Gibon et al., 2006; Stitt et al., 1985). While at the end of the night no steady state is reached yet, the whole background of the system shifts dramatically, since the photosynthetic apparatus, the Calvin-Benson Cycle and starch synthesis are turned on. Therefore,

[1] Usually, by analytic solution we mean that the functions $c_i(t)$ can be expressed either implicitly or explicitly in terms of elementary functions or in the form of a power series.

the following analysis concentrates on time-dependent observables and qualitative properties of temporal profiles.

Motivation and outline. The major interfacial enzymes in starch degradation seem to have been characterized and some pictorial models have emerged on their action mode (Delatte et al., 2006; Edner et al., 2007; Fulton et al., 2008; Hejazi et al., 2010). Increasingly, the presence of regulatory modifications is revealed, however, there are still some conflicting findings (Kötting et al., 2009). The aim here is to demonstrate that a dynamic model can further elucidate properties of interfacial catalysis and the potential function of reversible phosphorylation. A future prospect for models incorporating interfacial processes is to guide new experiments.

Section 3.2 gives the kinetic balance equations for *in vitro* degradation, derives the ODEs for the variables describing the interface quality and adsorption, and discusses how the helix-coil melting rate is included. Section 3.3 shows simulations with realistic system parameters from literature to find magnitudes of kinetic constants which reproduce the synergistic effect of interfacial catalysis. This effect is studied in more detail to formulate a hypothesis for the role of reversible phosphorylation.

3.2 Balance equations

The dynamic model to simulate the degradation by surface-active enzymes is based on the action mode as depicted in Fig. 3.2 which is basically the same as given in Fig. 2.12 with the sole modification that it includes the spontaneous melting of interfacial glucans. The 20 balance equations for both soluble and interfacial reactants are summarized in Table 3.1. In total, the model considers 31 variables. Three of the remaining 11 variables are describing the concentrations of ATP, AMP and Pi, while the other eight variables, which will be discussed below, consist of the two available area functions (ϕ^{cr} and ϕ^{am}) and the six surface-associated fractional concentration factors (f^*s).

Every reactant is considered in an even- and odd-numbered form. This is necessary to include the possibility that ISA can release both maltose and maltotriose by acting on G2b* and G3b*, respectively. The corresponding

degrees of polymerization of undigested branches are denoted $\mathrm{DP}^0_{\mathrm{eve}}$ and $\mathrm{DP}^0_{\mathrm{odd}}$. We assume that the parity remains constant for the interfacial helical glucans Gh*, that is

$$\chi^*_{\mathrm{Gh_{eve}}} = \mathrm{par} \cdot \chi^*_{\mathrm{h}}, \text{ and} \tag{3.5a}$$

$$\chi^*_{\mathrm{Gh_{odd}}} = (1 - \mathrm{par}) \cdot \chi^*_{\mathrm{h}}, \tag{3.5b}$$

where par is a parameter between 0 and 1. Due to conservation, an additional algebraic relation holds true for the total molar fraction of helical glucans at the interface, given by

$$\begin{aligned}\chi^*_{\mathrm{h}} = 1 &- \chi^*_{\mathrm{Gc_{eve}}} - \chi^*_{\mathrm{Gc_{odd}}} - \chi^*_{\mathrm{pG_{eve}}} - \chi^*_{\mathrm{pG_{odd}}} - \chi^*_{\mathrm{pGx_{eve}}} - \chi^*_{\mathrm{pGx_{odd}}} \\ &- \chi^*_{\mathrm{Gx_{eve}}} - \chi^*_{\mathrm{Gx_{odd}}} - \chi^*_{\mathrm{G2b}} - \chi^*_{\mathrm{G3b}}.\end{aligned} \tag{3.6}$$

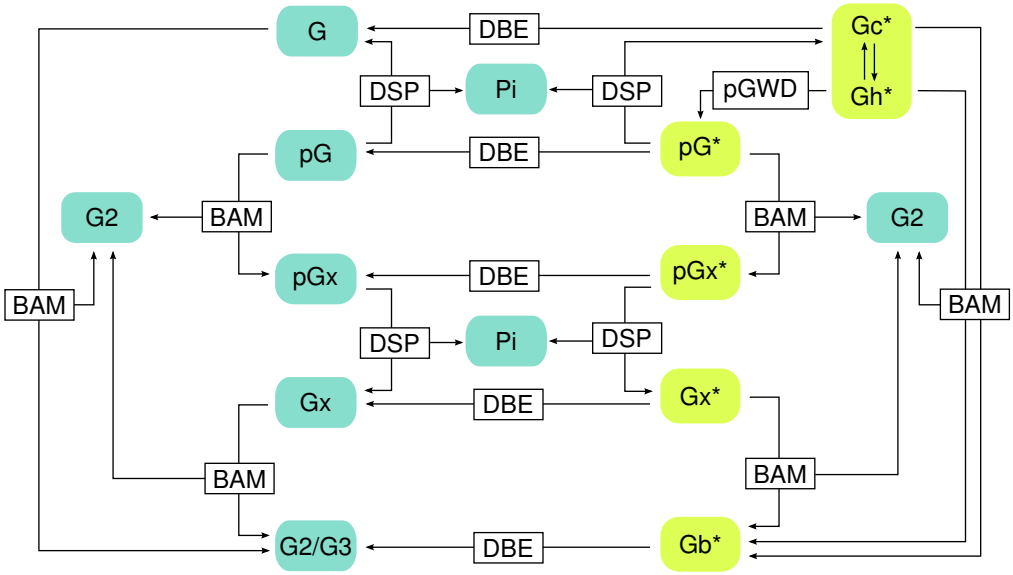

Figure 3.2: **Action mode of interfacial enzymes including spontaneous helix-coil transition**.

Another algebraic relation is valid for the interface area concentration a_{g} due to mass balance *in vitro*. Let $c_k(t)$ denote the concentrations of dissolved glucans at time t, and $M(k)$ and DP_k the corresponding molar mass and degree of polymerization, respectively, than the total mass concentration in the aqueous phase is given by

$$m_{\mathrm{aq}}(t) = \sum_k M(k) c_k(t) = M(\mathrm{AGU}) \sum_k \mathrm{DP}_k c_k(t), \tag{3.7}$$

Table 3.1: Balance equations of the kinetic model for *in vitro* starch degradation.

Interfacial reactants		
$\mathrm{d}\chi^*_{\mathrm{Gc_{eve}}}/\mathrm{d}t$	=	$\tilde{v}_{(\mathrm{DSP}\vert\mathrm{pG^*_{eve}})} - \tilde{v}_{(\mathrm{BAM}\vert\mathrm{Gc^*_{eve}})} - \tilde{v}_{(\mathrm{ISA}\vert\mathrm{Gc^*_{eve}})} + \widetilde{v}_{\mathrm{Meve}}$
$\mathrm{d}\chi^*_{\mathrm{Gc_{odd}}}/\mathrm{d}t$	=	$\tilde{v}_{(\mathrm{DSP}\vert\mathrm{pG^*_{odd}})} - \tilde{v}_{(\mathrm{BAM}\vert\mathrm{Gc_{odd}})} - \tilde{v}_{(\mathrm{ISA}\vert\mathrm{Gc^*_{odd}})} + \widetilde{v}_{\mathrm{Modd}}$
$\mathrm{d}\chi^*_{\mathrm{pG_{eve}}}/\mathrm{d}t$	=	$\tilde{v}_{(\mathrm{GWD}\vert\mathrm{Gh^*_{eve}})} - \tilde{v}_{(\mathrm{DSP}\vert\mathrm{pG^*_{eve}})} - \tilde{v}_{(\mathrm{BAM}\vert\mathrm{pG^*_{eve}})} - \tilde{v}_{(\mathrm{ISA}\vert\mathrm{pG^*_{eve}})}$
$\mathrm{d}\chi^*_{\mathrm{pG_{odd}}}/\mathrm{d}t$	=	$\tilde{v}_{(\mathrm{GWD}\vert\mathrm{Gh^*_{odd}})} - \tilde{v}_{(\mathrm{DSP}\vert\mathrm{pG^*_{odd}})} - \tilde{v}_{(\mathrm{BAM}\vert\mathrm{pG^*_{odd}})} - \tilde{v}_{(\mathrm{ISA}\vert\mathrm{pG^*_{odd}})}$
$\mathrm{d}\chi^*_{\mathrm{pGx_{eve}}}/\mathrm{d}t$	=	$-\tilde{v}_{(\mathrm{DSP}\vert\mathrm{pGx^*_{eve}})} + \tilde{v}_{(\mathrm{BAM}\vert\mathrm{pG^*_{eve}})} - \tilde{v}_{(\mathrm{ISA}\vert\mathrm{pGx^*_{eve}})}$
$\mathrm{d}\chi^*_{\mathrm{pGx_{odd}}}/\mathrm{d}t$	=	$-\tilde{v}_{(\mathrm{DSP}\vert\mathrm{pGx^*_{odd}})} + \tilde{v}_{(\mathrm{BAM}\vert\mathrm{pG^*_{odd}})} - \tilde{v}_{(\mathrm{ISA}\vert\mathrm{pGx^*_{odd}})}$
$\mathrm{d}\chi^*_{\mathrm{Gx_{eve}}}/\mathrm{d}t$	=	$\tilde{v}_{(\mathrm{DSP}\vert\mathrm{pGx^*_{eve}})} - \tilde{v}_{(\mathrm{BAM}\vert\mathrm{Gx^*_{eve}})} - \tilde{v}_{(\mathrm{ISA}\vert\mathrm{Gx^*_{eve}})}$
$\mathrm{d}\chi^*_{\mathrm{Gx_{odd}}}/\mathrm{d}t$	=	$\tilde{v}_{(\mathrm{DSP}\vert\mathrm{pGx^*_{odd}})} - \tilde{v}_{(\mathrm{BAM}\vert\mathrm{Gx^*_{odd}})} - \tilde{v}_{(\mathrm{ISA}\vert\mathrm{Gx^*_{odd}})}$
$\mathrm{d}\chi^*_{\mathrm{G2b}}/\mathrm{d}t$	=	$\tilde{v}_{(\mathrm{BAM}\vert\mathrm{Gc^*_{eve}})} + \tilde{v}_{(\mathrm{BAM}\vert\mathrm{Gh^*_{eve}})} + \tilde{v}_{(\mathrm{BAM}\vert\mathrm{Gx^*_{eve}})} - \tilde{v}_{(\mathrm{ISA}\vert\mathrm{G2b})}$
$\mathrm{d}\chi^*_{\mathrm{G3b}}/\mathrm{d}t$	=	$\tilde{v}_{(\mathrm{BAM}\vert\mathrm{Gc_{odd}})} + \tilde{v}_{(\mathrm{BAM}\vert\mathrm{Gh^*_{odd}})} + \tilde{v}_{(\mathrm{BAM}\vert\mathrm{Gx^*_{odd}})} - \tilde{v}_{(\mathrm{ISA}\vert\mathrm{G3b})}$
Soluble reactants		
$\mathrm{d}c_{\mathrm{ATP}}/\mathrm{d}t$	=	$-v_{(\mathrm{GWD}\vert\mathrm{Gh^*_{eve}})} - v_{(\mathrm{GWD}\vert\mathrm{Gh^*_{odd}})}$
$\mathrm{d}c_{\mathrm{AMP}}/\mathrm{d}t$	=	$v_{(\mathrm{GWD}\vert\mathrm{Gh^*_{eve}})} + v_{(\mathrm{GWD}\vert\mathrm{Gh^*_{odd}})}$
$\mathrm{d}c_{\mathrm{Pi}}/\mathrm{d}t$	=	$v_{(\mathrm{GWD}\vert\mathrm{Gh^*_{eve}})} + v_{(\mathrm{GWD}\vert\mathrm{Gh^*_{odd}})} + v_{(\mathrm{DSP}\vert\mathrm{pG_{eve}})} + v_{(\mathrm{DSP}\vert\mathrm{pG_{odd}})} + v_{(\mathrm{DSP}\vert\mathrm{pGx_{eve}})} +$ $v_{(\mathrm{DSP}\vert\mathrm{pGx_{odd}})} + v_{(\mathrm{DSP}\vert\mathrm{pG^*_{eve}})} + v_{(\mathrm{DSP}\vert\mathrm{pG^*_{odd}})} + v_{(\mathrm{DSP}\vert\mathrm{pGx^*_{eve}})} + v_{(\mathrm{DSP}\vert\mathrm{pGx^*_{odd}})}$
$\mathrm{d}c_{\mathrm{G_{eve}}}/\mathrm{d}t$	=	$v_{(\mathrm{DSP}\vert\mathrm{pG_{eve}})} - v_{(\mathrm{BAM}\vert\mathrm{G_{eve}})} + v_{(\mathrm{ISA}\vert\mathrm{Gc^*_{eve}})}$
$\mathrm{d}c_{\mathrm{G_{odd}}}/\mathrm{d}t$	=	$v_{(\mathrm{DSP}\vert\mathrm{pG_{odd}})} - v_{(\mathrm{BAM}\vert\mathrm{G_{odd}})} + v_{(\mathrm{ISA}\vert\mathrm{Gc^*_{odd}})}$
$\mathrm{d}c_{\mathrm{pG_{eve}}}/\mathrm{d}t$	=	$-v_{(\mathrm{DSP}\vert\mathrm{pG_{eve}})} - v_{(\mathrm{BAM}\vert\mathrm{pG_{eve}})} + v_{(\mathrm{ISA}\vert\mathrm{pG^*_{eve}})}$
$\mathrm{d}c_{\mathrm{pG_{odd}}}/\mathrm{d}t$	=	$-v_{(\mathrm{DSP}\vert\mathrm{pG_{odd}})} - v_{(\mathrm{BAM}\vert\mathrm{pG_{odd}})} + v_{(\mathrm{ISA}\vert\mathrm{pG^*_{odd}})}$
$\mathrm{d}c_{\mathrm{pGx_{eve}}}/\mathrm{d}t$	=	$-v_{(\mathrm{DSP}\vert\mathrm{pGx_{eve}})} + v_{(\mathrm{BAM}\vert\mathrm{pG_{eve}})} + v_{(\mathrm{ISA}\vert\mathrm{pGx^*_{eve}})}$
$\mathrm{d}c_{\mathrm{pGx_{odd}}}/\mathrm{d}t$	=	$-v_{(\mathrm{DSP}\vert\mathrm{pGx_{odd}})} + v_{(\mathrm{BAM}\vert\mathrm{pG_{odd}})} + v_{(\mathrm{ISA}\vert\mathrm{pGx^*_{odd}})}$
$\mathrm{d}c_{\mathrm{Gx_{eve}}}/\mathrm{d}t$	=	$v_{(\mathrm{DSP}\vert\mathrm{pGx_{eve}})} - v_{(\mathrm{BAM}\vert\mathrm{Gx_{eve}})} + v_{(\mathrm{ISA}\vert\mathrm{Gx^*_{eve}})}$
$\mathrm{d}c_{\mathrm{Gx_{odd}}}/\mathrm{d}t$	=	$v_{(\mathrm{DSP}\vert\mathrm{pGx_{odd}})} - v_{(\mathrm{BAM}\vert\mathrm{Gx_{odd}})} + v_{(\mathrm{ISA}\vert\mathrm{Gx^*_{odd}})}$
$\mathrm{d}c_{\mathrm{G2}}/\mathrm{d}t$	=	$\nu_{\mathrm{G_{eve}}} v_{(\mathrm{BAM}\vert\mathrm{G_{eve}})} + \nu_{\mathrm{G_{odd}}} v_{(\mathrm{BAM}\vert\mathrm{G_{odd}})} + \nu_{\mathrm{pG_{eve}}} v_{(\mathrm{BAM}\vert\mathrm{pG_{eve}})} +$ $\nu_{\mathrm{pG_{odd}}} v_{(\mathrm{BAM}\vert\mathrm{pG_{odd}})} + \nu_{\mathrm{Gx_{eve}}} v_{(\mathrm{BAM}\vert\mathrm{Gx_{eve}})} + \nu_{\mathrm{Gx_{odd}}} v_{(\mathrm{BAM}\vert\mathrm{Gx_{odd}})} +$ $\nu_{\mathrm{G^*_{eve}}} v_{(\mathrm{BAM}\vert\mathrm{Gc^*_{eve}})} + \nu_{\mathrm{G^*_{odd}}} v_{(\mathrm{BAM}\vert\mathrm{Gc_{odd}})} + \nu_{\mathrm{G^*_{eve}}} v_{(\mathrm{BAM}\vert\mathrm{Gh^*_{eve}})} +$ $\nu_{\mathrm{G^*_{odd}}} v_{(\mathrm{BAM}\vert\mathrm{Gh^*_{odd}})} + \nu_{\mathrm{pG^*_{eve}}} v_{(\mathrm{BAM}\vert\mathrm{pG^*_{eve}})} + \nu_{\mathrm{pG^*_{odd}}} v_{(\mathrm{BAM}\vert\mathrm{pG^*_{odd}})} +$ $\nu_{\mathrm{Gx^*_{eve}}} v_{(\mathrm{BAM}\vert\mathrm{Gx^*_{eve}})} + \nu_{\mathrm{Gx^*_{odd}}} v_{(\mathrm{BAM}\vert\mathrm{Gx^*_{odd}})} + v_{(\mathrm{ISA}\vert\mathrm{G2b})}$
$\mathrm{d}c_{\mathrm{G3}}/\mathrm{d}t$	=	$v_{(\mathrm{BAM}\vert\mathrm{G_{odd}})} + v_{(\mathrm{BAM}\vert\mathrm{Gx_{odd}})} + v_{(\mathrm{ISA}\vert\mathrm{G3b})}$

where $M(\mathrm{AGU})$ is the molar mass of an anhydroglucose unit (AGU, see Table 3.2 at p. 79). Hence, the interface concentration corresponds with granule

mass according to

$$\begin{aligned} a_{\mathrm{g}}(t) = \alpha m_{\mathrm{g}}(t) &= \alpha \left(m_{\mathrm{g}}^0 - m_{\mathrm{aq}}(t) \right) \\ &= \alpha \left(m_{\mathrm{g}}^0 - M(\mathrm{AGU}) \sum_k \mathrm{DP}_k c_k(t) \right) \end{aligned} \tag{3.8}$$

In the simulations, we will make the simplifying assumption that the specific surface area fulfills $\alpha \approx$ const.. This is a valid approximation for the initial phase of degradation which is of major interest here.

Dynamics of glucan species. The balance equations for the soluble species have a common form with the rate laws basically given as in Section 2.3. The different stoichiometric coefficients appearing in the balance equation for maltose, c_{G2}, are due to the action of BAM3. The number of maltose release per repetitive hydrolysis on a single species depends on

1. the DP of the substrate,
2. intrinsic constraints of the mechanism of BAM, and
3. the position of the phosphorylated glucosyl in a phosphoglucan.

Regarding the second aspect, structural data (Fulton et al., 2008) indicate that a glucan with at minimum DP 4 is needed to act, that is odd glucans are usually hydrolyzed up to maltotriose. Furthermore, β-limits with a maltosyl branch cannot be further hydrolyzed, since this would necessitate the cleavage of a α-1,6 bond. With respect to phosphoglucans, it is not known if there is a preferred position for the phosphate, whether it is rather placed close to a branching point or to the non-reducing end (M. Steup, pers. comm.). We introduce the parameter posP as a positive integer indicating the phosphorylated glucosyl residue of undigested species counted from the non-reducing end. For the initial simulations a value of posP = 4 is assumed, but subsequently the effect of changing this parameter on the degree of synergy is analyzed. The position of the phosphate is important, since hydrolysis of phosphorylated glucans (pG or pG*) presumably stops one or two glucosyl residues before the phosphorylated residue is reached (Kötting et al., 2009). The discussed constraints entail the following stoichiometric coefficients for maltose release per attacked branch:

- for soluble reactants we have (sup denotes the least upper integer bound of the number in brackets)
  - $\nu_{\mathrm{G_{eve}}} = \mathrm{DP}^0_{\mathrm{eve}}/2$,
  - $\nu_{\mathrm{G_{odd}}} = \left(\mathrm{DP}^0_{\mathrm{odd}} - 3\right)/2$,
  - $\nu_{\mathrm{pG_{eve}}} = \sup[(\mathrm{posP} - 3)/2]$,
  - $\nu_{\mathrm{pG_{odd}}} = \sup[(\mathrm{posP} - 3)/2]$,
  - $\nu_{\mathrm{Gx_{eve}}} = \left(\mathrm{DP}^0_{\mathrm{eve}} - 2 \cdot \nu_{\mathrm{pG_{eve}}}\right)/2$,
  - $\nu_{\mathrm{Gx_{odd}}} = \left(\mathrm{DP}^0_{\mathrm{odd}} - 2 \cdot \nu_{\mathrm{pG_{odd}}} - 3\right)/2$,
- and for interfacial reactants
  - $\nu_{\mathrm{G^*_{eve}}} = \left(\mathrm{DP}^0_{\mathrm{eve}} - 2\right)/2$,
  - $\nu_{\mathrm{G^*_{odd}}} = \left(\mathrm{DP}^0_{\mathrm{odd}} - 3\right)/2$,
  - $\nu_{\mathrm{pG^*_{eve}}} = \sup[(\mathrm{posP} - 3)/2]$,
  - $\nu_{\mathrm{pG^*_{odd}}} = \sup[(\mathrm{posP} - 3)/2]$,
  - $\nu_{\mathrm{Gx^*_{eve}}} = \left(\mathrm{DP}^0_{\mathrm{eve}} - 2 \cdot \nu_{\mathrm{pG_{eve}}} - 2\right)/2$,
  - $\nu_{\mathrm{Gx^*_{odd}}} = \left(\mathrm{DP}^0_{\mathrm{odd}} - 2 \cdot \nu_{\mathrm{pG_{odd}}} - 3\right)/2$.

The balance equations for the interfacial reactants are written in terms of mole fractions, hence the rate laws are modified. Consider the case of a single enzyme where the bulk concentration of an interfacial reactant changes according to

$$\frac{\mathrm{d}\left(a_{\mathrm{g}} c^*\right)}{\mathrm{d}t} = v. \tag{3.9}$$

A rearrangement similar to that in Eq. (2.14) and division by the total surface number density $c^{*\max} = (N_{\mathrm{A}} A_{\mathrm{R}})^{-1}$ yields

$$\frac{\mathrm{d}\left(\chi^*\right)}{\mathrm{d}t} = \widetilde{v} - \chi^* r_{\mathrm{g}}, \tag{3.10}$$

where the interface growth rate r_{g} will again be assumed to be very small such that the second term is negligible. Thus, the modified rate laws are formed by

$$\widetilde{v} = \frac{v}{a_{\mathrm{g}} c^{*\max}}. \tag{3.11}$$

The equations for the native coiled side chains involve additional rates, $\widetilde{v}_{\mathrm{Meve}}$ and $\widetilde{v}_{\mathrm{Modd}}$, for the transition from helical to random coil conformation (M stands for melting). We will break down the probably more complicated process to one that includes only the essential ingredients of a cooperative transition. It can be depicted as the following scheme:

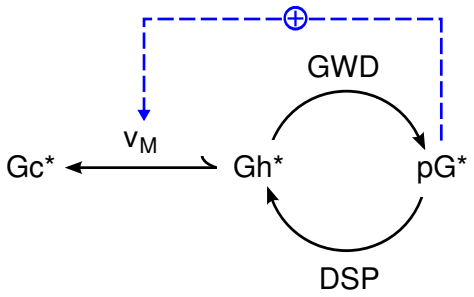

Here, the spontaneous transition from the helical (Gh^*) to the random coil (Gc^*) conformation with the rate v_{M} is thought of as a reversible process being stimulated by phosphorylated glucans (blue arrow). All phosphorylated (pG^* an pGx^*) and degraded glucans (Gx^* an Gb^*)[2] are assumed to be in the coiled state only. The outcome of the simulations will be compared to the case when $v_{\mathrm{M}} = 0$. In general one would expect that without such transitions a higher interfacial phosphorylation is necessary to make the surface susceptible to hydrolytic attack. The helix-coil melting rate can be written for both even and odd glucans in a form generally applied for cooperative processes (cf. Sec. 2.4 in Reich and Sel'kov, 1981):

$$v_{\mathrm{M}} = k_{\mathrm{M}} \cdot (a_{\mathrm{g}} c^*_{\mathrm{Gh}}) \cdot T \cdot p. \tag{3.12}$$

Here, k_{M} is of dimension $[k_{\mathrm{M}}] = \mathsf{T}^{-1}$, setting the characteristic time of the melting process, and the term

$$T = \left(1 - \frac{\Gamma}{\Gamma^{\mathrm{eq}}}\right), \tag{3.13}$$

determines the reaction direction and its distance from equilibrium, where

$$\Gamma = \frac{\chi^*_{\mathrm{Gc}}}{\chi^*_{\mathrm{Gh}}}$$

denotes the mass action ratio. The signal term p models the stimulatory effect on melting exerted by phosphoglucans. Introducing the *signal quality* s (>1

[2] A certain chain length is necessary to establish stable hydrogen bonding (see O'Sullivan and Perez, 1999).

for activator, <1 for inhibitor), the *half-effect constant* K_P and the *coefficient of cooperativity* n, the signal term reads

$$p = \frac{1 + s \cdot (c_\mathrm{P}^*/K_\mathrm{P})^n}{1 + (c_\mathrm{P}^*/K_\mathrm{P})^n}, \tag{3.14}$$

where

$$c_\mathrm{P}^* = c^{*\,\max}\chi_\mathrm{P}^* = c^{*\,\max}\left(\chi_{\mathrm{pG_{eve}}}^* + \chi_{\mathrm{pG_{odd}}}^* + \chi_{\mathrm{pGx_{eve}}}^* + \chi_{\mathrm{pGx_{odd}}}^*\right) \tag{3.15}$$

is the surface concentration of all phosphorylated species at the interface. Note, that $p = 1$ if $s = 1$ (i.e., if the signal is neutral) or $c_\mathrm{P}^* = 0$. Eq. (3.14) can be written in terms of mole fractions using Eq. (3.15) resulting in

$$p = \frac{1 + s \cdot (\chi_\mathrm{P}^*/\Lambda_\mathrm{P})^n}{1 + (\chi_\mathrm{P}^*/\Lambda_\mathrm{P})^n}, \tag{3.16}$$

where

$$\Lambda_\mathrm{P} = \frac{K_\mathrm{P}}{c^{*\,\max}}.$$

Finally, the melting rate in terms of the change of mole fractions reads

$$\widetilde{v}_\mathrm{M} = \frac{1}{a_\mathrm{g} c^{*\,\max}} v_\mathrm{M} \tag{3.17}$$

$$= k_\mathrm{M} \cdot \chi_\mathrm{Gh}^* \cdot T \cdot p. \tag{3.18}$$

Dynamics of available area functions and surface fractions of enzymes. While the right-hand sides of the ODEs for the reactants have a common form, the ODEs for the variables associated with the adsorption process need to be explained. On the face of it, it may seem contradictory to consider changing concentration factors, since we are using rate laws derived precisely under the condition of equilibrating adsorption. The reason why time-dependency of the available area function has to be considered is the presence of enzymatic processes which alter the interfacial properties. Phosphorylation and hydrolysis will reduce the crystalline surface fraction ω^cr and concomitantly increase ω^am. These quantities enter the available area functions ϕ^cr and ϕ^cr, see Eq. (2.32a), thus we have to derive ODEs which tell us how these variables precisely change.

The transition from crystalline to amorphous surface patches may be supported by spontaneous helix-coil transitions $\mathrm{Gh}^* \rightleftharpoons \mathrm{Gc}^*$. It may be counteracted

by enzymatic dephosphorylation of pG* and removal of the stubs G2b* and G3b*, enabling the emergence of crystalline substrates Gh at the interface. To not complicate matters, we assume that the crystalline surface fraction ω^{cr} is, at any instant of time, proportional to the molar fraction of helical glucans χ^*_{h} (proportionality constant=1). Hence for the associated rates of change we get

$$\frac{\mathrm{d}\omega^{\mathrm{cr}}}{\mathrm{d}t} = \frac{\mathrm{d}\chi^*_{\mathrm{h}}}{\mathrm{d}t} = -\sum_k \frac{\mathrm{d}\chi^*_k}{\mathrm{d}t} \quad \text{and} \tag{3.19}$$

$$\frac{\mathrm{d}\omega^{\mathrm{am}}}{\mathrm{d}t} = +\sum_k \frac{\mathrm{d}\chi^*_k}{\mathrm{d}t}, \tag{3.20}$$

consistent with the condition $\omega^{\mathrm{cr}} + \omega^{\mathrm{am}} = 1$. The sum of derivatives of the interfacial species, $\sum_k \frac{\mathrm{d}\chi^*_k}{\mathrm{d}t}$, is given by summing up the associated right-hand sides of the equations given in Table 3.1. Therefore, the derivative of the available area function is given by

$$\begin{aligned}\frac{\mathrm{d}\phi^{\mathrm{cr}}}{\mathrm{d}t} &= \frac{\mathrm{d}}{\mathrm{d}t}\left[\omega^{\mathrm{cr}} - \sum_j F^{\mathrm{cr}}_j \left(\theta^{\mathrm{cr}}_j + \sum_c [\theta^{\mathrm{cr}}_{j,c}]^{\mathrm{ss}}\right)\right] \\ &= -\sum_k \frac{\mathrm{d}\chi^*_k}{\mathrm{d}t} - \sum_j F^{\mathrm{cr}}_j \frac{\mathrm{d}\theta^{\mathrm{cr}}_j}{\mathrm{d}t},\end{aligned} \tag{3.21a}$$

and analogously

$$\frac{\mathrm{d}\phi^{\mathrm{am}}}{\mathrm{d}t} = +\sum_k \frac{\mathrm{d}\chi^*_k}{\mathrm{d}t} - \sum_j F^{\mathrm{am}}_j \frac{\mathrm{d}\theta^{\mathrm{am}}_j}{\mathrm{d}t}. \tag{3.21b}$$

F^{cr}_j is the enzyme-patch function and the derivative of the sum $\sum_c [\theta^{\mathrm{cr}}_{j,c}]^{\mathrm{ss}}$, taken over all enzyme intermediates c in the catalytic cycle of enzyme j, vanishes because of the QSSA.

Apparently, in order to integrate the ODEs we must know the time derivatives of the surface coverages θ^{cr}_j and θ^{am}_j. Here it is important to realize that any variation in the coverages is constrained by the equilibrium condition (see Eq. 2.34)

$$\frac{[\theta^i_j]^{\mathrm{eq}}}{[e_j]^{\mathrm{eq}}} = \frac{\phi^i}{\widetilde{K}^i_{\mathrm{d},j}}. \tag{3.22}$$

The right-hand side is an apparent equilibrium 'constant' for enzyme j adsorbing onto patch i. Thus, a changing available area function ϕ^i entails a changing equilibrium constant of adsorption, which means that the ratio of $[\theta^i_j]^{\mathrm{eq}}$ to $[e_j]^{\mathrm{eq}}$ is altered. This interdependency can be used to eliminate $[e_j]^{\mathrm{eq}}$, employing the

fact that according to the rate laws the whole rapid-equilibrium segment is in a quasi-steady state, hence $x_j = [x_j]^{\mathrm{ss}}$. Since the fractional concentration factors of a segment always sum up to unity we get

$$[\theta_j^i]^{\mathrm{eq}} = f_j [x_j]^{\mathrm{ss}} \frac{\phi^i}{\widetilde{K}_{\mathrm{d},j}^i} = \left(1 - \sum_i f_j^i\right) \frac{[x_j]^{\mathrm{ss}} \phi^i}{\widetilde{K}_{\mathrm{d},j}^i} \tag{3.23}$$

where it shall be understood that f_j^i refers to the adsorbed fraction of the rapid-equilibrium segment. With the last equation we can calculate the derivative $\mathrm{d}_t \theta_j^i$ to be replaced in Eqs. (3.21a) and (3.21b) yielding the differential equations

$$\frac{\mathrm{d}\phi^{\mathrm{cr}}}{\mathrm{d}t} = -\frac{\sum_k \frac{\mathrm{d}\chi_k^*}{\mathrm{d}t} + \phi^{\mathrm{cr}} \sum_j F_j^{\mathrm{cr}} \frac{[x_j]^{\mathrm{ss}}}{\widetilde{K}_{\mathrm{d},j}^{\mathrm{cr}}} \frac{\mathrm{d}f_j^{\mathrm{cr}}}{\mathrm{d}t}}{1 + \sum_j \left[F_j^{\mathrm{cr}} \frac{[x_j]^{\mathrm{ss}}}{\widetilde{K}_{\mathrm{d},j}^{\mathrm{cr}}} \left(1 - f_j^{\mathrm{cr}} - f_j^{\mathrm{am}}\right) \right]}, \tag{3.24a}$$

$$\frac{\mathrm{d}\phi^{\mathrm{am}}}{\mathrm{d}t} = +\frac{\sum_k \frac{\mathrm{d}\chi_k^*}{\mathrm{d}t} - \phi^{\mathrm{am}} \sum_j F_j^{\mathrm{am}} \frac{[x_j]^{\mathrm{ss}}}{\widetilde{K}_{\mathrm{d},j}^{\mathrm{am}}} \frac{\mathrm{d}f_j^{\mathrm{am}}}{\mathrm{d}t}}{1 + \sum_j \left[F_j^{\mathrm{am}} \frac{[x_j]^{\mathrm{ss}}}{\widetilde{K}_{\mathrm{d},j}^{\mathrm{am}}} \left(1 - f_j^{\mathrm{cr}} - f_j^{\mathrm{am}}\right) \right]}, \tag{3.24b}$$

The QSS concentrations $[x_j]^{\mathrm{ss}}$ were basically already determined in finding the solution for the rate laws. The remaining unknowns are the rates of change $\mathrm{d}_t f_j^{\mathrm{cr}}$ and $\mathrm{d}_t f_j^{\mathrm{am}}$. These derivatives are obtained by dividing the equations describing the fast adsorption dynamics (see Eq. 2.33a) by the slow variable $[x_j]^{\mathrm{ss}}$ giving

$$\frac{\mathrm{d}f_j^{\mathrm{cr}}}{\mathrm{d}t} = F_j^{\mathrm{cr}} \cdot \widetilde{k}_{\mathrm{a},j}^{\mathrm{cr}} e_j^{*\max} \cdot \left[a_{\mathrm{g}} \phi^{\mathrm{cr}} \left(1 - f_j^{\mathrm{cr}} - f_j^{\mathrm{am}}\right) - K_{\mathrm{d},j}^{\mathrm{cr}} f_j^{\mathrm{cr}} \right], \tag{3.25a}$$

$$\frac{\mathrm{d}f_j^{\mathrm{am}}}{\mathrm{d}t} = F_j^{\mathrm{am}} \cdot \widetilde{k}_{\mathrm{a},j}^{\mathrm{am}} e_j^{*\max} \cdot \left[a_{\mathrm{g}} \phi^{\mathrm{am}} \left(1 - f_j^{\mathrm{cr}} - f_j^{\mathrm{am}}\right) - K_{\mathrm{d},j}^{\mathrm{am}} f_j^{\mathrm{am}} \right]. \tag{3.25b}$$

Let us recapitulate why the extra ODEs (3.24a) to (3.25b) are necessary. The rapid equilibrium segment is considered in equilibrium after a fast initial transient. However its apparent equilibrium constant is drifting due to processes on the slow time scale (the metabolic reactions) which affect the available area function. The rapid subsystem obeys this perturbation. It adapts the fractional concentration factors almost immediately and remains in equilibrium. In a certain sense, the available area function figures as a field or reservoir variable for the equilibrating adsorption process, like for example

temperature does for any chemical reaction. Thus, in contrast to rate laws derived solely with the QSS assumption the partial equilibrium mechanism admits changes in surface coverages to be considered, whether due to degradation in general or due to interfacial phase transitions which change the relevant surface fractions ω_i.

3.3 Simulations

Model parameters. Table 3.2 below summarizes the parameters used for the simulations. The experimental setting with amounts of ATP, starch and enzymes is according to Kötting et al. (2009) while the extra parameters in the Table are necessary to obtain derived quantities.

Figure 3.3 shows a randomly generated granule size distribution typical for the parameters chosen in Table 3.2. Similar distributions can be found for starch granules of other botanical origin (Tatsumi and Katano, 2005). The artificial distribution is used along with the value for the shape factor z and the density ρ to calculate the specific surface area α of the random sample according to Eq. (2.4).

Another derived parameter is the enzyme parking area. Assuming a spherical molecule shape, the molecule radius can be calculated using the molecular mass of the respective enzyme, $m(\mathrm{E}_j)$, and the value around which the partial specific volume, ν_B, clusters for proteins (Ramsden, 2002), hence

$$r_j = \left(\frac{3}{4\pi} m(\mathrm{E}_j) \nu_\mathrm{B} \right)^{1/3}, \tag{3.26}$$

giving the parking areas as $A_j = \pi \cdot r_j^2$.

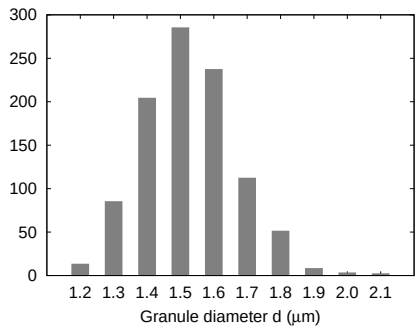

Figure 3.3: **Typical granule size distribution**. Randomly generated log-normal distributions using `lognrnd` of the Matlab Statistics Toolbox with $\mu = 1.5$ μm, $\sigma^2 = 0.02$ and a sample of 1000.

Table 3.2: Fixed system parameters for fitting model to *in vitro* starch degradation.

Simulation parameter	**Value**	**Reference**
Total volume V	120 μL	Kötting et al. (2009)
Substrates		
ATP concentration	$a_3^0 = 1$ mM	Kötting et al. (2009)
Starch mass	$M^0 = 2.5$ mg	Kötting et al. (2009)
	($\equiv 15,432$ nmol Glc)	
Granule size distribution	$\mu = 1.5$ μm, $\sigma^2 = 0.02$	Zeeman et al. (2002)
Granule shape	$z = 2 \quad (h \approx 1/4)$	Zeeman et al. (2002)
Granule density	$\rho = 1.5$ g cm^{-3}	Buléon et al. (1982)
Parity interfacial glucans	par $= 0.5$	see text
DPs of native side chains	$\mathrm{DP}^0_{\mathrm{eve}} = 16$	see text
	$\mathrm{DP}^0_{\mathrm{odd}} = 15$	
Effective area[‡]	$A_{\mathrm{R}} = 8.5 * 10^{-17}$ cm^2	Buléon et al. (1998)
Average phosphate position	posP $= 4$	see text
Molar mass anhydroglucose unit	$M(\mathrm{AGU}) = 162$ g mol^{-1}	periodic table
Enzymes		
Partial specific volume of proteins	$\nu_{\mathrm{B}} = 0.74$ cm^3 g^{-1}	Ramsden (2002)
Adsorption constant[§]	$\widetilde{k}^{\mathrm{cr,am}}_{\mathrm{a},j} = 60 \cdot 10^5$ M^{-1}min^{-1}	Wegner et al. (2004)
Molecular mass *At*GWD	$m(\mathrm{GWD}) = 157$ kDa	`www.uniprot.org`
*At*SEX4/Laforin	$m(\mathrm{DSP}) = 40$ kDa	Niittylä et al. (2006)
*At*BAM3	$m(\mathrm{BAM}) = 61$ kDa	`www.uniprot.org`
*At*ISA3	$m(\mathrm{ISA}) = 80$ kDa	Delatte et al. (2006)
Initial mass concentration	$m^0_{\mathrm{GWD}} = 16.6$ μg mL^{-1}	Kötting et al. (2009)
	$m^0_{\mathrm{DSP}} = 16.6$ μg mL^{-1}	
	$m^0_{\mathrm{BAM}} = 16.6$ μg mL^{-1}	
	$m^0_{\mathrm{ISA}} = 8.3$ μg mL^{-1}	
Helix-coil transition		
Characteristic rate	$k_{\mathrm{M}} = 10^6$ min^{-1}	fitted values
Equilibrium constant	$\Gamma^{\mathrm{eq}} = 10^{-2}$	
Signal quality	$s = 1.1$	
Half-effect constant	$\Lambda_{\mathrm{P}} = 10^{-1}$	
Coefficient of cooperativity	$n = 2$	

[‡] The given value represents an estimate of the lower bound on the effective area occupied by an interfacial reactant. It assumes the unit cell area of the B-type allomorph where at maximum four side-chains can pack, see Fig. 3 in Buléon et al. (1998).

[§] Value represents the expected order of magnitude.

With the given set of system parameters the kinetic parameters of the model have been varied, in order to reproduce the stimulatory effects of combining different surface-active enzymes observed experimentally, see Fig. 3.1. That is the fitting was done comparing the released amount of glucose equivalents. I opted for a rather coarse fitting by hand to see at which orders of magnitude the parameters have to be, particularly in relation to each other. If a model has too many parameters, there is always the danger of over-fitting. Beyond a certain degree, computer-precision is artificial and does not convey any useful extra information (Aris, 1994; Heinrich and Schuster, 1996). The glucan release showed only very little standard deviations when different size distributions were used, randomly generated with one and the same mean and variance. The fitted values of the kinetic parameters will be discussed at the end of this section and are given in Table 3.3 at p. 88.

Including helix-coil melting leads to better approximation of experimental results. Figure 3.4 compares the temporal glucan release in a system assumed without helix-coil melting (Fig. 3.4a) with a system, where this spontaneous process is present.

In both cases a stimulatory effect is observed. However, the non-melting case shows a drastic deviation from experimental results: First, there is an unrealistically large gap between those combinations comprising BAM+GWD plus at least one other enzyme (solid brown, orange and green curves) and the remaining settings, respectively. Second, the higher release of BAM+GWD+DSP (orange) compared to BAM+ISA+GWD (brown) contradicts experimental findings qualitatively, see Fig. 3.1b.

In contrast to that Fig. 3.4b, calculated using the same kinetic parameters, concurs qualitatively with the experimental findings. Like in Fig. 3.1b, the enzyme combinations can be separated into more or less four ranges according to the released amounts. The separation becomes more pronounced with the extent of reaction, illustrating that the results also depend on the time of measurement. For example, the stimulatory effect of adding GWD to BAM+ISA (brown) is only visible before ≈300 min. After that, interfacial phosphorylation rather limits further release compared to BAM+ISA (blue). The interpretation is that the phosphate esters prevent a high processivity of BAM, which

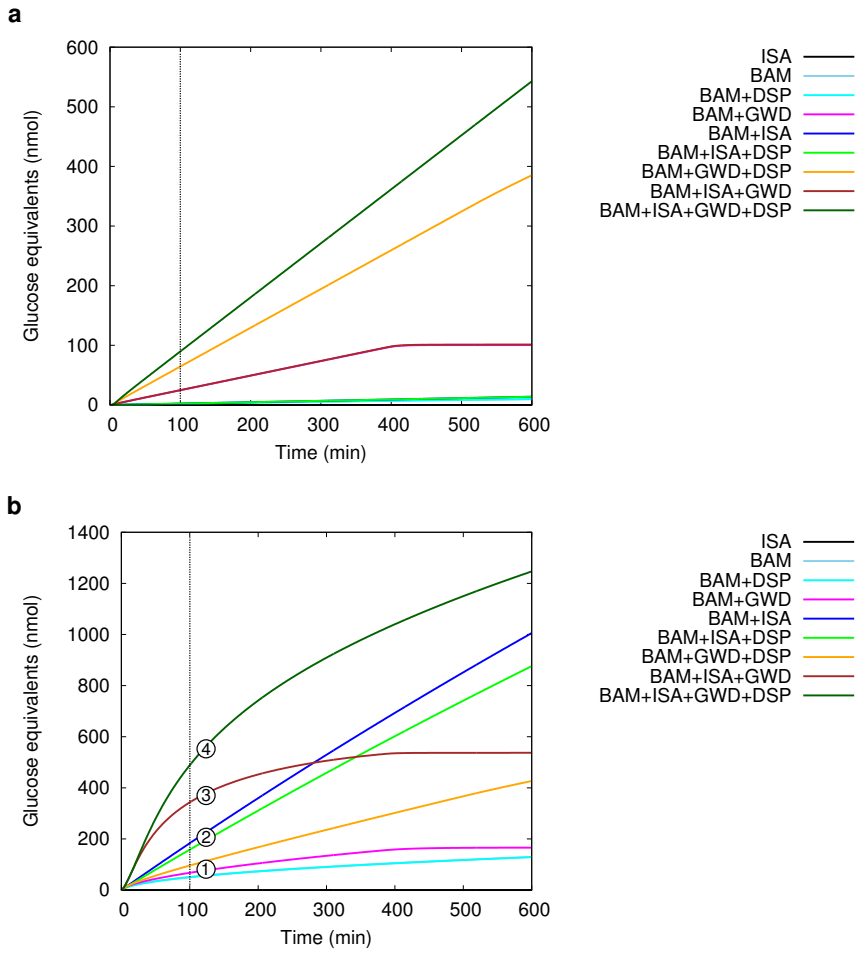

Figure 3.4: **Time-resolved glucan release by interfacial enzyme combinations favors model with interfacial helix-coil transitions**. Simulations over 600 min using a granule size distribution resulting in $\alpha = 5.2571 \cdot 10^4$ $\mathrm{cm^2 g^{-1}}$. The dashed vertical line indicates an early time point. **a**, Temporal profiles of total release without helix-coil transition (i.e. $v_\mathrm{M} = 0$) shows mostly a linear increase. Maximally ∼550 glucose equivalents are released which amounts to ∼3.5% of the whole mass as given in Table 3.2. **b**, The same picture with interfacial glucan melting producing more realistic results in the early phase. The separation into basically four groups of combinations also seen in experiments is indicated by the numbers. The BAM curve is hidden behind the BAM+DSP curve. Approximately 8% of the whole mass is released when all enzymes are present.

effectively reduces the amount of β-limit dextrin like stubs. These, however, are the preferred substrates of ISA which thus shows a decreased activity. In

the remaining part only the model with spontaneous melting is analyzed.

Figure 3.5 compares the glucan release after 100 min (values at the vertical line in Fig. 3.4b) to the values from Kötting et al. (2009). The results are qualitatively in good agreement but in the simulations the stimulatory effect of DSP is less pronounced than in experiments.

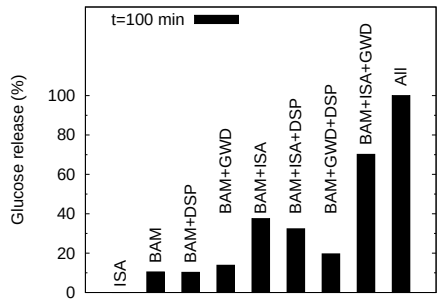

Figure 3.5: **Simulation results after 100 min are qualitatively comparable to experiments**. As in Kötting et al. (2009), see Fig. 3.1, the release is normalized to the maximum. The placing of the labels shows that the assays can be grouped similarly according to the release of glucose equivalents both in experiment (indicated by height of the labels) and simulation.

Degree of synergy and the role of reversible phosphorylation. Figure 3.6 shows the degree of synergy depending on time. For the simulated time span, combining all four enzymes results in a ≈10-fold higher release compared to the sum released by the individual enzymes. However, the synergism of the hydrolytic set (see blue curve) is steadily increasing and eventually rises above that of BAM+ISA+GWD (brown). A general observation is, that combinations with GWD have a local maximum early during degradation and subsequently decrease. An exception is BAM+GWD+DSP (orange) which, however, will come to halt if only β-limit like stubs are left, since these can only be removed by ISA. In contrast to that, combining exo- and endo-acting amylases has a more positive effect when longer time periods are considered.

To look at this more closely Fig. 3.7 shows for a longer time span the degree of synergy $\Xi(Z;W)$ with Z being the full set of enzymes and W comprising the hydrolytic subset {BAM,ISA} and the subset {GWD,DSP}. This confirms that the stimulatory effect of reversible interfacial phosphorylation is maximal

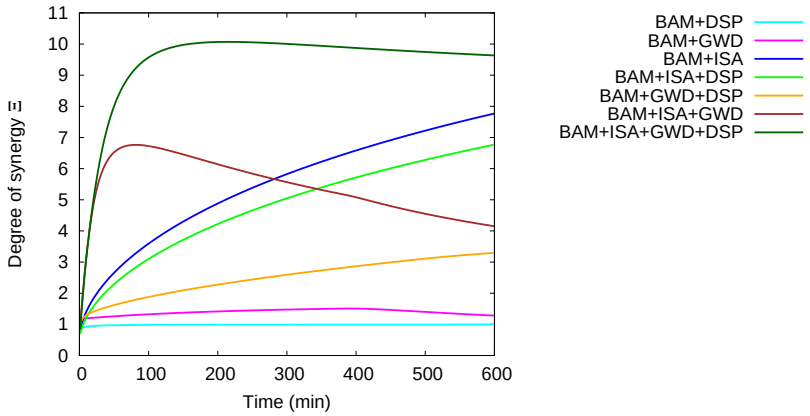

Figure 3.6: **Degrees of synergy change during starch degradation**. The glucan release for the enzyme sets is normalized according to the definition of the degree of synergy, Eq. (3.2) at p. 65, summing the release of the individual members in the denominator. Exactly the same data set as in Fig 3.4b is used.

in the early phase of degradation. The peak is slightly increased and delayed if the phosphate ester is consistently positioned more closely to the branching point (higher posP!), but qualitatively the curves are similar. Thus, the model confirms that reversible phosphorylation has unambiguously a positive effect, but in addition to that it allows to suggest a refinement: namely that reversible phosphorylation is especially important for a rapid onset of degradation, which allows for roughly the 3-fold amount of glucosyl residues to be mobilized in comparison to hydrolysis alone. Physiologically, a rapid switch from starch synthesis to degradation could be important for the diurnal regulation of carbon allocation (Graf et al., 2010).

Time course of variables. Finally, we take a look at how the reactants and the associated interfacial quantities change during degradation and discuss the fitted kinetic parameters.

Figure 3.8a confirms that the major products released are maltose and maltotriose with considerably less maltotriose (Edner et al., 2007). Phosphoglucans with a phosphate ester close to the non-reducing end (pGx) are also present but only in minute concentrations not visible in the plot. Much higher levels of maltose compared to other malto-oligosaccharides are also found *in vivo* in wild type *Arabidopsis* leaves (Critchley et al., 2001).

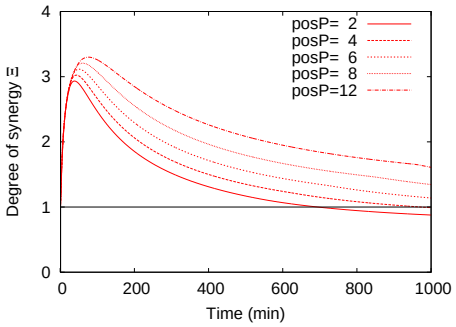

Figure 3.7: **Stimulatory effect of reversible phosphorylation is mainly in the early phase of starch mobilization**. The time-dependency of the degree of synergy Ξ of the full enzyme set relative to the (hydrolytic) subset {BAM, ISA} is shown. Values above $\Xi = 1$ indicate stimulation. The curves differ in the phosphate position. Simulations are done with the model including helix-coil melting.

Figure 3.8b shows an effectively linear decrease of helical glucans with a concomitant increase in partially degraded phosphoglucans. The remaining reactants make up only around 1% of the surface. This suggest that DSP-catalyzed hydrolysis of phosphate esters may become more and more limiting for exo-acting amylases during the course of reaction.

In Fig. 3.8c the temporal change in the surface-bound fractions of the rapid equilibrium segments are shown. The adsorption reaction is in equilibrium, which has been tested and confirmed during numerical integration by simultaneously printing out a term which has to be one after an initial transient. During most of the time span (until ≈600 min) the equilibria of GWD and pGWD do not shift. *In vitro* experiments show that a virtually constant partition of enzymes between both phases is reached after approximately ten minutes, which is very rapid compared to catalytic turnover (M. Hejazi, pers. comm.).

GWD is almost exclusively in the soluble phase, that is the unphosphorylated form desorbs very quickly and is not residing at the interface in significant amounts. In contrast to that, pGWD is almost exclusively localized at the interface (corresponding f^* ≈100%). This is reasonable, since otherwise pGWD could become hydrolyzed and the catalytic cycle would burn ATP without turning over carbohydrates (Hejazi et al., 2010). Approximately 40% of BAM

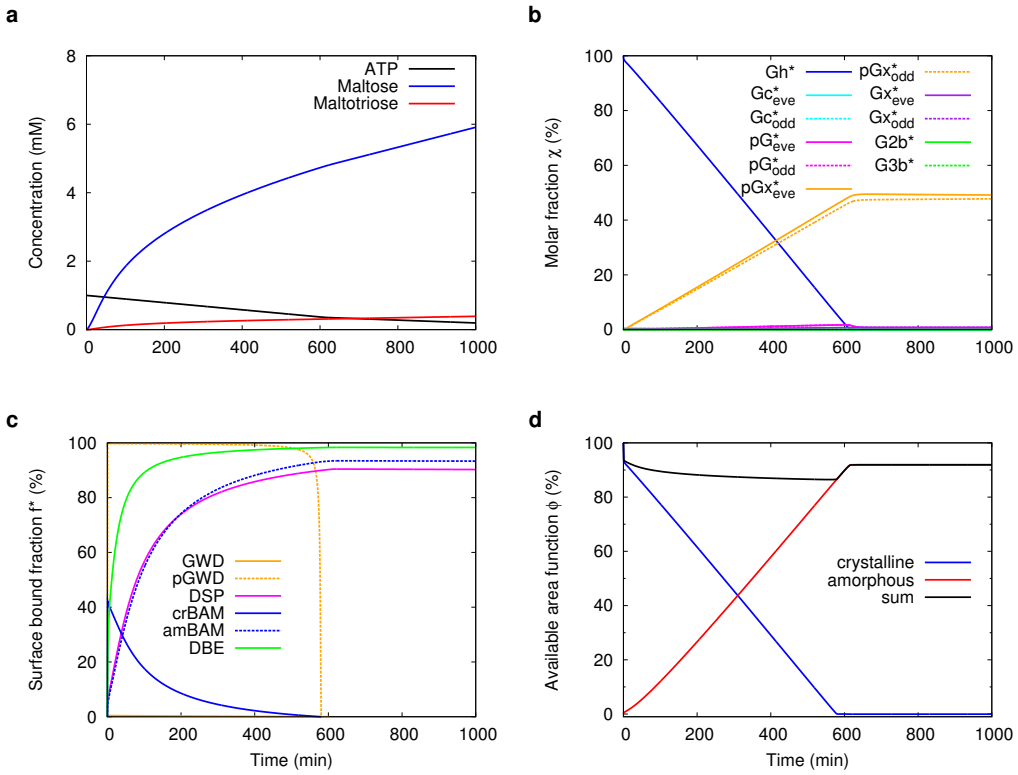

Figure 3.8: **Temporal evolution of soluble and interfacial quantities in *in vitro* starch degradation**. **a**, Major forms of carbohydrates in the soluble phase are maltose and, to a smaller extent, maltotriose. Partially digested phosphoglucans (pGx) are also present, but the very small amounts are not visible at the range of the plot. **b**, At the interface the fraction of helical glucans (Gh*) decreases linearly accompanied by a significant increase only in the partially digested phosphoglucan side-chains (pGx*, both even and odd in similar amounts). **c**, The adsorbed fractions of the rapid equilibrium segments are shown. The colors distinguish the enzymes. Note, that GWD and pGWD belong to separate segments, while both the crystalline- and amorphous-bound BAM belong to the same segment, see the mechanisms in the last chapter. See the discussion in the main text for the behavior around 600 min. **d**, The free crystalline area decreases while the amorphous area increases almost at the same rate. The sum shows the slow change in the total available area indicating that throughout the reaction approximately 10% of the interface is occupied by enzymes.

is adsorbed at crystalline regions in the beginning, a value which decreases with decreasing crystallinity of the surface (see Fig. 3.8d). Concomitantly, BAM localized to amorphous patches increases. Interestingly, it does so at the same rate as DSP, although the dissociation constants (see Table 3.3) and their $e^{*\max}$ values differ. Presumably this dynamic pattern reflects the tight cooperation between both enzymes, where BAM produces from phosphoglucans (pG*) the preferred substrate (pGx*) of DSP, and DSP has to act in order to produce Gx*. The surface bound fraction of the debranching enzyme is steadily increasing to almost 100%.

Figure 3.8d shows that the available area on the crystalline phase changes complementary to that associated with the amorphous phase. The curve showing the sum indicates that approximately only 10% of the total available area is occupied by enzymes throughout degradation.

At around 600 min, the time when the crystalline region almost vanishes, a sharp transition takes place in the fractional concentration factors, where I encountered some numerical problems with negative values which I could not resolve. Presumably, this is related to the stiffness of the ODE system, since different time scales are considered simultaneously. Therefore, a cautionary remark regarding the trajectories after this time point is necessary although in some simulations done with other parameter sets this problem was not observed.

It seems most probable, however, that the QSS assumptions force the simulation to comply with conservation relations which may produce negative values when the crystallinity (i.e. χ_{h}^*), hence the associated fractional concentration factors for crBAM and GWD, approach zero. There is an indication that indeed this is the reason: I tried the option `NonNegative` of the MATLAB ODE solver to force non-negative values with the result that this violated conservation relations, for example the available area function increased above one. It may be that at low values of crystallinity changes in the quasi-steady state concentrations of the enzyme-complexes are not negligible anymore (see Eq. 3.21a at p. 76, where this was assumed). As already mentioned, approximations exploiting time scale considerations are powerful but never valid throughout the whole reaction progress. Singular perturbation techniques (Bender and Orszag, 1999) can be used to analyze when certain

approximations break down. See also the discussion in Ciliberto et al. (2007) for these issues especially relating to conserved quantities.

Regarding the kinetic parameters shown in Table 3.3 we will focus attention on the comparison of affinities to interfacial substrates (i.e. the interfacial K^*_{m} values) which are shared among enzymes. For example, the simulations suggest that Gc* and Gx* are more readily bound by BAM than by ISA. BAM has also a higher affinity to long phosphoglucans (pG*) than DSP and ISA. On the other hand, partially degraded phosphoglucans are bound rather by DSP than by ISA, whereas BAM is rather inhibited by these (small value of q^*_{pGx}, see rate equation denominator, p. 47) and by the β-limit dextrin like stubs (q^*_{Gb}).

3.4 Discussion

Summary. This chapter demonstrates the applicability of interfacial rate laws developed in Chapter 2. To this end a kinetic model is formulated in Section 3.2. The analysis of interfacial processes in Section 3.3 suggests the existence of spontaneous helix-coil transitions of the interfacial amylopectin side-chains as a mechanistic explanation for the experimentally observed (Edner et al., 2007; Kötting et al., 2009) synergistic effect when dikinase, phosphatase, as well as exo- and endo-amylases act in concert. Based on the model results, a reasonable guess is that reversible phosphorylation is especially effective in initiating starch mobilization whereas in the long run the hydrolytic enzymes take over.

The preceding section has demonstrated that the rate laws proposed can be used to describe biochemical reactions at interfaces. Although some uncertainties about the parameter values remain, it is possible to reproduce, at least semi-quantitatively, experimental findings. To verify the reliability of the rate laws and analyze some basic characteristics of the interfacial reactions it was necessary to exploit the best data available which is why I restricted myself to *in vitro* experiments. To my knowledge, this is the first model of starch degradation which thoroughly studies interfacial dynamics and considers the cooperation of starch-degrading enzymes. Since it relies on the rate laws derived by myself it is of course also the first one using rate laws with the

Table 3.3: Comparison of coarsely fitted kinetic parameters for simulation of *in vitro* starch degradation. N/D Not Defined.

Parameter[†]	**GWD**	**DSP/SEX4**	**BAM**	**DBE/ISA**
k_{cat}	$k_{\mathrm{aut}} = 10^3$ $k_{\mathrm{leak}} = 10^{-2}$	1	10^3	N/D
k^*_{cat}	5	1	10^3	10^3
[‡]$\widetilde{K}^{\mathrm{cr}}_{\mathrm{d}}$	GWD: 1 pGWD: 10^{-5}	N/D	10^{-2}	N/D
$\widetilde{K}^{\mathrm{am}}_{\mathrm{d}}$	N/D	10^{-3}	$5 \cdot 10^{-4}$	10^{-4}
K_{atp}	10^{-3}	N/D	N/D	N/D
K_{G}	N/D	N/D	10^{-2}	N/D
K_{Gx}	N/D	N/D	10^{-2}	N/D
K_{pG}	N/D	10^{-1}	10^{-2}	N/D
K_{pGx}	N/D	10^{-2}	N/D	N/D
q_{md}	N/D	1	N/D	N/D
q_{mt}	N/D	N/D	10^1	N/D
$K_{\mathrm{i,G}}$	N/D	10^{-3}	N/D	N/D
$K_{\mathrm{i,Gx}}$	N/D	10^{-3}	N/D	N/D
K^*_{Gh}	10^{-3}	N/D	10^4	N/D
K^*_{Gc}	N/D	N/D	10^{-2}	10^5
K^*_{Gx}	N/D	N/D	10^{-1}	10^5
K^*_{G3b}	N/D	N/D	N/D	10^{-4}
K^*_{G2b}	N/D	N/D	N/D	10^{-4}
K^*_{pG}	N/D	1	10^{-1}	10^5
K^*_{pGx}	N/D	10^{-6}	N/D	10^5
q^*_{Gb}	N/D	N/D	10^{-4}	N/D
q^*_{pGx}	N/D	N/D	10^{-2}	N/D
$K^*_{\mathrm{i,Gb}}$	N/D	N/D	10^{-5}	N/D
$K^*_{\mathrm{i,pGx}}$	N/D	N/D	10^{-5}	N/D

[†] Simulations were carried out using the units μmol, g, cm throughout. For the dimensions see Sections 2.3.1–2.3.4 describing the rate laws. Usually, parameters have dimensions associated with the reaction space in which the interactions take place.

[‡] $K_{\mathrm{d},j} = \widetilde{K}_{\mathrm{d},j}/e^{*\,\max}_j$

available area function.

A general observation is that there exist almost no kinetic models of chloroplast metabolism which incorporate starch breakdown at all (Morgan and Rhodes, 2002; Rios-Estepa and Lange, 2007). In Poolman et al. (2000), for example, starch breakdown is considered as a single (moreover phosphorolytic!) step. The absence of mathematical models which consider the reactions at the interface explicitly is of course due to the fact that these processes were simply unknown until very recently. Surely, the coming years will evidence an increasing effort to tackle this system with modeling.

The degree of synergy, is a quantity which frequently has been studied in cellulose degradation (Zhang and Lynd, 2004). Both, Converse and Optekar (1993) and Zhang and Lynd (2006) are good examples and suggest further investigation of the starch system, for example the dependence of synergistic kinetics on enzyme loading. Here, it has been studied how it depends on reaction time, different enzyme combinations and the phosphate position.

As the elucidation of the role of interfacial enzymes in starch metabolism is ongoing, new physiological problems will emerge, which can hopefully be tackled by the methods provided here.

Chapter 4

Carbohydrate-active enzymes exemplify entropic principles in metabolism

> Eine Theorie ist desto eindrucksvoller, je größer die Einfachheit ihrer Prämissen ist, je verschiedenartigere Dinge sie verknüpft und je weiter ihr Anwendungsbereich ist. Deshalb der tiefe Eindruck, den die klassische Thermodynamik auf mich machte. Es ist die einzige physikalische Theorie allgemeinen Inhalts, von der ich überzeugt bin, daß sie im Rahmen der Anwendbarkeit ihrer Grundbegriffe niemals umgestoßen werden wird (zur besonderen Beachtung der grundsätzlichen Skeptiker).
>
> Albert Einstein (1870 - 1955)

The nocturnal breakdown of transitory starch provides dissolved malto-oligosaccharides (MOS) which are further metabolized in stroma and cytosol to support downstream pathways like glycolysis and sucrose synthesis. In this respect, it is noteworthy that many reactions taking place in MOS metabolism consist only of transfers of glucosyl residues. The plastidial 4-α-

glucanotransferase (GTase) shuffles glucosyl residues mainly between two maltotrioses to produce glucose and maltopentaose as a substrate for BAM (Critchley et al., 2001). Maltose is the primary product of starch degradation directed to the cytosol (Niittylä et al., 2004), while only a minor fraction is exported as glucose. Intriguingly, a second cytosolic GTase takes up maltose immediately, producing glucose and transferring the second glucosyl residue to a heterogeneous pool of soluble glycans (Fettke et al., 2006, 2009b). Yet another transferase, albeit phosphorolytic, is able to withdraw the glucosyl residue in the form of Glucose-1-phosphate (G1P), which is fed into central metabolism. Certainly, this shuffling of glucose is not superfluous in an evolved system, however, to this date there is no conclusive theory regarding the regulatory role of such a pathway design. The enzymes themselves seem to be unregulated although DPE2 and α-glucan-phosphorylase are subject to post-translational modifications (Kötting et al., 2010). Moreover, these enzymes are relatively unspecific with respect to the size of the α-1,4-linked glucans and thus cannot be associated with any single reaction. Thus, one has to take into account the whole reaction system mediated by GTases.

The following chapter outlines a way to consistently characterize carbohydrate-active transferases and the associated reaction systems. Although their importance is recognized, glycans are notoriously difficult to analyze due to their structural and functional diversity (Seeberger, 2005). This is mirrored by the versatile action patterns of CAZymes, which accept structurally distinct glycans as substrates and often act iteratively. A combinatorial explosion of reactions is observed, making classical enzyme assays problematic. In Section 4.2 a statistical thermodynamics approach is proposed, which elucidates the pivotal role of entropy for both the equilibrium and temporal patterns of these reaction systems. Each reactant is interpreted as an energy level, transitions between which are constrained by the enzymatic mechanisms. Application to combinations of *in vitro* assays of polymer-active CAZymes essential for carbon metabolism in plants confirmed the dominance of entropic gradients (Section 4.3). Supported by stochastic simulations our results suggest how randomization of metabolites may contribute to robustness of metabolic functions (Section 4.4).

Based on the theoretical predictions, the experiments were designed and

conducted together with Sebastian Mahlow from AG Steup, University of Potsdam. It is appropriate here to emphasize that a much larger part of the experimental work is due to him. Details on the experiments are given in Appendix B. On the theoretical side there was a fruitful interaction with Oliver Ebenhöh and Alexander Skupin.

4.1 Introduction

Background. Polysaccharides constitute the most abundant biopolymers found in nature but are far less investigated than proteins and nucleic acids. They govern a remarkably wide range of functions, including carbon and energy storage (Ball and Morell, 2003; Zeeman et al., 2010), mechanical stabilization of cells or tissues (Cosgrove, 2005), cell-cell or cell-protein interactions (Varki, 2007) and organelle division (Yoshida et al., 2010). They have recently attracted considerable interest as renewable energy source (Himmel et al., 2007; Zeeman et al., 2010), and serve as starting materials or additives for many technological applications (Takaha and Smith, 1999).

Biosynthesis and -degradation of polysaccharides involve the concerted action of numerous CAZymes (Cantarel et al., 2009; Davies and Henrissat, 2002), each of which can act on an enormous number of distinct substrates (Coutinho et al., 2003). They typically catalyze a very specific reaction *pattern* and as a result, catalyze a complex network of reactions involving a potentially infinite number of different chemical species. Evidently, a classical description in terms of Michaelis-Menten parameters and a single thermodynamic equilibrium constant is insufficient to describe the complex reaction patterns and the resulting equilibrium distributions. Nevertheless, this simplistic approach was applied for example in Schmidt and John (1979), where bacterial glucanotransferases were incubated with varying amounts of maltodextrins of different lengths and glucose levels observed after a certain incubation time (10–30 minutes) were taken as a measure of the reaction velocity. From the resulting Lineweaver-Burk plots, Michaelis parameters $v_{\max}$ and K_{m} were estimated. However, the observed glucose levels depend on the concerted action of *all* proceeding reactions, regardless whether they act on the initially applied substrate or re-utilize products of previous reactions. Moreover, the apparent $v_{\max}$ values are biased

by the fact that the equilibrium distribution is different for different initial substrates. Similarly, the K_m values do not only reflect binding affinities of the initially applied substrate but result from a multitude of reactions. Taking these difficulties into account, it becomes apparent that interpretations of parameters derived in analogy to classical, highly substrate specific enzymes are problematic.

Comprehensive models based on differential equations would require the introduction of one equation for each substrate species which is unfeasible due to potentially infinite numbers. Novel rule-based approaches (Feret et al., 2009) have intended to overcome this limitation and increase numerical tractability, but despite a vast amount of experimental studies (Colleoni et al., 1999b; Jones and Whelan, 1969; Kakefuda and Duke, 1989; Lin and Preiss, 1988; Steichen et al., 2008) and some attempts to model the kinetics of CAZymes (Allen and Thoma, 1976a,b; Nakatani, 1999; Thoma, 1976; Thoma et al., 1971), a generally applicable theoretical description is still lacking.

Systems with potentially infinite states are consistently described in the framework of statistical thermodynamics (Landau and Lifschitz, 1979). Interpreting the distinct chemical species as different energy states, the reactant mixture can be described as a statistical ensemble (Alberty, 2003; Flory, 1944). In this thermodynamic view, enzymes mediate transitions between different states and the enzymatic mechanisms define how these transitions are constrained. This concept allows the development of a consistent formalism in which the entropy of the entire reactant mixture is highlighted as an important thermodynamic driving force of the reactions. To develop and experimentally validate our concept, we focus on enzymatic interconversion of α-1,4-D-glucans. Each distinct substrate, hence different energy state, can be characterized by the number of glucose residues, denoted as degree of polymerization (DP). This offers a straightforward generalization to reaction systems in which bond enthalpy is not conserved. Taking the energies of formation into account, the equilibrium is determined by a minimum in Gibbs free energy (Alberty, 2003). A generalization to other glucans and transferases is straightforward.

While former applications of minimizing the Gibbs energy are restricted to single reactions or based on numerical methods (Alberty, 2003), our approach enables analytic solutions even for complex systems where it is essential to

take into account all constraints of the system, including those arising from the enzymatic mechanisms. Thus, we show that the equilibrium distributions of CAZymes can be characterized uniquely by the coefficient β of the resulting Boltzmann-like distribution of degrees of polymerization, which serves as a generalization of equilibrium constants.

4.2 Development of the theoretical approach

In this section, we provide a deductive derivation of the proposed formalism. As a starting point we use a general formula for the Gibbs free energy of a mixture of dilute solutions in water. With this strategy, we first develop a general formalism and subsequently apply this formalism in Section 4.3 to arrive at formulas valid for different plant CAZymes of importance in starch degradation.

4.2.1 Background

The second law of thermodynamics implies that in an isolated system the entropy can only increase and assumes a maximum if the system is in equilibrium. As a consequence, a chemical reaction taking place in an isolated system (a reaction without heat production), the driving force must be an increase in entropy.

For a closed system σ, which is in contact to a thermal reservoir Θ the total change of entropy is the sum of the changes of entropy in the system and its environment (see for example Craig, 1992),

$$\Delta S_{\text{tot}} = \Delta S_\sigma + \Delta S_\Theta. \tag{4.1}$$

The change of entropy in the reservoir at a given temperature T is given by

$$\Delta S_\Theta = \frac{\Delta U_\Theta}{T}, \tag{4.2}$$

where the internal energy U_Θ of the reservoir is a thermodynamic state variable. If additionally the pressure p is constant, as is usually assumed for biochemical reactions, then the change in reservoir energy is exclusively derived from enthalpy changes within the reaction system, $\Delta U_\Theta = -\Delta H_\sigma$. Thus, for closed

chemical reaction systems the second law asserts that

$$\Delta S_{\text{tot}} = \Delta S_\sigma - \frac{\Delta H_\sigma}{T} \geq 0. \tag{4.3}$$

In equilibrium, $\Delta S_{\text{tot}} = 0$ and the total entropy is maximized, $S_{\text{tot}} \to \max$. With the definition of the Gibbs energy of the reaction system,

$$G_\sigma = H_\sigma - TS_\sigma, \tag{4.4}$$

the equilibrium condition that the total entropy is maximized can equivalently be formulated as the condition that the Gibbs energy of the system is minimized, $G_\sigma \to \min$.

4.2.2 General formalism

Gibbs energy of a dilute solution mixture and generalised mixing entropy. We begin with a general expression for the Gibbs energy of a dilute solution in which different substances i are dissolved with n_i moles in N moles solvent (Landau and Lifschitz, 1979, Eq. (87,3)):

$$G = N\mu^\circ + RT \sum_i n_i \ln \frac{n_i}{eN} + \sum_i n_i \psi_i, \tag{4.5}$$

where e is Euler's number, R is the universal gas constant, T the temperature and μ° is the chemical potential of the pure solvent. The constants ψ_i are independent of the concentrations and are characteristics of the solutes i. They are directly related to the chemical potentials μ_i which, by definition, are given by

$$\mu_i = \frac{\partial G}{\partial n_i} = RT \ln \frac{n_i}{N} + \psi_i. \tag{4.6}$$

To introduce common units of concentrations, we denote by c° the concentration of the solvent and by c_i the concentration of the solutes, measured in the same standard unit. Typically, concentrations are measured in moles per liter (M), resulting in $c^\circ = 55.5\text{M}$ for pure water. The quantities of the concentrations are related to the particle numbers quantified in moles by

$$\frac{c_i}{c^\circ} = \frac{n_i}{N}. \tag{4.7}$$

This implies that for a solute present in one standard unit concentration ($c_i = 1\text{M}$), $n_i/N = 1/c^\circ$. Thus, according to Eq. (4.6), the *standard* chemical

potential of solute i reads

$$\mu_i^0 = \psi_i - RT \ln c^\circ. \tag{4.8}$$

Therefore, Eq. (4.5) can be written as

$$\begin{aligned} G &= N \cdot \left[\mu^\circ + RT \sum_i \frac{c_i}{c^\circ} \left(\ln \frac{c_i}{c^\circ} - 1 \right) + \sum \frac{c_i}{c^\circ} \psi_i \right] \\ &= \frac{N}{c^\circ} \cdot \left[c^\circ \mu^\circ + \sum_i c_i \mu_i^0 + RT \sum_i c_i \left(\ln c_i - 1 \right) \right]. \end{aligned} \tag{4.9}$$

The expression

$$G^{\mathrm{f}} = \frac{N}{c^\circ} \left[c^\circ \mu^\circ + \sum_i c_i \mu_i^0 \right] \tag{4.10}$$

depends only on the *standard* chemical potentials of the solvent and solutes scaled by their respective concentrations. The value of G^{f}, however, is independent on the fact whether the substances are present in a mixture or in separate containers. To illustrate how the Gibbs energy changes as a result of mixing various solutions, we consider K different containers with N/K moles solvent. In each container only one type of solute is dissolved with concentration Kc_i. The Gibbs energies of the separate containers are

$$G_i = \frac{N}{Kc^\circ} \left[c^\circ \mu^\circ + Kc_i \mu_i^0 + RT\, Kc_i \left(\ln Kc_i - 1 \right) \right]. \tag{4.11}$$

After mixing these containers, the resulting mixture will contain N moles solvent in which the K different solutes are dissolved with concentrations c_i. Due to the mixing process, the Gibbs energy will decrease,

$$\Delta_{\mathrm{mix}} G = G - \sum_i G_i = -RT \frac{N \ln K}{c^\circ} \sum_i c_i = -T \Delta \tilde{S}_{\mathrm{mix}}. \tag{4.12}$$

This decrease of Gibbs energy results from an increase in mixing entropy. Defining

$$\tilde{S}_{\mathrm{mix}} = -R \frac{N}{c^\circ} \sum_i c_i \left(\ln c_i - 1 \right), \tag{4.13}$$

and using (4.10) allows to compactly rewrite Eq. (4.9) as

$$G = G^{\mathrm{f}} - T \tilde{S}_{\mathrm{mix}}. \tag{4.14}$$

This notation illustrates the two contributions to the Gibbs energy resulting from the mere *abundance* (G^{f}) of the substances in solution and their *mixing*

($\tilde{S}_{\mathrm{mix}}$). This separation of the Gibbs energy is only defined up to an additive constant. Simultaneously redefining $G^{\mathrm{f}} \to G^{\mathrm{f}} - k$ and $\tilde{S}_{\mathrm{mix}} \to \tilde{S}_{\mathrm{mix}} + k$ leaves Eq. (4.14) unchanged and also does not influence the position of the extrema.

Since G and $\tilde{S}_{\mathrm{mix}}$, as defined in Eqs. (4.10) and (4.13), are extensive quantities directly proportional to the total system size, extremal values do not depend on the volume. Without loss of generality we therefore consider systems with one standard unit volume and in the following set $N = c^{\circ}$.

Chemical reactions in a mixture of solutions. Consider the general chemical reaction

$$\sum_i \nu_i A_i = 0, \tag{4.15}$$

in which A_i are the involved chemical species and the ν_i are the stoichiometric coefficients, denoting how many molecules are consumed (negative) or produced (positive) per reaction. Introducing the extent of reaction, ζ, the concentration changes that result from an infinitesimal progress in the reaction are given by $\mathrm{d}c_i = \nu_i \mathrm{d}\zeta$. Thus, the associated change in Gibbs energy (4.14) is

$$\begin{aligned} \mathrm{d}G &= \mathrm{d}G^{\mathrm{f}} - T\mathrm{d}\tilde{S}_{\mathrm{mix}} \\ &= \left[\sum_i \nu_i \mu_i^0 - T\left(-R\sum_i \nu_i \ln c_i\right)\right]\mathrm{d}\zeta. \end{aligned} \tag{4.16}$$

The contribution $\mathrm{d}G^{\mathrm{f}}$ reflects the changes of the Gibbs free energies as a result from the chemical conversion of substances. This quantity is independent on the amount of chemical species. The concentration dependent contribution $-T\mathrm{d}\tilde{S}_{\mathrm{mix}}$ takes into account that the composition of the reaction mixture, and thus the mixing entropy, will also change as a result of the chemical reactions. By definition, the Gibbs free energy of reaction is

$$\begin{aligned} \Delta_{\mathrm{r}}G := \frac{\partial G}{\partial \zeta} &= \sum_i \nu_i \mu_i^0 - T\left[-R\sum_i \nu_i \ln c_i\right], \\ &= \Delta_{\mathrm{r}}G^0 - T\Delta_{\mathrm{r}}\tilde{S}_{\mathrm{mix}}. \end{aligned} \tag{4.17}$$

The *standard* Gibbs free energy of reaction,

$$\Delta_{\mathrm{r}}G^0 = \sum_i \nu_i \mu_i^0, \tag{4.18}$$

holds when all reactants are present in one unit concentration. In this case, $\Delta_\mathrm{r}\tilde{S}_\mathrm{mix} = 0$.

It is important to note that the entropy change $\Delta_\mathrm{r}\tilde{S}_\mathrm{mix}$ exclusively results from the change of the composition of the reaction mixture as a consequence of the chemical reaction. This expression does not include the *molar* entropies, s_i, which reflect the dispersal of energy within the molecules and which, of course, do also contribute to the Gibbs free energy in quantities proportional to the respective amounts of chemical species. However, the effect of molar entropy change is implicitly taken into account via the term G^f: The standard molar entropies, s_i^0, are related to the standard Gibbs energies of formation, $\Delta_\mathrm{f}G_i^0$, by

$$\Delta_\mathrm{f}G_i^0 = \Delta_\mathrm{f}H_i^0 - Ts_i^0, \tag{4.19}$$

where the $\Delta_\mathrm{f}H_i^0$ are the standard enthalpies of formation. Further, the standard Gibbs free energy of reaction is related to the standard Gibbs energies of formation by

$$\Delta_\mathrm{r}G^0 = \sum_i \nu_i \Delta_\mathrm{f}G_i^0. \tag{4.20}$$

Comparing this expression with Eq. (4.18) shows that

$$\mathrm{d}G^\mathrm{f} = \left(\sum_i \nu_i \Delta_\mathrm{f}G_i^0\right) \mathrm{d}\zeta. \tag{4.21}$$

Therefore, G^f can be expressed as

$$G^\mathrm{f} = const. + \sum_i c_i \Delta_\mathrm{f}G_i^0 \tag{4.22}$$

demonstrating how this quantity includes the molar entropies through the Gibbs energies of formation. It is highly useful to express the Gibbs free energy as

$$G = const. + \sum_i c_i \Delta_\mathrm{f}G_i^0 - T\tilde{S}_\mathrm{mix}, \tag{4.23}$$

because the energies of formation $\Delta_\mathrm{f}G_i^0$ represent experimentally accessible and tabulated quantities. Note, that the energies of formation encompass properties of the solvent like pH, temperature and ionic strength. If their values have to be considered as independent (or reservoir) variables, appropriate thermodynamic potentials can be defined by Legendre transforms. See Alberty (2003) for an excellent elaboration on this.

4.2.3 General solution and equivalence to law of mass action

To demonstrate that the presented formalism is equivalent to the classical treatment of reaction equilibria, and to illustrate how chemical equilibria can be determined in general by our formalism, we again consider a general reaction of the form (4.15). This reaction implies a constraint on the values of the concentrations, since they cannot change completely arbitrary. This constraint is most generally written in terms of a conserved quantity

$$\sum_i q_i c_i = C, \tag{4.24}$$

where the coefficients q_i are determined through the condition (see e.g. Heinrich and Schuster, 1996)

$$\sum_i q_i \nu_i = 0. \tag{4.25}$$

In equilibrium, G assumes a minimum. Therefore, the equilibrium concentrations can be identified by determining the minimum of G under the constraints given by Eq. (4.24). This can be achieved using the method of Lagrangian multipliers. We define the function

$$L(c_i;\alpha) = \sum_i c_i \mu_i^0 + RT \sum_i c_i(\ln c_i - 1) - \alpha \left(\sum q_i c_i - C \right). \tag{4.26}$$

A necessary condition for the minimum of G under the given constraints is that all partial derivatives vanish:

$$0 = \frac{\partial L}{\partial c_i} = \mu_i^0 + RT \ln c_i - \alpha q_i. \tag{4.27}$$

Thus

$$0 = \sum_i \nu_i \frac{\partial L}{\partial c_i} = \sum_i \nu_i \mu_i^0 + RT \sum_i \nu_i \ln c_i - \alpha \sum_i q_i \nu_i. \tag{4.28}$$

The last term equals zero because of relation (4.25). With Eq. (4.18) it follows that

$$\Delta_\mathrm{r} G^0 + RT \sum_i \nu_i \ln c_i = 0 \quad \Leftrightarrow \quad \prod_i c_i^{\nu_i} = e^{-\frac{\Delta_\mathrm{r} G^0}{RT}}, \tag{4.29}$$

which is identical to the law of mass action. Of course, the formalism is consistent with $\Delta_\mathrm{r} G = 0$ in equilibrium as is clear from a comparison of (4.29) with (4.17).

4.2.4 Systems with constant numbers of reactants

For a reaction system which conserves the total number of reactants, $c^{\mathrm{tot}} = \sum c_i$ is constant. The equilibrium distribution can be found by identifying the minimum of the molar Gibbs energy

$$g = \frac{G}{c^{\mathrm{tot}}} = \frac{c^{\circ}\mu^{\circ}}{c^{\mathrm{tot}}} + \sum_i \frac{c_i}{c^{\mathrm{tot}}}\mu_i^0 + RT\sum_i \frac{c_i}{c^{\mathrm{tot}}}(\ln\frac{c_i}{c^{\mathrm{tot}}} + \ln c^{\mathrm{tot}} - 1). \qquad (4.30)$$

Introducing the molar fractions $\chi_i = c_i/c^{\mathrm{tot}}$, this can be compactly written as

$$g = const. + \sum_i \chi_i\mu_i^0 + RT\sum_i \chi_i \ln\chi_i = const. + \sum_i \chi_i\Delta_{\mathrm{f}}G_i^0 - TS_{\mathrm{mix}}, \quad (4.31)$$

where, in analogy to Eq. (4.23), the standard Gibbs energies of formation, $\Delta_{\mathrm{f}}G_i^0$, and the entropy of mixing,

$$S_{\mathrm{mix}} = -R\sum_i \chi_i \ln\chi_i, \qquad (4.32)$$

have been introduced.

This description highlights the equivalence of a chemical reaction system with conserved total number of reactants and the well-known Boltzmann distribution for identical particles in statistical physics. The reacting molecular species i represent different energy states with the associated energy $\Delta_{\mathrm{f}}G_i^0$. Correspondingly, the molar fractions χ_i can be interpreted as the probabilities that a particle is in state i.

This analogy is very powerful since the complete mathematical formalism that has been developed for statistical physics can directly be applied to such reaction systems. However, the reaction systems considered here in general underlie further constraints imposed by the stoichiometries of the enzyme catalyzed reactions.

4.2.5 Systems with conserved energy

A special class of reaction systems is realized by enzymes catalyzing energetically neutral reactions (as the disproportionating enzymes, see section 4.3 below), for which the *standard* Gibbs energy of reaction, $\Delta_{\mathrm{r}}G^0$, equals zero (Tewari et al., 1997). In this case, the sum of the Gibbs energies of formation remains constant and Eq. (4.31) further simplifies to

$$g = const. - TS_{\mathrm{mix}}. \qquad (4.33)$$

It becomes apparent that in this kind of system the equilibrium is exclusively determined by a maximum of the entropy of mixing S_{mix}. Without further constraints, a uniform distribution of concentrations over all possible species i would be expected. However, due to the chemical constraints, this is in general not the case. The structure of the constraints considered here (conservation of inter-molecular bonds) leads to a distribution of the exponential family and can be specified as a Boltzmann distribution, since a reflecting boundary condition holds (we will see what that means). Here, the total (conserved) number of bonds assumes an analogous role to the total energy of an isolated system of identical particles, which is characterized by the system's temperature. We will exploit this analogy in the next section for the calculation of equilibrium distributions of selected systems.

4.3 Application to plant CAZymes

The example systems discussed in this section all act on polydisperse mixtures of α-1,4 linked polyglucans. Every different polyglucan is uniquely identified by its degree of polymerization, DP. Throughout this section, we will denote the molar fractions by χ_k, where k denotes the number of α-1,4-glucosidic *linkages*, which means that $k = \text{DP} - 1$. We introduce this notation for convenience to exploit the analogy to statistical thermodynamics, where usually the state with the lowest energy carries the index 0. Here, χ_0 denotes the molar fraction of glucose, the simplest molecule within the polydisperse mixture possessing no inter-sugar linkage. All CAZymes discussed are important in plant carbon metabolism and their characterization is backed up with experimental verifications of the predictions. We will start with the paradigmatic case of DPE1.

4.3.1 Disproportionating enzyme 1 (DPE1)

Background. In bacteria and plants the transfer of glucosyl chains between α-1,4-D-glucans is an integral part of glucan metabolism. The corresponding enzymes are members of the glycoside hydrolase family 77 and classified as α-1,4-glucanotransferases (GTase, EC 2.4.1.25). Since the first discovery in potato juice, plant biologists are more familiar with the term dispropor-

tionating enzyme or D-Enzyme (Peat et al., 1953), while in bacteria similar enzymes with a different action pattern are often designated as amylomaltases. A fairly comprehensive review of the characteristic action pattern of GTases with different specificities is given in Takaha and Smith (1999).

Basically, a pair of saccharides yields a disproportionated pair of products in a bi-bi reaction, retaining the overall number of α-1,4-linkages and glucose residues. The readily reversible reactions can be written as

$$\mathrm{G}_n + \mathrm{G}_m \rightleftharpoons \mathrm{G}_{n-x} + \mathrm{G}_{m+x}, \tag{4.34}$$

where the index denotes the DP and $x = 1, 2, 3$ is the number of transferred glucosyl residues. In this scheme, G_n represents the glucosyl donor, whereas G_m figures as the acceptor molecule, the equality $n = m$ being allowed in general.

The prevalent mechanistic model of the catalytic cycle largely stems from detailed structural studies on glucanotransferases from bacteria, especially from the genus *Thermaceae* (Barends et al., 2007). The ping-pong mechanism (Segel, 1993) is briefly summarized in Scheme 4.1, not going too much into detail. Most notably, the mechanism shows that acceptor binding can be thought of as an integral part of catalyzing the disproportionation reaction, avoiding hydrolysis to occur.

Equilibrium distribution. The reaction system consisting of all reactions of type (4.34) is constrained by two conserved quantities. Every reaction converts two substrate molecules in two product molecules and thus the total number of reactant molecules is conserved. Further, in every elementary step one α-1,4-glucosidic linkage is opened and another is formed. Thus, the total number of linkages also remains constant. With the notation introduced above, these constraints can be written as

$$\sum_k \chi_k = 1 \tag{4.35}$$

$$\sum_k k \cdot \chi_k = b. \tag{4.36}$$

Here, b is the average number of linkages. This number is defined by the average degree of polymerization, $\mathrm{DP}_{\mathrm{ini}}$, of the initially applied substrates. If,

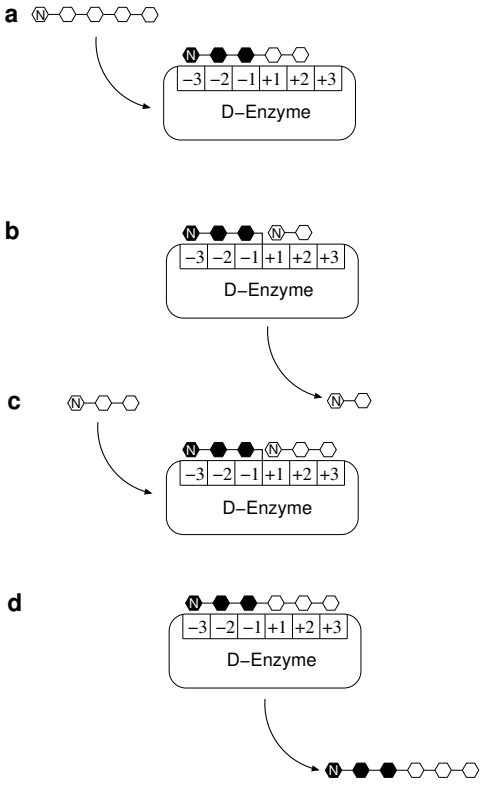

Figure 4.1: **Mechanism of D-enzyme (DPE1)**. **a**, Upon binding the donor (G_n) a positional isomer is formed, in which the more or less random alignment of the polymer defines the scissile glucosidic bond x (counted from the non-reducing end N) between subsites -1 and +1. **b**, An amino acid residue (most likely glutamin) acting as an acid/base catalyst protonates the oxygen atom of the scissile bond, and the associated C-1 is attacked by a nucleophilic residue to form a β-glycosydic bond. Through a planar oxocarbenium-like transition state this results in a covalent glycosyl enzyme intermediate and the first product G_{n-x} is released. **c**, An acceptor G_m binds to the exposed positive subsites with its non-reducing end towards the saccharide to be transferred. **d**, Acceptor binding is thought to release the acid/base catalyst from an unproductive positioning, upon which the deprotonation of the 4-OH group of the acceptor triggers the nucleophilic substitution of the enzyme to form an α-1,4-glycosydic bond, thus leading to the second product G_{m+x}.

for example, the enzyme is incubated with maltotriose (G_3, corresponding to χ_2), then $b = 2$. In general, $b = \mathrm{DP}_{\mathrm{ini}} - 1$ holds.

The bond enthalpy of α-1,4-glucosidic linkages is independent on the link location within the polymer and the standard Gibbs reaction energy equals zero,

$\Delta_r G^0 = 0$ (Tewari et al., 1997). It can therefore be assumed with high confidentiality that the sum of the energies of formation of the molecules within the system remains constant and DPE1 represents a system with conserved energy (see Subsection 4.2.5). For such a system, the equilibrium distribution is obtained by identifying the maximum of the entropy of mixing (4.32) under constraints (4.35) and (4.36). To the best of our knowledge Nakatani (1999) was the first to propose, based on stochastic simulations, that in equilibrium the DP distribution has maximal entropy. The statistical description presented here rigorously proves that this must indeed be the case, being a direct consequence of the second law of thermodynamics. In analogy to the general treatment outlined in Section 4.2.3, we define the Lagrange function

$$L(\chi_k; \alpha, \beta) = -\sum_k \chi_k \ln \chi_k - \alpha \left(\sum_k \chi_k - 1 \right) - \beta \left(\sum_k k \cdot \chi_k - b \right) \quad (4.37)$$

and set the partial derivatives to zero,

$$0 = \frac{\partial L}{\partial \chi_0} = -(\ln \chi_0 + 1) - \alpha, \quad (4.38)$$

$$0 = \frac{\partial L}{\partial \chi_k} = -(\ln \chi_k + 1) - \alpha - k \cdot \beta. \quad (4.39)$$

This yields

$$\chi_k = \chi_0 \cdot e^{-k\beta} = \chi_0 \, y^k, \quad (4.40)$$

where $y = e^{-\beta}$ is introduced for convenience. This result demonstrates that in equilibrium the molar fractions of different DPs are exponentially distributed. The specific values for χ_0 and y are determined from the constraints, where it is convenient to exploit the analogy to the formalism in statistical physics and introduce the partition function $Z = \sum y^k$, such that

$$\chi_0 = \frac{1}{Z} \quad \text{and} \quad b = \frac{y}{Z} \frac{\partial Z}{\partial y}. \quad (4.41)$$

These expressions fully characterize the equilibrium distribution. The entropy in equilibrium is

$$\begin{aligned} S^{\mathrm{eq}} = S_{\mathrm{mix}}/R &= -\sum_k \chi_0 y^k \ln(\chi_0 y^k) \\ &= -\ln \chi_0 - b \ln y \\ &= \ln Z - \ln y \cdot \frac{\partial \ln Z}{\partial \ln y}. \end{aligned} \quad (4.42)$$

These expressions are valid regardless of the precise range over which the sums in Eqs. (4.35), (4.36) and (4.37) have to be extended. To realistically characterize the biochemical reaction system catalyzed by DPE1, the sums must be extended over all possible DPs which are accessible to the enzyme. In particular, DPE1 catalysis transfers of glucose, maltose and maltotriose, corresponding to $x = 1, 2, 3$ in (4.34). The evolving reaction scheme with a pure substrate DP_{ini} is shown in Figure 4.2, where each reaction step consists of a transfer from a donor, following a dashed arrow, to an acceptor, following a solid arrow of the same color. The reaction system exhibits a fast combinatorial explosion. The lower limit of glucose as smallest maltodextrin induces a symmetry break in the reaction system which corresponds to a reflecting boundary condition. This is visible in Scheme 4.2 in the third step, where fewer donor paths than acceptor paths exist. Mathematically, this asymmetry

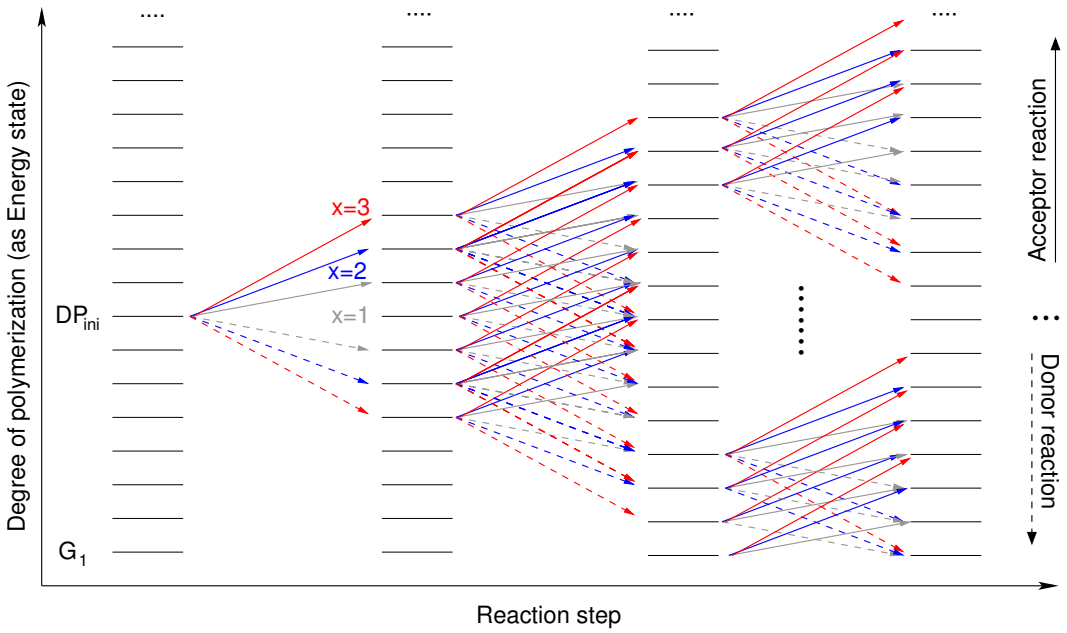

Figure 4.2: **Scheme of the DPE1 mediated reaction system**. DPE1 mediates transfers of glucose, maltose and maltotriose units, i.e. $x = 1, 2, 3$. In each reaction step the system follows an arbitrary dashed and solid arrow of the same col-our simultaneously. This leads to a combinatorial explosion of the reaction system. The lower limit of DP leads to a reflecting boundary condition for G_1 which causes the Boltzmann distribution.

is the underlying reason for the observed exponential equilibrium distributions.

We assume that all glucans of arbitrary DPs can be metabolized. In this case, the sums extend over all integers and the resulting expressions have a particularly simple form. The partition sum reads

$$Z = \sum_{k=0}^{\infty} y^k = \frac{1}{1-y}. \tag{4.43}$$

It follows that

$$\chi_0 = \frac{1}{b+1} \quad \text{and} \quad y = \frac{b}{b+1}. \tag{4.44}$$

The latter expression characterizes β in terms of the initial conditions and generalizes the equilibrium constant.

Thus, the equilibrium distribution is

$$\chi_k = (1-y)y^k = (1-e^{-\beta})e^{-\beta k} = (e^{-\beta}-1)e^{-\beta \cdot \mathrm{DP}}. \tag{4.45}$$

Clearly, for all values of $b = \mathrm{DP_{ini}} + 1$, $y < 1$ implying that β is always positive, hence the exponential decay is predicted to decrease when the average initial degree of polymerization, $\mathrm{DP_{ini}}$, increases. In the limit of very long initial DPs,

$$\lim_{b\to\infty} y = 1. \tag{4.46}$$

The entropy in equilibrium amounts to

$$S^{\mathrm{eq}} = -\sum_{k=0}^{\infty} \chi_k \ln \chi_k = (b+1)\ln(b+1) - b \ln b. \tag{4.47}$$

These predictions have been tested by incubating DPE1 with defined maltodextrins. The reactions were followed until no change in the patterns was detectable and the reaction system apparently reached equilibrium. The glucan patterns confirm the prediction that an exponential distribution is approximated and that the factor β, characterizing the equilibrium distribution, depends only on the average initial DPs (Fig. 4.3a-c) Furthermore, the observed distributions quantitatively confirm the predicted decrease of β with increasing DP_{ini} (Fig. 4.3d, e). From the observed glucan patterns the experimental entropy can be calculated which also is in accordance with the predicted entropy in equilibrium (Fig. 4.3f).

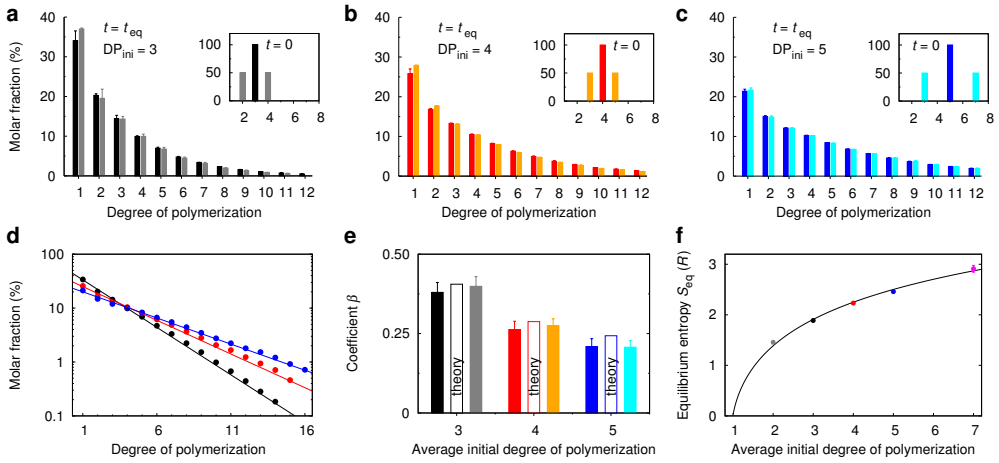

Figure 4.3: **DPE1 maximizes entropy *in vitro***. **a-c**, All DP patterns obey the theoretically expected exponential distribution (4.45) where the exponential factor β depends on the initial substrates, as demonstrated by maltotriose G_3 (black in **a**), maltotetraose G_4 (red in **b**) and maltopentaose G_5 (blue in **c**). The distributions are independent of how DP_{ini} is realized since in each panel the distributions obtained by 50:50 mixtures of G_{n-m} and G_{n+m} ($m = 1$ in **a** and **b**, $m = 2$ in **c**) are indistinguishable from the patterns obtained for G_n. **d**, Comparison between the experimental results (dots) and the theoretical predictions (solid lines) in a semi-log plot demonstrates the differences of the coefficients β (corresponding to the slopes) for different initial substrates. **e**, Agreement of observed and predicted β demonstrates the entropic mechanism of glucanotransferases. **f**, The experimentally determined equilibrium entropies S^{eq} (dots) in dependence on the average initial degree of polymerization DP_{ini} match with the values predicted by formula Eq. 4.47, indicated by the solid line. (All error bars denote standard deviation of 3 independent experiments.)

Quasi Equilibrium without maltose and time scales of relaxation. The classical experiments on D-enzyme from Peat et al. (1957, 1956), Walker and Whelan (1957) and especially Jones and Whelan (1969) have shown that in the digest of D-enzyme malto-oligos of different length can be detected but that DPE1 from white potato is incapable of utilizing maltose as glucosyl donor nor does it form maltose. These findings led to the rule of "forbidden" linkages that

later was applied to DPEs from other species, such as *Arabidopsis thaliana* (Lin and Preiss, 1988) and *Chlamydomonas reinhardtii* (Colleoni et al., 1999a,b).

However, our measurements (Fig. 4.4) clearly demonstrate that this rule is not valid for recombinant DPE1 from *A. thaliana*. Presumably, this discrepancy is due to differences in the length of the incubation period. As revealed by our measurements, approximately 10 minutes after incubation a quasi-stationary state is reached in which maltose is undetectable. This "quasi-equilibrium" is close to the true equilibrium of a system which excludes maltose from being utilized. Subsequently, the maltose level rises and approaches its theoretically predicted equilibrium concentration after several days. These data are consistent with the assumption that 4-α-glucanotransferases prefer distinct glucan binding modes (Nakatani, 1999; Suganuma et al., 1991; Takaha and Smith, 1999). Based on this view, a stochastic model was developed with only two kinetic parameters reflecting the interaction of the different subsites of the enzyme with glucosyl residues(see Sec. 4.4). The observed time-resolved glucan patterns can be reproduced under the sole assumption that glucosyl transfers occur with an 800-fold smaller probability than transfers of maltosyl or maltotriosyl residues (Fig. 4.4a). In the vicinity of the quasi-equilibrium, the mixing entropy (Fig. 4.4b) increases more slowly, while steadily evolving towards the predicted maximum entropy state. Our simulations demonstrate that the kinetics of DPE1 can appropriately be characterized by three values, a rate constant reflecting maximal turnover, and two constants reflecting the different subsite affinities (Thoma et al., 1971). Experimentally, these values are not accessible through simple incubation experiments in analogy to the classical treatment of enzymes catalyzing single reactions but rather require monitoring of the entire reactant mixture.

On time scales on which observed amounts of maltose are very small, we can approximately assume that maltose acts neither as substrate nor as product of DPE1. This assumption allows to calculate analytically the quasi equilibrium distribution and the corresponding entropy for this intermediary state which is assumed after $\sim$10 minutes and prevails approximately for several hours. For this, maltose ($k = 1$) has to be excluded from the sums. Thus, the partition

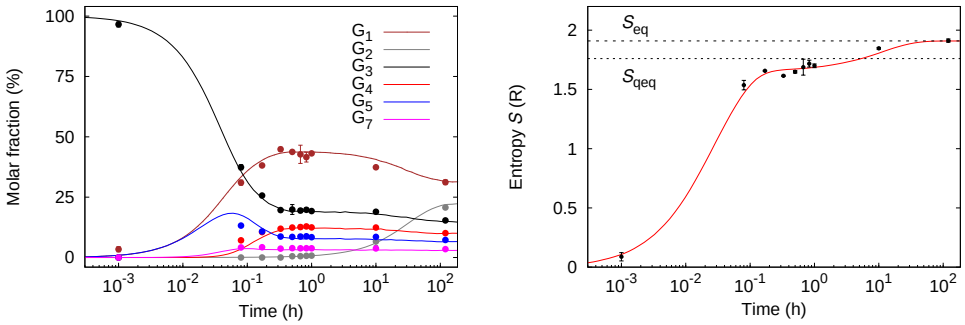

Figure 4.4: **Low binding affinity for maltose induces a quasi equilibrium distribution**. **a**, The experimental time course (dots) shows the generation of the different glucans for DPE1 incubated with maltotriose, demonstrating that maltose is produced on a slower time scale compared to the other glucans. Stochastic simulations (solid lines) assuming an 800-fold reduced probability for the transfer of single glucosyl residues compared to maltosyl and maltotriosyl residues accurately reproduce the data. **b**, The increase in entropy exhibits two time scales. In the first phase, the entropy rapidly increases towards a quasi equilibrium state without detectable maltose. The dotted line at S^{qeq} indicates the predicted equilibrium entropy for a constrained system not capable of producing maltose (see Fig. 4.5). The second phase is characterized by a much slower relaxation towards the real equilibrium S^{eq} (dashed line). (All error bars describe standard deviation of 3 independent experiments.)

sum is

$$Z = \sum_{\substack{k=0 \\ k\neq 1}}^{\infty} y^k = \frac{1-y+y^2}{1-y} = \frac{1}{\chi_0}. \tag{4.48}$$

Relations (4.41) define the implicit equation determining y from b,

$$b = \frac{y}{1-y} \cdot \frac{2y-y^2}{1-y+y^2} = \frac{y}{1-y} + \frac{2y^2-y}{1-y+y^2}. \tag{4.49}$$

To test the assumption that maltose is produced with a smaller time scale and that the results in Fig. 4.4 are not caused by unspecific reactions, DPE1 was incubated with pure maltose. The resulting experimental time course is shown in Figure 4.5a by dots and corresponding simulations by lines.

The temporal changes in the experimental data could be described rather well by simulations with the same parameters as for the case with $\mathrm{DP}_{\mathrm{ini}} = 3$

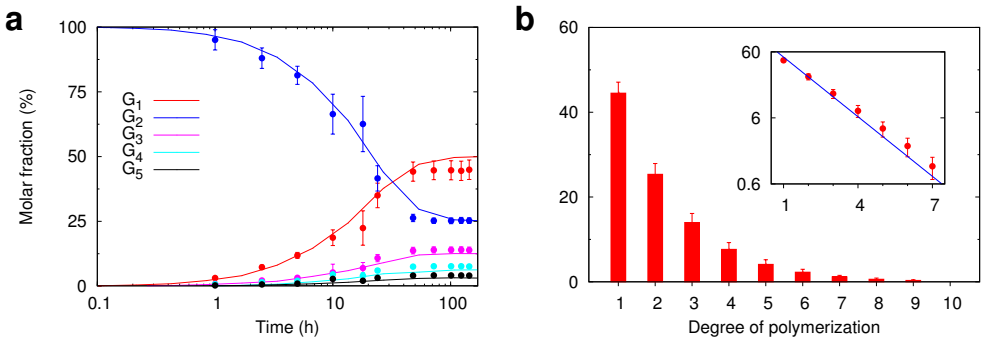

Figure 4.5: **Action of DPE1 incubated with maltose G_2 as initial substrate DP_{ini} only.** **a**, The temporal glucan patterns can be described by simulations using the same parameters as in Fig. 4.4. Since maltose is the exclusive glucan source, only the slowest time scale dominates the process and no quasi equilibrium is observed. **b**, As predicted, an exponential equilibrium distribution is experimentally observed (red bars). The logarithmic scale (inset) shows that the predicted (blue line) and the observed distributions (red dots) show slight deviations where the predictions are still in the error limits taking technical errors into account.

shown in Fig. 4.4 which are given in in Section 4.4. The difference is that no quasi-equilibrium is observed since conversion of G_2 is the limiting step and thus only the slow time scale is observable. The small deviations of the data from the simulations for large times are also visible in the equilibrium distributions shown in panel b. In the inset, the data (red dots) are plotted on a semi-logarithmic scale and additionally compared with the theoretical predictions (blue line) by Eq. (4.41). Interestingly, the simulations approach an equilibrium reflecting the theoretical predictions, hinting at a systematic deviation which might result from technical errors of the measurements.

4.3.2 Disproportionating enzyme 2 (DPE2)

Background. DPE2 catalysis the transfer of a single glucose residue from one α-1,4-linked glucan to another. It therefore also belongs to the class of energetically neutral enzymes (Subsection 4.2.5) and obeys the constraints of conserved number of molecules (4.35) and conserved total number of bonds (4.36).

However, if, as our and other (Steichen et al., 2008) experimental findings suggest, maltose (χ_1) never acts as an acceptor of glucosyl residues and maltotriose (χ_2) never acts as a donor, DPE2 effectively obeys a third constraint, namely the conservation of the sum of glucose and maltose molecules,

$$\chi_0 + \chi_1 = p, \tag{4.50}$$

where p is determined by the initially applied glucose and maltose. The DPE2 mediated reaction scheme is shown in Figure 4.6 where the separation of the glucose-maltose pool from the pool of larger DPs is shown by the red dashed line which is not crossed by any possible reaction path. In each DPE2 reaction step, one arbitrary donor reaction (dashed arrows) occurs simultaneously with one arbitrary acceptor reaction (solid arrows). Starting from an initial substrate mixture of maltohexaose and maltose, the 5 first possible reactions are shown in Scheme 4.6, where in each step the reaction system follows a dashed and a solid line simultaneously. Here, the conservation of the glucose/-maltose pool from the longer polyglucans results in an additional symmetry break, or reflecting boundary condition, causing the exponential equilibrium distribution.

Equilibrium distribution. Again, the maximal entropy is determined using the method of Lagrangian multipliers. We define the Lagrangian

$$\begin{aligned} L(\chi_k;\alpha,\beta,\gamma) = &-\sum_k \chi_k \ln \chi_k \\ &- \alpha\left(\sum_k \chi_k - 1\right) \\ &- \beta\left(\sum_k k\cdot\chi_k - b\right) \\ &- \gamma(\chi_0 + \chi_1 - p) \end{aligned} \tag{4.51}$$

and set the partial derivatives to zero:

$$0 = \frac{\partial L}{\partial \chi_0} = -(\ln\chi_0 + 1) - \alpha - \gamma, \tag{4.52}$$

$$0 = \frac{\partial L}{\partial \chi_1} = -(\ln\chi_0 + 1) - \alpha - \beta - \gamma, \tag{4.53}$$

$$0 = \frac{\partial L}{\partial \chi_k} = -(\ln\chi_k + 1) - \alpha - k\cdot\beta \quad \text{for } k \geq 2. \tag{4.54}$$

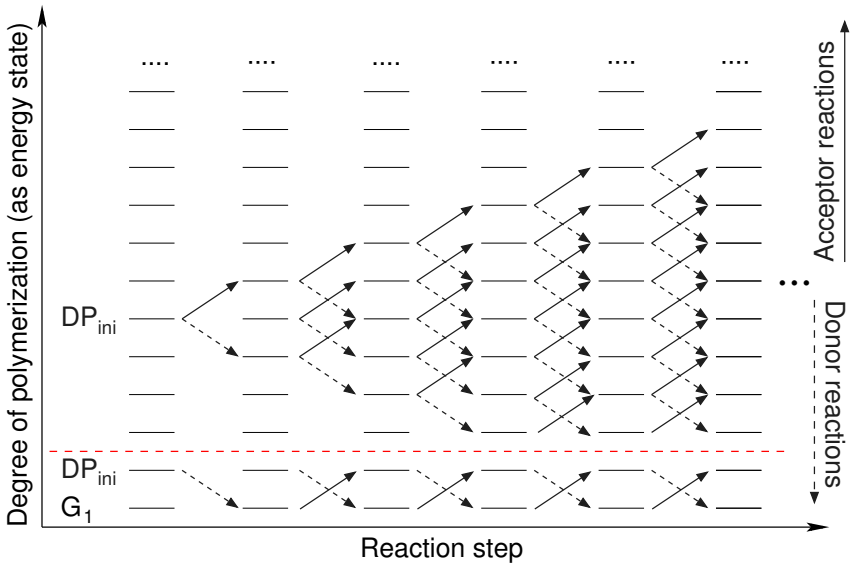

Figure 4.6: **Scheme of the DPE2 mediated reaction system**. Each DPE2 reaction step consists of one donor and one acceptor reaction depicted by a dashed and a solid arrow, respectively. Due to the restriction that maltose is never an acceptor and maltotriose is never a donor, the maltose and glucose pool is separated from the other DPs as shown by the red dashed line. The scheme exhibits all possible reaction pathways starting from the two indicated initial substrates maltohexaose and maltose, where in each step one arbitrary solid and one arbitrary dashed path is taken.

Defining $y = e^{-\beta}$ it follows that

$$\frac{\chi_1}{\chi_0} = y \quad \text{and} \quad \chi_k = \chi_2 \cdot y^{k-2}, \tag{4.55}$$

showing that the DPs again follow an exponential distribution. The difference to DPE1 is that the ratio $\chi_{k+1}/\chi_k = y$ is not observed for the ratio χ_2/χ_1. Constraints (4.35) and (4.50) imply

$$\chi_0 = \frac{p}{1+y} \quad \text{and} \quad \chi_2 = (1-p)(1-y). \tag{4.56}$$

Constraint (4.36) allows to derive the formula

$$b - 2(1-p) = p \cdot \frac{y}{1+y} + (1-p) \cdot \frac{y}{1-y}, \tag{4.57}$$

from which y can be determined from the initial conditions b (average number of bonds) and p (initially applied molar fraction of glucose and maltose).

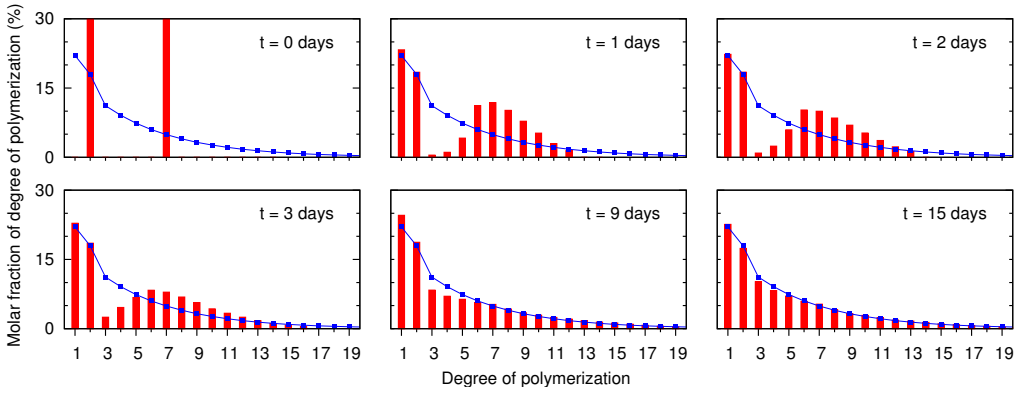

Figure 4.7: **Predicted equilibrium distributions of the degree of polymerization (blue) and experimental validation (red) of DPE2**. The temporal relaxation of the measured distribution towards the predicted one for an initial 40:60 mixture of maltose (G_2) and maltoheptaose (G_7). The two separated pools exhibit different time scales. While the small pool of G_1 and G_2 is very close to equilibrium after one day, the larger pool needs around 15 days caused by the larger configuration space.

These predictions were tested experimentally by incubating DPE2 with an initial mixture containing 40% maltose and 60% maltoheptaose. The experimentally observed DP distributions are plotted for several time points in Figure 4.7 as red bars. Clearly, the approached equilibrium closely matches the theoretically predicted equilibrium distribution depicted by the blue lines in Figure 4.7.

4.3.3 DPE1 + Hexokinase

As an example system in which the total energy of formation is not conserved,the combined action of DPE1 and hexokinase (HK) is considered. This particular combination has been chosen to study the effect of an exothermic reaction on the distribution of glucans produced by isenthalpic reactions. A great advantage is that the degree of reversibility of the HK reaction can be experimentally controlled by adding different amounts of ATP. Because the HK reaction diminishes the glucose pool accessible to DPE1 but keeps the number of inter-glucose bonds constant, the equilibrium patterns are shifted

towards larger DPs.

Additional to reactions (4.34), hexokinase catalysis the conversion

$$\mathrm{Glc} + \mathrm{ATP} \leftrightarrow \mathrm{G6P} + \mathrm{ADP}, \tag{4.58}$$

with a standard Gibbs energy of reaction Δg. We denote again a polyglucan with k linkages by χ_k, glucose-6-phosphate by u, ATP by a_3 and ADP by a_2. Four conserved quantities give rise to side constraints:

$$\text{Total number of molecules:} a_2 + a_3 + u + \sum_k \chi_k = 1 \tag{4.59}$$

$$\text{Conservation of interglucose linkages:} \sum_k k\chi_k = b \tag{4.60}$$

$$\text{Conservation of adenosine moieties:} a_2 + a_3 = A \tag{4.61}$$

$$\text{Simultaneous production of ADP and G6P:} a_2 - u = B. \tag{4.62}$$

The molar Gibbs energy of formation can be written as

$$g^f = const. + u \cdot \Delta g \tag{4.63}$$

and the mixing entropy reads

$$S_{\mathrm{mix}} = -R \left[a_2 \ln a_2 + a_3 \ln a_3 + u \ln u + \sum_k \chi_k \ln \chi_k \right]. \tag{4.64}$$

The equilibrium distribution is now determined by identifying the minimum of the Gibbs free energy (4.31)

$$G = g^f - TS_{\mathrm{mix}} \tag{4.65}$$

under the constraints (4.59)–(4.62). Setting the partial derivatives of the Lagrange function

$$\begin{aligned} L(a_2, a_3, u, \chi_k; \alpha, \beta, \gamma, \delta) =& g^f - TS_{\mathrm{mix}} \\ &+ \alpha \left(a_2 + a_3 + u + \sum_k \chi_k - 1 \right) \\ &+ \beta \left(\sum_k k\chi_k - b \right) \\ &+ \gamma(a_2 + a_3 - A) \\ &+ \delta(a_2 - u - B) \end{aligned} \tag{4.66}$$

to zero, we get

$$\frac{a_2}{a_3} = e^{-\frac{\delta}{RT}} = z, \quad \frac{u}{\chi_0} = e^{-\frac{\Delta g}{RT}} \cdot e^{\frac{\delta}{RT}} = \frac{k_0}{z} \quad \text{and} \quad \frac{\chi_k}{\chi_0} = e^{-\frac{k\beta}{RT}} = y^k, \tag{4.67}$$

where

$$y = e^{-\frac{\beta}{RT}}, \quad z = e^{-\frac{\delta}{RT}} \quad \text{and} \quad k_0 = e^{-\frac{\Delta g}{RT}}. \tag{4.68}$$

The constraints (4.59)–(4.62) yield the equations

$$a_3(1+z) = A, \tag{4.69}$$

$$\chi_0 \left(\frac{k_0}{z} + \frac{1}{1-y} \right) = 1 - A, \tag{4.70}$$

$$\chi_0 \cdot \frac{y}{(1-y)^2} = b \tag{4.71}$$

$$\text{and} \quad \frac{Az}{1+z} - \chi_o \cdot \frac{k_0}{z} = B. \tag{4.72}$$

From Eqs. (4.70)–(4.72), the two variables χ_0 and z can be eliminated to result in one single equation which implicitly determines the equilibrium distribution parameter y:

$$b \cdot \frac{1-y}{y} \left[k_0(1-y) \cdot \left(\frac{A}{B+1-A-b \cdot \frac{1-y}{y}} - 1 \right) + 1 \right] + A - 1 = 0. \tag{4.73}$$

This equation implicitly defines β as a function of the initial concentrations and the equilibrium constant of the HK reaction. The equation has been numerically solved to determine the equilibrium parameter β which was used to compare experimental and theoretical results in Fig. 4.8. Additional results from the set of experiments are plotted in Figure 4.9.

Our results concur with earlier findings (Kakefuda and Duke, 1989; Walker and Whelan, 1959) on the DPE1-mediated synthesis of amylose which now experience a quantitative theoretical explanation. Moreover, this scenario exemplifies a situation with relevance *in vivo* when DPE1 is active while simultaneously the glucose molecules are subject to the action of other enzymes, such as the plastidial HK or the glucose transporter. When the plastidial HK or the glucose exporter is active, this results in a sequestration of glucoses from the DPE1-mediated transfer reactions. Under these conditions, DPE1 mediates an energy-independent elongation of glucans and thereby provides substrates for the plastidic α-glucan phosphorylase or even supports starch synthesis directly. The latter conjecture is consistent with the phenotype of

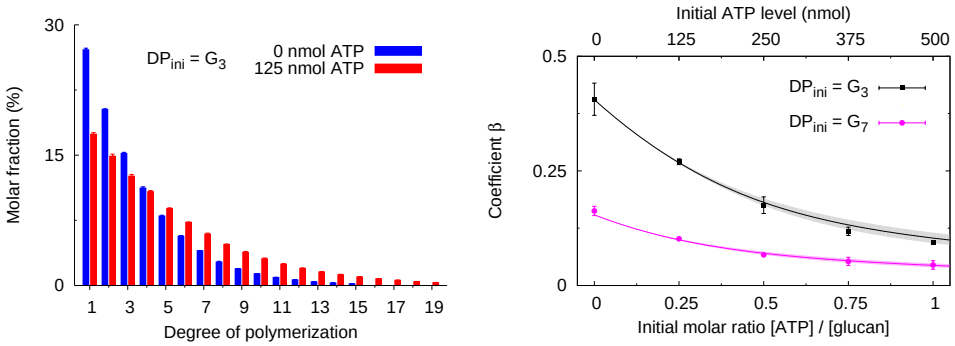

Figure 4.8: **Influence of the Hexokinase activity on the equilibrium distribution of DPE1**. In the presence of hexokinase (HK), the DPE1-mediated equilibrium distribution depends on the applied amount of ATP, the Gibbs energy of the HK reaction and the average initial degree of polymerization, DPini. a, The equilibrium distribution of DPE1, incubated with 500 nmol maltotriose (G3) and 125 nmol ATP (red) is shifted towards longer DPs compared to the distribution without ATP (blue). The semi-logarithmic plot (inset) shows that observed (circles) and predicted (lines) distributions are in good agreement. b, In systematic experiments the ATP level was varied between 0 and 500 nmol leading to an ATP/glucan ratio between 0 and 1 for the two different initial substrates G3 (black) and G7 (magenta). From distributions corresponding to those in panel a, the equilibrium parameter β was determined by fitting to data (symbols) and compared with the theoretical prediction (lines) according to Eq. (4.73). Predictions were calculated with the experimentally determined average equilibrium constant of the HK reaction. Shadowed regions describe the corresponding standard deviation of 4 independent experiments. (All error bars correspond to standard deviation of 3 independent experiments.)

a *C. reinhardtii* mutant lacking a functional DPE1 which displays aberrant starch synthesis (Colleoni et al., 1999a,b).

4.3.4 α-glucan phosphorylase

Background. The enzyme α-glucan phosphorylase catalyzes the transfer of a single glucose residue from the non-reducing end of a glucan onto inorganic

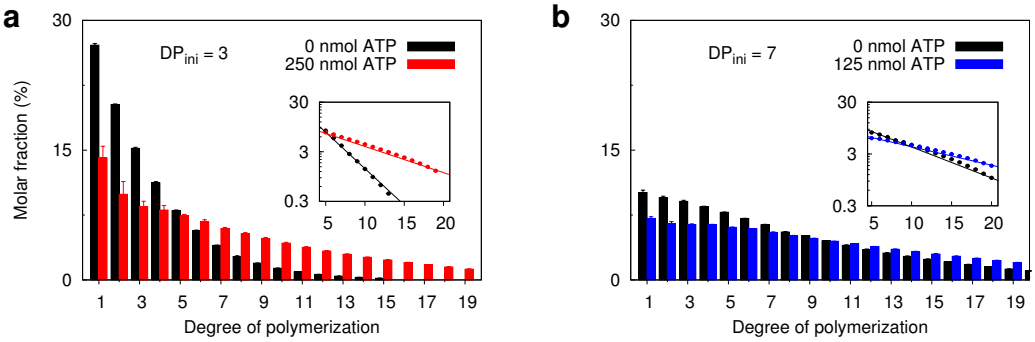

Figure 4.9: **Further results on the influence of Hexokinase on the equilibrium distribution**. **a**, Distributions for $\mathrm{DP_{ini}} = 3$ with [ATP] = 0 nmol (black) and [ATP] = 250 nmol (red) corresponding to a ratio R=[ATP]/[glucan] of 0 and 0.5 respectively. **b**, Distributions for $\mathrm{DP_{ini}} = 7$ with [ATP] = 0 nmol (black) and [ATP] = 125 nmol (blue) corresponding to a ratio R=[ATP]/[glucan] of 0 and 0.25 respectively. (Error bars indicate standard deviation of 3 independent experiments.)

phosphate to form glucose-1-phosphate. The general reaction is (Steup and Schächtele, 1981)

$$\mathrm{P_i} + \mathrm{G}_n \leftrightarrow \mathrm{G1P} + \mathrm{G}_{n-1}, \tag{4.74}$$

Apparently, this enzyme also conserves the total number of molecules. However, since the bond enthalpies of the α-1,4 glucosidic linkages in polyglucans and the phosphoester bond in glucose-1-phosphate are different, the total energy of formation is not a conserved quantity. As a consequence, the equilibrium distribution will be determined by a combined effect of minimizing the Gibbs energy of reaction and maximizing the entropy.

Equilibrium distribution. We denote by Δg the change in Gibbs energy when breaking one mole of α-1,4 glucosidic linkages and simultaneously closing one mole of phosphoester bonds. The molar fractions of inorganic phosphate Pi and of glucose-1-phosphate are denoted by u and v, respectively. We assume that phosphorylase can be active on glucans with a minimal number of bonds, denoted m. As above, we denote with χ_k the molar fraction of the glucan with k bonds. The total energy of formation of the reaction mixture (per mole) is

thus

$$g^f = const. + u \cdot \Delta g \tag{4.75}$$

and the mixing entropy reads

$$S_{\text{mix}} = -R \left[u \ln u + v \ln v + \sum_k \chi_k \ln \chi_k \right]. \tag{4.76}$$

The equilibrium distribution is determined by identifying the minimum of the Gibbs free energy (4.31) under the constraints

$$\text{total number of molecules:} \qquad u + v + \sum_{k \geq m} \chi_k = 1, \tag{4.77}$$

$$\text{conservation of bonds:} \qquad v + \sum_{k \geq m} k\chi_k = b, \tag{4.78}$$

$$\text{conservation of phosphate groups:} \qquad u + v = p. \tag{4.79}$$

These constraints are analogous to the three constraints (4.35), (4.36) and (4.50) which apply to DPE2. Indeed, they formally become identical if u is identified with χ_0, v with χ_1 and $m = 2$. The main difference is that here the Lagrange function

$$\begin{aligned} L(u, v, \chi_k; \alpha, \beta, \gamma) =& v \cdot \Delta g + RT \left[u \ln u + v \ln v + \sum_k \chi_k \ln \chi_k \right] \\ &+ \alpha \left(u + v + \sum_k \chi_k - 1 \right) \\ &+ \beta \left(v + \sum_k k\chi_k - b \right) \\ &+ \gamma(u + v - p) \end{aligned} \tag{4.80}$$

contains the molar change in Gibbs energy Δg. Here, introducing

$$y = e^{-\frac{\beta}{RT}} \quad \text{and} \quad k_0 = e^{-\frac{\Delta g}{RT}} \tag{4.81}$$

and setting the partial derivatives to zero yields

$$\frac{v}{u} = y \cdot k_0 \quad \text{and} \quad \frac{\chi_{k+1}}{\chi_k} = y \quad \text{for} \quad k \geq m. \tag{4.82}$$

An analogous calculation to that performed in Section 4.3.2 yields

$$u = \frac{p}{1 + yk_0} \quad \text{and} \quad \chi_m = (1 - p)(1 - y) \tag{4.83}$$

and y is determined by solving the equation

$$b - m \cdot (1 - p) = p\frac{yk_0}{1 + yk_0} + (1 - p)\frac{y}{1 - y}. \tag{4.84}$$

The implicit formula (4.57) for DPE2 represents a special case of Eq. (4.84) when $k_0 = 1$, which corresponds to identical bond energies ($\Delta g = 0$). The analogous structure of the solutions is not surprising considering the parallels in the constraints that the respective enzymes observe. In both, the number of molecules as well as the number of bonds is conserved and both obey an additional, third, constraint. In the case of DPE2, the sum of the glucose and maltose moieties is conserved, in the case of phosphorylase the conservation of phosphate groups results in a conserved sum of the moieties of inorganic phosphate and glucose-1-phosphate.

To test our theoretical approach experimentally, we start with the left side of Eq. (4.74). Recombinant phosphorylase was incubated with 250 nM G_7 and 12.5 μM P_i. Together with Eq. (4.84), this extreme ratio of 1:50 enables a fine fitting of the unknown k_0 which depends on the change in Gibbs energy by Eq. (4.81). As shown in Figure 4.10b by the red bars, the high P_i concentration leads to a very steep experimental distribution of DP. The small amount of detected G_3 indicates either some contamination of the initial substrate or a quasi equilibrium caused by essentially smaller binding rates for G_4 similar to the scenario described in the main text for DPE1 binding to maltose. For the prediction we assume $m = 3$ and exclude the contribution of G_3 to the molar fraction, finding that $k_0 = 0.19$ describes the data sufficiently well. The logarithmic plot in the inlet illustrates how the slope decreases with decreasing k_0 from $k_0 = 0.4$ (black line), $k_0 = 0.19$ (blue line) to $k_0 = 0.1$ (dashed line).

In further experiments the right side of Eq. (4.74) was used as a starting point and incubated phosphorylase with G1P and the polyglucans G_4 and G_7, respectively. The resulting patterns are shown in Figure 4.10c. Both distributions include again a minor fraction of G_3. Besides this, the comparison demonstrates again the dependence of the distribution on the initial conditions. The logarithmic plot in panel c demonstrates the Boltzmann-like distributions, and the comparison with the theoretical predictions shown by the solid lines again validate the theoretical approach for systems with a net change in enthalpy. This underlines the meaning and importance of the coefficient β as a

general equilibrium parameter, since it allows for an estimation of the change in Gibbs energy.

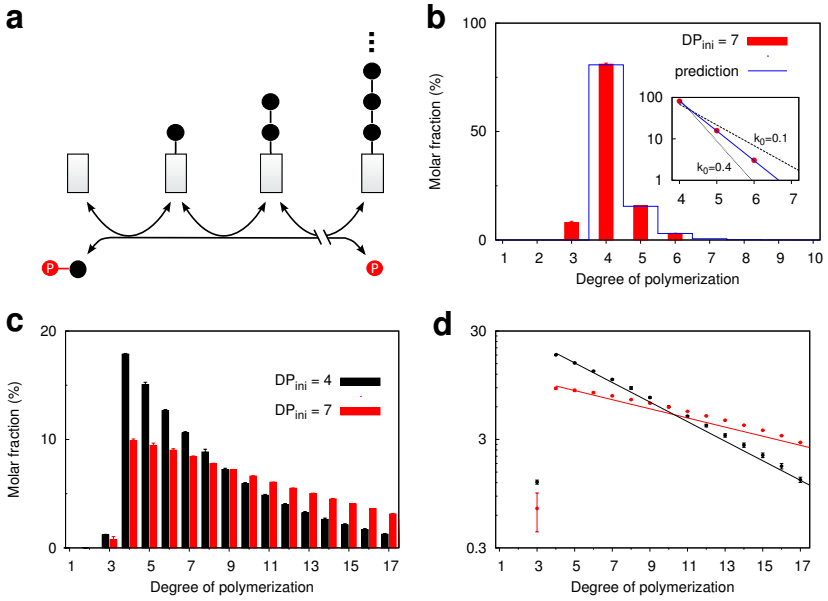

Figure 4.10: **Equilibrium distributions of the degree of polymerization for phosphorylase experiments**. **a**, Schematic representation of the mechanism of phosphorylase. From a polyglucan one glucose residue is reversibly transferred to orthophosphate, producing glucose 1-phosphate. **b**, The experimental distribution (red bars) for a 1:50 mixture of $\mathrm{DP_{ini}} = 7$ and Pi exhibits a steep decrease. From the theoretical prediction Eq. (4.84) shown in blue, we can fit the unknown k_0 parameter as 0.19. The inlet shows the logarithmic data (red) and further predictions for $k_0 = 0.1$ (dashed) and $k_0 = 0.4$ (solid). **c**, Comparison between G4 (black) and G7 (red) incubated with G1P demonstrates the dependence on the initial substrate. **d**, Both distributions obey an exponential distribution as shown by the logarithmic plot. The agreement of experiments (dots) and theoretical predictions (lines) validates the theoretical approach. (Error bars indicate standard deviation of 3 independent experiments.)

4.4 Simulation: *in vitro* reactions and a minimal model of SHG metabolism

In order to complement and substantiate the experimental and analytical results, a stochastic algorithm to simulate coupled chemical reactions has been employed (Gillespie, 1977). This approach enables the kinetic characterization of the glucan patterns and thereby elucidates the effect of different affinities between enzymes and substrates on the concentration trajectories.

4.4.1 Algorithm

The algorithm simulates the reaction systems by a discrete number of polyglucan molecules and enzymes which interact through enzyme-substrate complex formation and enzymatically catalyzed chemical conversions. In analogy to classical thermodynamics, each glucan G_n, n denoting the degree of polymerization, DP, can be interpreted as a defined energy state which may be occupied by an arbitrary number of particles (see Figures 4.2 and 4.6).

In the reaction systems catalyzed by DPE1 and DPE2, the enzymes catalyze transfers of x glucose units from one molecule to another corresponding to the general reaction scheme

$$G_n + G_m \overset{\text{DPE}}{\longleftrightarrow} G_{n-x} + G_{m+x} \ ,$$

where the entropic principle implies the mixing of the corresponding occupation numbers, until the equilibrium distributions as described in Sections 4.3.1 and 4.3.2 are reached.

The algorithm simulates this mixing of discrete occupation numbers and exploits the dynamic memory allocation of the vector class in `C++` that enables simulations of unlimited chain lengths. A two-step sequential mechanism, having basically two types of rate constants, turned out to be sufficient to simulate the temporal patterns:

$$E + G_n \xrightarrow{k_b} EG_n \tag{4.85}$$

$$EG_n + G_m \xrightarrow{k_t} G_{n-x} + G_{m+x} + E, \tag{4.86}$$

where E denotes a free enzyme, EG_n the enzyme-donor complex, and k_b and k_t are the rate constants of donor binding and the glucosyl transfer, respec-

tively. The rate constant k_b may depend on x, $k_\mathrm{b}(x)$, reflecting the different probabilities of forming positional isomers (Thoma et al., 1971). A positional isomer is defined by the alignment of the donor polymer at the enzyme subsite, which already determines one of the products, G_{n-x}.

Former studies reported that DPE1 catalysis maltosyl and maltotriosyl transfers only ($x = 2, 3$), whereas we have shown here, that also single glucose units can be transferred although with a much smaller rate. Taking into account that from maltose (G_2) only glucosyl residues ($x = 1$), and from maltotriose only glucosyl and maltosyl ($x = 1, 2$) residues can be transferred, the experimental data could be fitted well with simulations using the parameters $k_\mathrm{t} = k_\mathrm{b}(x = 2, 3) = 0.2\ \mathrm{s}^{-1}$ and $k_\mathrm{b}(x = 1) = 0.00025\ \mathrm{s}^{-1}$.

The algorithm can be summarized as follows:

1. In dependence on the propensities, a G_n is randomly chosen to bind to a free enzyme E (Eq. (4.85)) or to an enzyme-oligoglucan complex EG_n (Eq. (4.86)) leading to a positional isomer or a transfer reaction, respectively.

2. If the reaction corresponds to donor binding the binding probability of a glucan depends on the number of glucosyl residues which will be transferred.

3. In the catalytic step, x glucosyl residues are transferred, the processed glucans are released and the enzyme returns into its free state.

Simulations of the Phosphorylase and of the DPE2–Phosphorylase (see below) systems are implemented in an analogous flavor.

4.4.2 Entropy-induced robustness in cytosolic SHG metabolism

The developed algorithm is able to reproduce both the experimental equilibrium distributions as well as the temporal changes in the reaction patterns as demonstrated in Section 4.3. Furthermore, simulations allow us to investigate the role of enzymes generating mixing entropy in non-equilibrium open systems. Here, we want to exemplify this for carbon metabolism in plants.

The degradation of transitory starch in chloroplasts of leaf cells during darkness (Fettke et al., 2009a; Sulpice et al., 2009) provides essentially maltose, which is exported to the cytosol in order to support glycolysis as well as sucrose synthesis. Glycolysis is the ubiquitous pathway of energy metabolism to produce chemical energy equivalents in form of ATP and NADH, and sucrose is the major form in which carbon is transported to sink organs of plants. It turns out that by exporting maltose, using it as a glucosyl donor, plants can bypass the first reaction of glycolysis (hexokinase) and produce the intermediate glucose-1-phosphate (G1P) via a soluble heteroglycan pool, SHG (Fettke et al., 2009b). G1P is necessary for both the downstream processes of glycolysis and sucrose synthesis.

It has been hypothesized that the SHG pool has a buffering function and supports the integration of carbon fluxes but it is not known by which mechanism to explain this. In this respect, it is interesting that a significant fraction of SHG consists of polyglucans, which serve as substrates for DPE2 and cytosolic α-glucan phosphorylase (Pho), two 'entropic enzymes' characterized in this work. Thus, it is tempting to suggest that the entropy-driven maintenance of a polydisperse pool by these enzymes provides an explanation for the putative role of SHG in buffering carbon fluxes.

A minimal model which mimics the physiological scenario found in the cytosol of plant leaves during darkness is shown in Figure 4.11a. In order to study the role of the SHG pool, we compare this system to an alternative one which does not exploit entropy gradients. Consider a noisy maltose input resulting from a spatially inhomogeneous plastidial export of maltose (G_2) into the cytosol. A single process consuming G1P represents the activity of downstream processes. We study the output performance for two mechanisms: 1) Maltose is converted into glucose and G1P by the concerted action of the entropic enzymes DPE2 and Pho; 2) Maltose is directly split by a single reaction according to, $G_2 + P_i \longleftrightarrow G_1 + G1P$, which could for example be catalyzed by maltose phosphorylase (MPho, EC 2.4.1.8). In contrast to system 2, system 1 is to a large extent driven by entropic gradients (see Sections 4.3.2 and 4.3.4, respectively).

The downstream activity represented by the G1P output rate differs for the two systems. As shown in Figure 4.11b, the MPho system (red) strongly follows

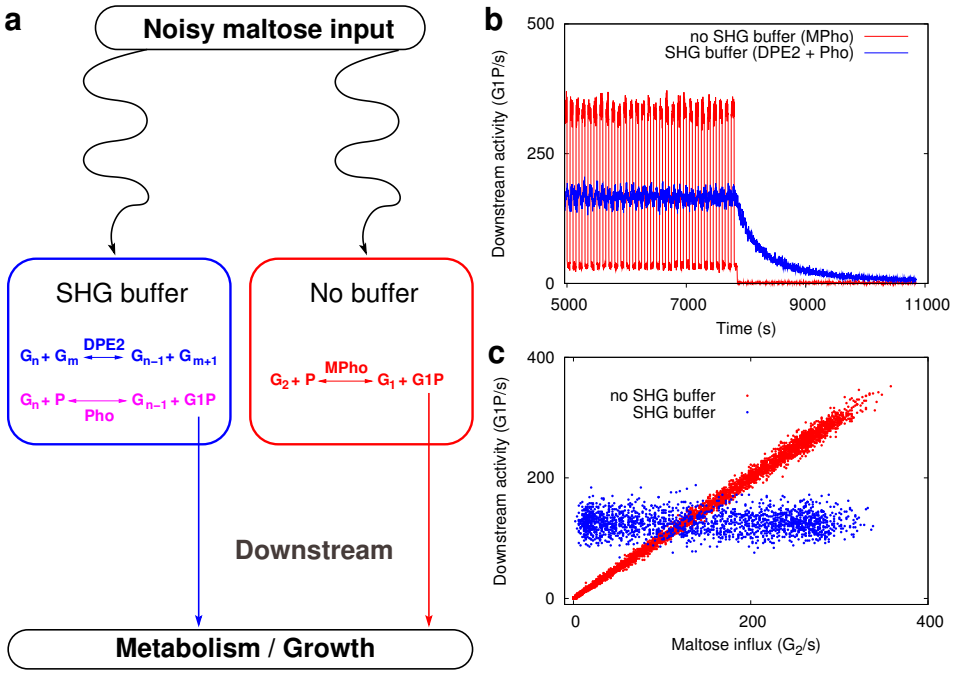

Figure 4.11: **Entropic enzymes induce metabolic robustness**. **a**, We compare the downstream activity of a system with the entropic enzymes DPE2 (blue) and Pho (magenta) catalyzing the turnover of a SHG pool with a system which directly converts a fluctuating maltose input into glucose (G_1) and glucose-1-phosphate (G1P) using maltose phosphorylase (MPho, red). **b**, The simulated temporally resolved output activity indicates that the higher entropy due to the SHG pool smears out the large fluctuation of the noisy maltose influx while the MPho system follows the fluctuations fastly. The difference becomes dramatic in the case of very small maltose influx, where the downstream activity of the MPho system stops abruptly whereas the SHG buffer system can still provide energy from the pool of larger glucans. **c**, The dependence of the G1P output on the maltose input demonstrates that the SHG pool acts as a buffer and ensures a robust support of downstream metabolism with carbon even under large and rapid external fluctuations, whereas the MPho system reacts strongly to changes in influx.

the noisy input leading to large fluctuations in downstream activity, whereas the increased internal entropy due to the SHG buffer (blue) dampens the the fast fluctuations in analogy to a low pass filter. Although the MPho system

can reach higher output rates, the SHG system exhibits a larger physiological robustness because, in case of starvation it can for a limited time still provide energy from buffered glucans with larger DPs. This is visible by the exponential damping of metabolic activity after setting the influx to very small values at around 8000 s in panel b.

Analyzing the dependence of the output on the maltose influx into the (cytosolic) system in panel c, demonstrates that the SHG system exhibits a rather constant metabolic activity independent of the influx strength as long as the temporal average of input does not vary too much. In contrast, the MPho system reacts nearly immediately to changes in the input as shown by the linear relation. These simulation results provide a strong hint that the enzymatic exploitation of entropy gradients to increase polydispersity provides the mechanistic basis for the integrating and buffering function of the metabolic system mediating SHG turnover.

4.5 Discussion

Summary. In plant carbohydrate metabolism, transfer of glucosyl moieties is a crucial process in pathways providing sugars for energy metabolism. The quantitative description of the responsible enzymes in isolation is met with problems, since a comprehensive characterization requires the simultaneous monitoring of a multitude of reactants. Thus polymer-active enzymes like the GTases do not fit into the classical Michaelis-Menten scheme.[1] Section 4.2 develops the theoretical framework in order to characterize the equilibrium of CAZyme-mediated reaction systems and emphasizes the mixing entropy of the reactant distribution. This is applied in Section 4.3 to prove that GTases (DPE1 and DPE2) catalyze entropy-driven reaction systems. Also Pho and a system combined with HK is shown to be tractable. The analytical results are confirmed by experiments and supported by stochastic simulations. The latter approach is explained in Section 4.4 and a model is formulated to explain the function of the cytosolic SHG pool as a low pass filter.

[1] Chetkarov and Kolev (1984) proposed a model of hydrolytic enzymes acting on polymers where both the maximal rate and the Michaelis-Menten constant turn out to be time-dependent.

We have shown that reaction systems catalyzed by carbohydrate-active transferases can be comprehensively characterized by the entropy of the chain length (DP) distribution of the reactants and their Gibbs energies of formation. The statistical description is illuminating since it allows to treat enzymes which catalyze many distinct reactions simultaneously. Moreover, constraints in the reaction pattern which arise from the enzyme mechanism and its subsite structure can be consistently incorporated. By this it was possible to explain the temporal patterns observed for DPE1 and DPE2. The stochastic approach to CAZymes has been especially pursued by NAKATANI (Nakatani, 1997, 1999, 2001, 2002).

The DPE reactions occur without noticeable net enthalpy changes since the total number of glucosidic bonds remains constant and every inter-sugar linkage contains approximately the same enthalpy (Goldberg et al., 1991). This raises the question of the reaction's driving force. To the best of our knowledge Nakatani (1999) was the first to propose that in equilibrium the DP distribution has maximal entropy. Our statistical description rigorously proves that this must indeed be the case, being a direct consequence of the second law of thermodynamics applied to dilute solutions. This entropic principle entails that the molar fractions of the different DPs approach an exponential distribution. The corresponding exponential factor β fully characterizes the equilibrium distribution of CAZyme-mediated reaction systems and thus represents an adequate generalization of the classical equilibrium constant. While the equilibrium constant is $q = 1$ for every individual reaction (Tewari et al., 1997), the functional form of β is determined by constraints imposed by the enzymatic mechanism and reveals the dependence on the initial conditions. It is predicted to decrease when the average initial degree of polymerization, $\mathrm{DP}_{\mathrm{ini}}$, increases.

We expect that the principle of constrained entropy maximization provides a sound framework applicable to "entropic" enzymes beyond the examples presented herein. One possible example with relevance for plant physiology is the transketolase (TK) which catalyzes several transfer reactions in the Calvin-Benson Cycle (or reductive pentose phosphate cycle) in chloroplasts (Stitt et al., 2010). Recently, Raines (2010) has proposed a TK-centric viewpoint of the Calvin-Benson Cycle and it would be interesting to see if the entropic

viewpoint could provide any insights here as well.

The empiric observations which led us to a description of polysaccharide equilibria in terms of distribution functions resemble those found by Alberty and Oppenheim (1986) for the homologous series of alkanes and alkenes. However, by putting the emphasis on entropy and the dispersal of reactants, our approach rather follows the philosophy expressed by Wicken (1978) and Craig (1992). Note, that every flux, whether mechanical, electrical or chemical, is a thermodynamically irreversible process and insofar dissipates energy and increases the system's entropy. Whereas usually the associated increase in entropy is attributed to mere "friction", that is transformation of chemical energy into heat, the inquiry at hand considers the dispersal of energy *among the reactants*. Especially in the case of isenthalpic transglycosilations, the bond energy is then retained in a useful form in the biochemical system. Thus, entropy increase per se does not lead to a waste of energy.

Frequently misinterpreted, entropy has been an elusive concept ever since its introduction by Rudolf Clausius.[2] Even up to this day foundational studies are concerned with explaining the second law (Esposito and Van den Broeck, 2010; Lieb and Yngvason, 1999; Mackey, 1989; Uffink, 2001). Ultimately, the entropy law is based on the statistical motion of a large number of microscopic bodies. Nevertheless, macroscopic thermodynamics as developed by Gibbs has proven to be successful again and again and will remain a cornerstone of the natural sciences (Landau and Lifschitz, 1979). Although a more detailed treatment using statistical mechanics is possible (see e.g. Flory, 1944), a macroscopic approach is often preferable, since it does not rely on a specific model of the microscopic realization of a system or as Callen puts it,

> *predictions should be drawn from the most general and least detailed assumptions possible. Models, endemic to statistical mechanics, should be eschewed whenever the general methods of macroscopic thermodynamics are sufficient.* (Callen, 1985)

Entropy, in terms of which a rigorous criterion for equilibrium is formulated, is a Janus-faced concept since it is also seen as a key in developing a non-equilibrium theory. It is sometimes stated that thermodynamics, as it

[2] see e.g. http://entropysite.oxy.edu/

refers to its classical form, is a misnomer and that it should rather be called thermostatics. This is attributed to the fact that all observables in this theory are defined for equilibrium only. However, the outcome of change from one equilibrium state to another can be assessed. Also, it is possible to predict in which direction a system will move if a certain constraint (a 'plug') is removed. In our *in vitro* system, the 'plug' consists of a practically infinitely high activation energy, and it is 'removed' by supplying enzymes which open up a feasible path for the reaction. Moreover, the deceleration in the temporal increase of the mixing entropy in the DPE1 system (cf. Fig. 4.4) became more clear because we knew exactly which entropy the system should approach if DPE1 would not use maltose.

Thus, equilibrium thermodynamics is useful to interpret dynamics, but indeed, the path taken by a changing system cannot be synthesized using this framework. For this we had to use stochastic simulations based on Gillespie's algorithm (Gillespie, 1977). To date, there is no rigorous variational principle (like maximum entropy) accepted for non-equilibrium systems which would provide a solution to this problem. Onsager (1931) provided first steps but the subsequent development of irreversible thermodynamics based on the principle of local equilibrium and extremal entropy production density has been criticized due to logical flaws and contradictory consequences (see the discussion in Jaynes, 1980). The most promising candidates for the future seem to be the principle of maximum caliber (Ghosh et al., 2006; Jaynes, 1980) and thermodynamics based on the second entropy formulation (Attard, 2009). Both share the emphasis on the probability of micro-trajectories.

It can be expected that a clarification in this field would be a great leap forward both for understanding classical thermodynamics[3] and processes in living systems.

As an example, we studied a dynamic property of an open metabolic system using a stochastic model. Regarding the role of different GTases and phosphorylases *in vivo*, several studies have provided a wealth of information to re-

[3] "Human anatomy contains a key to the anatomy of the ape. The intimations of higher development among the subordinate animal species, however, can be understood only after the higher development is already known." (Marx, 1983, translation from http://www.marxists.org)

construct the pathway of starch degradation (Colleoni et al., 1999a; Critchley et al., 2001; Fettke et al., 2006; Lu and Sharkey, 2004; Lu et al., 2006). From an evolutionary perspective we have posed the problem of why the downstream pathway is found to have such a peculiar design involving a heteroglycan pool in the cytosol. D. E. Atkinson, who introduced the adenylate energy charge, gave a characterization of the interplay between physiology and evolution. His statement would rather loose in clarity if it were to be rephrased:

> *Evolution is the purposeless process by which purpose and function arise.* [...] *It must be evident that any attempt to deal separately with function and evolution is a particularly unfortunate example of the establishment of a distinction where there is no difference.* [...] Evolution occurs through selection of function. [...] *A paleontologist or taxonomist whose only concern is with the details of structure for their own sake, without regard to function, is as limited in his view as is a biochemist who is interested only in the physical or kinetic properties of enzymes, without regard to the significance of those properties in the complex evolved interrelations of the living cell.* (Atkinson, 1977)

Backed up by our thermodynamic approach and using stochastic simulations we have proposed that the entropy-driven turnover of the SHG pool realizes the function of a low pass filter, translating a fluctuating maltose input from the chloroplasts into a constant provision of carbohydrates for downstream pathways. This provided interesting hints as to the buffering function of the SHG pool, but a non-equilibrium theory would definitely allow to infer more general results.

In conclusion, our concept offers a shift in perspective by suggesting that cellular metabolism is organized as an intricate interplay of energy- and entropy-driven processes. Apparently, living cells have evolved to use internal entropy gradients constructively, using multifarious polymer-active enzymes which efficiently produce and consume polydisperse pools of metabolites.

Chapter 5

Conclusions

> But who am I to doubt or question the
> inevitable being
> For these are but a few discoveries
> We find inside the Secret Life of Plants
>
> Stevie Wonder

Throughout this treatise the reader will have noticed that the author is optimistic regarding the important role physical methods and principles can have in understanding living systems and metabolism in particular. As long as we are totally aware what physics can tell us, we will never fall into the pit of reductionism and maintain a systems viewpoint. Such reductionism would be wrong since it neglects the semantic gap between different scientific theories. Biological processes do have a physical correlate, but that does not mean necessarily that a better understanding of a system is reached if the biological explanation is replaced by a physical one. The **physical realization** is a crucial but not the only aspect of a **biological function**. One could equally well argue that biology is the higher truth, since living systems can control the constraints of their physico-chemical subsystems for survival.

In my opinion, it should be our goal to emphasize the unity of science by showing that their exist transitions between the disciplines. The interfacial catalysis of starch degradation is one interesting example. We have seen that interfacial enzymes of plant carbohydrate metabolism can almost immediately trigger spontaneous physical changes on the meso- to macro-scale. These changes feed back to the **adsorption** of the enzyme. Based on this system we

could formulate the hypothesis that reversible phosphorylation at the interface is an effective system to rapidly adjust the starch degradation. The regulatory principles to control the **synergistic effect** remain to be shown but it is hoped that even more sophisticated methods from surface science can make it into the biochemistry of interfacial enzymes. The framework using the **available area function** is hopefully a good starting point.

Another example where physics has provided insight is the case of **entropy-driven transferases**. I think with this we could provide a convincing rationale for some peculiar properties of DPEs observed in the literature over the last decades. Moreover, it proved to be a relatively simple system in which the 2nd law of thermodynamics can be quantitatively observed over time.

The latter work, I believe, has much more potential and we may have seen only the tip of the iceberg. I cannot think of an example where entropy has been discussed in the context of metabolism in the way it was done here. Usually, entropy is associated with self-assembly processes and ligand interactions but not with enzymatic reactions.

In conclusion, one may say that in a time with a great fragmentation of science one should now and then try to bring together different concepts and elaborate these in conjunction. In the long run, I do not see any other possible lingua franca than **mathematics**, whatever structure it may have in the future.

Appendix A

Nondimensionalizing balance equations for competitive adsorption on a heterogeneous interface

Consider the equation for the interfacial species in (2.33b),

$$\frac{\mathrm{d}\mathbf{e}^*}{\mathrm{d}t} = \mathbf{F} \circ \left[(\mathrm{dg}\boldsymbol{\phi})\, \mathbf{k}_\mathrm{a}\, (\mathrm{dg}\mathbf{e}) - \left(\mathbf{k}_\mathrm{d} + r_\mathrm{g} \mathbf{1}_{(p\times m)} \right) \circ \mathbf{e}^* \right].$$

First, it is easy to nondimensionalise the bulk enzyme concentrations and the desorption constants, leading to

$$= \mathbf{F} \circ \left[(\mathrm{dg}\boldsymbol{\phi})\, \mathbf{k}_\mathrm{a}\, (\mathrm{dg}\underline{\mathbf{e}})\, e_\mathrm{t} - \max_{ij}\{k^i_{\mathrm{d},j}\} \left(\boldsymbol{\kappa}_\mathbf{d} + \varrho_\mathrm{g} \mathbf{1}_{(p\times m)} \right) \circ \mathbf{e}^* \right].$$

Next, the left-hand side is nondimensionalized by multiplying the equation with $1/\max_{ij}\{k^i_{\mathrm{d},j}\}$ and with $(\mathrm{dg}\mathbf{e}^{*\max})^{-1}$ from the right (since the enzyme concentrations are organized columnwise in the matrix $\mathbf{e}^*$):

$$\frac{\mathrm{d}\boldsymbol{\theta}}{\mathrm{d}\tau} = \mathbf{F} \circ \left[(\mathrm{dg}\boldsymbol{\phi})\, \frac{\mathbf{k}_\mathrm{a}}{\max_{ij}\{k^i_{\mathrm{d},j}\}}\, (\mathrm{dg}\underline{\mathbf{e}}) \left(\mathrm{dg}\frac{\mathbf{e}^{*\max}}{e_\mathrm{t}} \right)^{-1} - \left(\boldsymbol{\kappa}_\mathbf{d} + \varrho_\mathrm{g} \mathbf{1}_{(p\times m)} \right) \circ \boldsymbol{\theta} \right].$$

Now, we (Hadamard) multiply $\mathbf{k}_\mathrm{a}$ with $\mathbf{k}_\mathrm{d} \circ \mathbf{k}_\mathrm{d}^- = \mathbf{1}_{(p\times m)}$, where $\mathbf{k}_\mathrm{d}^-$ is the Hadamard inverse, to introduce the matrix of association constants:

$$= \mathbf{F} \circ \left[(\mathrm{dg}\boldsymbol{\phi})\, (\boldsymbol{\kappa}_\mathbf{d} \circ \mathbf{K}_\mathrm{a})\, (\mathrm{dg}\underline{\mathbf{e}}) \left(\mathrm{dg}\frac{\mathbf{e}^{*\max}}{e_\mathrm{t}} \right)^{-1} - \left(\boldsymbol{\kappa}_\mathbf{d} + \varrho_\mathrm{g} \mathbf{1}_{(p\times m)} \right) \circ \boldsymbol{\theta} \right].$$

According to a rule for the Hadamard product (Lemma 5.1.2 in Horn and Johnson, 1991, p. 304) the term on the left-hand side in the brackets can be rewritten as

$$(\mathrm{dg}\boldsymbol{\phi})\,(\boldsymbol{\kappa}_{\mathbf{d}} \circ \mathbf{K}_{\mathrm{a}})\,(\mathrm{dg}\underline{\mathbf{e}}) = (\mathrm{dg}\boldsymbol{\phi})\,\boldsymbol{\kappa}_{\mathbf{d}} \circ \mathbf{K}_{\mathrm{a}}\,(\mathrm{dg}\underline{\mathbf{e}})\,,$$

where the usual matrix product takes precedence over the Hadamard product. Permuting the diagonal matrices to the right of the Hadamard product allows to introduce the rescaled association constants, $\Lambda^{i}_{\mathrm{a},j}$, leading to

$$\frac{\mathrm{d}\boldsymbol{\theta}}{\mathrm{d}\tau} = \mathbf{F} \circ \left[(\mathrm{dg}\boldsymbol{\phi})\,\boldsymbol{\kappa}_{\mathbf{d}} \circ \boldsymbol{\Lambda}_{\mathbf{a}}\,(\mathrm{dg}\underline{\mathbf{e}}) - \left(\boldsymbol{\kappa}_{\mathbf{d}} + \varrho_{\mathrm{g}}\mathbf{1}_{(p\times m)}\right) \circ \boldsymbol{\theta}\right].$$

Hadamard multiplication with $\boldsymbol{\kappa}_{\mathbf{d}}^{-} \circ \boldsymbol{\kappa}_{\mathbf{d}} = \mathbf{1}_{(p\times m)}$ from the right and exploiting associativity and distributivity laws yields

$$= \mathbf{F} \circ \left[(\mathrm{dg}\boldsymbol{\phi})\,\boldsymbol{\kappa}_{\mathbf{d}} \circ \boldsymbol{\kappa}_{\mathbf{d}}^{-} \circ \boldsymbol{\Lambda}_{\mathbf{a}}\,(\mathrm{dg}\underline{\mathbf{e}}) - \left(\mathbf{1}_{(p\times m)} + \varrho_{\mathrm{g}}\boldsymbol{\kappa}_{\mathbf{d}}^{-}\right) \circ \boldsymbol{\theta}\right] \circ \boldsymbol{\kappa}_{\mathbf{d}}.$$

Again, we look at the left term in the brackets. Applying the rule referred to above yields

$$\begin{aligned}
(\mathrm{dg}\boldsymbol{\phi})\,\boldsymbol{\kappa}_{\mathbf{d}} \circ \boldsymbol{\kappa}_{\mathbf{d}}^{-} \circ \boldsymbol{\Lambda}_{\mathbf{a}}\,(\mathrm{dg}\underline{\mathbf{e}}) &= (\mathrm{dg}\boldsymbol{\phi})\left(\boldsymbol{\kappa}_{\mathbf{d}} \circ \boldsymbol{\kappa}_{\mathbf{d}}^{-}\right)\mathbf{I}_{(m\times m)} \circ \boldsymbol{\Lambda}_{\mathbf{a}}\,(\mathrm{dg}\underline{\mathbf{e}}) \\
&= (\mathrm{dg}\boldsymbol{\phi})\,\mathbf{1}_{(p\times m)} \circ \boldsymbol{\Lambda}_{\mathbf{a}}\,(\mathrm{dg}\underline{\mathbf{e}}) \\
&= (\mathrm{dg}\boldsymbol{\phi})\left(\mathbf{1}_{(p\times m)} \circ \boldsymbol{\Lambda}_{\mathbf{a}}\right)(\mathrm{dg}\underline{\mathbf{e}}) \\
&= (\mathrm{dg}\boldsymbol{\phi})\,\boldsymbol{\Lambda}_{\mathbf{a}}\,(\mathrm{dg}\underline{\mathbf{e}})\,,
\end{aligned}$$

where $\mathbf{I}_{(m\times m)}$ is the usual identity matrix with only ones in the diagonal and zero otherwise. Finally, Eq. (2.36) results from substituting this and setting $\varrho_{\mathrm{g}} = 0$. The conservation relation is nondimensionalized by using elementary matrix rules for the transpose.

Appendix B

Materials and methods

Chemicals. ATP was purchased from Roche (product no. 10519979001, Germany). Maltose (product no. EC 200-716-5), α-glucans, glucose 1-phosphate (product no. EC 260-154-1) and glycogen (from oyster, type II) were obtained from Sigma-Aldrich (Taufkirchen, Germany). Commercial maltodextrins (product no. EC 232-940-4) were separated into larger (50-60%[v/v]) and smaller (60-70%) sized compounds by precipitation with varying concentrations of ethanol following precrystallization (Hejazi et al., 2009).

Recombinant proteins. Recombinant plastidial α-glucan phosphorylase (Pho1) from *Oryza sativa* was expressed and purified as described elsewhere (Fettke et al., 2010).

Cloning. For cloning of dpe1 (At5g64860) and dpe2 (At2g40840) from *Arabidopsis thaliana*, total RNA was isolated from leaves (100 mg fresh weight each) by using the Nucleo Spin RNA Plant Kit (Machery-Nagel; Düren, Germany).

For first strand cDNA synthesis encoding DPE1, the SuperScript II Reverse Transcriptase (Invitrogen, Darmstadt, Germany) and a specific 3' primer (5'-3'): AAGCCGTCCGTACAATGACAAAAGATCTCT were used following the instructions of the manufacturer. The resulting cDNA was then amplified by PCR using the EcoRI and XhoI linked primers (5' forward primer [5'-3']: GAATCCGATGGAGGTCGTTTCGAGTAATTC and 3' reverse primer [5'-3']: CTCGAGAAGCCGTCCGTACAATGAACCAAG) that include the complete cDNA except the predicted transit sequence (135 bp from the start). In a final volume of 50 μl, the PCR reaction mixture contained 2 μl of the re-

verse transcription mixture and Phusion Taq Polymerase (Finnzymes, Espoo, Finland). Subsequently, the 2,2 kb dpe1 encoding fragment was subcloned into pGEM T-easy vector (Promega, Mannheim, Germany). Finally, the dpe1 fragment was restricted by EcoRI/XhoI and ligated to the expression vector pET23b (Novagen, Darmstadt, Germany).

For cloning of dpe2, first strand cDNA was synthesised by using the 3' primer (5'-3'): TTATGGGTTTGGCTTAGTCGAGCCATTGGC (see above) and was then amplified by HF Polymerase (product no. 11732650001, Roche, Mannheim, Germany) by use of the following primers: 5' forward primer (5'-3'): ATGATGAATCTAGGATCTCTTTCGTTGAG and 3' reverse primer (5'-3'): TTATGGGTTTGGCTTAGTCGAGCCATTGGC. Subsequently, the dpe2 encoding cDNA was ligated to the pGEM-T Easy vector. Subcloning was performed by the Gateway Technology (Invitrogen, Darmstadt, Germany) following the instructions of the manufacturer. Subsequently, the pDONR221 was recombined with the attB1- and attB2 flanked dpe2 cDNA (primers: attB1 [5'-3']: AAAAAGCAGGCTTAATGATGAATCTAGGAT and attB2 [5'-3']: AGAAAGCTGGGTATGGGTTTGGCTTAGTCG). Finally, the PCR product was cloned into pDEST17.

DPE1 and DPE2 were expressed in *E.coli* BL21 (DE3) harboring the plasmid pET23b and pDEST17, respectively. Cells were grown in LB medium containing 100 μg/ml ampicillin at 37 $^\circ$C until the suspension reached an OD_{600} of approximately 0.8. Following the addition of IPTG (final concentration 1 mM) the suspension was cooled to 18 $^\circ$C and incubated over night. Cells were harvested, washed with 50 mM Tris-HCl (pH 7.5), resuspended in grinding buffer (20 mM NaH_2PO_4, 500 mM NaCl, 2.5 mM DTT, 20 mM imidazole and 1% [v/v] protease inhibitor cocktail III [Calbiochem, Darmstadt, Germany], pH 7.4).and sonicated on ice. Following centrifugation (20 min at 20000 g) the supernatant was passed through a nitrocellulose filter (pore size 0.45 μm) and the filtrate was loaded onto a HisTrap-HP-column (1 ml; GE Healthcare, München, Germany). For elution, a stepwise increasing imidazole concentration (up to 500 mM, dissolved in grinding buffer) was used. Fractions containing the desired protein were combined, concentrated and were then transferred to storage buffer (50 mM Hepes-KOH, pH 7.5, 1 mM EDTA, 2 mM DTT), using Amicon Ultra-4 centrifugal filter-unit concentrator (MWCO 30000, Mil-

lipore, Schwalbach am Taunus, Germany). Finally, glycerol was added (final concentration of 20% [v/v]) and aliquots were frozen at -80 ° C.

Capillary Electrophoresis (CE). Glucans were separated from denatured proteins by using a centrifugal filter device (YM-30; Microcon, Millipore, Schwalbach am Taunus, Germany) and were freeze dried. Each sample was diluted in 2μl 0.2 M 8-aminopyrene-1,3,6-trisulfonic acid (APTS) in 15% [v/v] aqueous acetic acid plus 2 μl 1 M Na-cyanoborohydride. Following incubation (4 h at 37 ° C) and 250- to 500fold dilution with water, the labeled samples were applied to CE using a PA-800 (Beckman Coulter, Krefeld, Germany).

Protein concentrations. Soluble proteins were quantified using Bio-Rad protein assay (Bio-Rad, München, Germany). BSA served as standard (Roth, Karlsruhe, Germany).

Photometric assay of the activity of recombinant DPE1 and DPE2 (PA). Activity was measured using a slightly modified version of the coupled photometric assay described by Lu et al. (2006). For DPE1 maltotriose (final concentration 2 mM) served as substrate. The assay of DPE2 contained maltose (2 mM maltose) and glycogen from oyster (1 mg/ml; final concentrations each).

Long-term assay of the recombinant transferases (LTA). For LTA, all reaction mixtures containing 0.025% [w/v] sodium azide were incubated at 30 ° C for several days. The following reaction mixtures were used: a) DPE1 or DPE2 (25 mU each; 100 μl final volume) were incubated with 500 nmol α-glucans, 2.5 mM citrate-NaOH (pH 7.0). In some experiments, the citrate buffer was replaced by 25 mM Hepes-KOH pH 7.0. Under these conditions the same α-glucan patterns were observed. b) DPE1/ATP: DPE1 (25 mU DPE1 each; 100 μl final volume), 25 mM Hepes-KOH (pH 7.0), 6.5 mM $MgCl_2$, 500 nmol maltotriose or maltoheptaose, 0 to 500 nmol ATP and 500 mU hexokinase (from yeast, Roche, Mannheim, Germany). c) Pho1/G1P: Pho1 (0.5 μg each; 100 μl final volume), 25 mM Hepes-KOH (pH 7.0) 1 μmol G1P, 250 nmol maltotetraose or 250 nmol maltoheptaose. d) Pho1/ Pi: Pho1 (0.5 μg; 100 μl final volume), 25 mM Hepes-KOH (pH 7.0), 250 nmol maltoheptaose, 12.5 μmol orthophosphate.

All enzymes were replaced by a fresh preparation every day. At intervals, aliquots (equivalent to 50 nmol α-glucans) were withdrawn and reactions were

terminated by heating (95 ° C for 5min).

Patterns of α-glucans. Patterns of α-glucans were monitored by capillary electrophoresis (CE) following coupling to APTS.

Bibliography

Alberty RA (2003) Thermodynamics of Biochemical Reactions. John Wiley & Sons.

Alberty RA (2008) Rapid-Equilibrium Enzyme Kinetics. J Chem Educ 85: 1136.

Alberty RA, Oppenheim I (1986) Analytic expressions for the equilibrium distributions of isomer groups in homologous series. J Chem Phys 84: 917–920.

Allen JD, Thoma JA (1976a) Subsite mapping of enzymes. Application of the depolymerase computer model to two α-amylases. Biochem J 159: 121–132.

Allen JD, Thoma JA (1976b) Subsite mapping of enzymes. Depolymerase computer modelling. Biochem J 159: 105–120.

Amann H, Escher J (1998) Analysis 1. Birkhäuser.

Aris R (1994) Mathematical Modelling Techniques. Dover.

Atkinson DE (1977) Cellular Energy Metabolism and its Regulation. 1st ed., Academic Press.

Attard P (2009) The second entropy: a general theory for non-equilibrium thermodynamics and statistical thermodynamics. Annu Rep Prog Chem, Sect C: Phys Chem 105: 63–173.

Ball SG, Morell MK (2003) From bacterial glycogen to starch: understanding the biogenesis of the plant starch granule. Annu Rev Plant Biol 54: 207–233.

Barends TRM, Bultema JB, Kaper T, van der Maarel MJEC, Dijkhuizen L, et al. (2007) Three-way stabilization of the covalent intermediate in amylomaltase, an α-amylase-like transglycosylase. J Biol Chem 282: 17242–17249.

Beard DA, Qian H (2008) Chemical Biophysics. Quantitative Analysis of Cellular Systems. Cambridge University Press.

Bender CM, Orszag SA (1999) Advanced Mathematical Methods for Scientists and Engineers. Springer-Verlag.

Berg OB, Jain MK (2002) Interfacial Enzyme Kinetics. John Wiley & Sons.

Berman KM, Cohn M (1970a) Phosphoenolpyruvate synthetase of *Escherichia coli*. Purification, some properties, and the role of divalent metal ions. J Biol Chem 245: 5309–5318.

Berman KM, Cohn M (1970b) Phosphoenolpyruvate synthetase. Partial reactions studied with adenosine triphosphate analogues and the inorganic phosphate-$H_2{}^{18}O$ exchange reaction. J Biol Chem 245: 5319–5325.

Blennow A, Engelsen SB (2010) Helix-breaking news: fighting crystalline starch energy deposits in the cell. Trends Plant Sci 15: 236–240.

Blennow A, Nielsen TH, Baunsgaard L, Mikkelsen R, Engelsen SB (2002) Starch phosphorylation: a new front line in starch research. Trends Plant Sci 7: 445–450.

Boraston AB (2005) The interaction of carbohydrate-binding modules with insoluble non-crystalline cellulose is enthalpically driven. Biochem J 385: 479–484.

Boraston AB, Bolam DN, Gilbert HJ, Davies GJ (2004) Carbohydrate-binding modules: fine-tuning polysaccharide recognition. Biochem J 382: 769–781.

Brown RF, Holtzapple MT (1990) A comparison of the Michaelis-Menten and HCH-1 models. Biotechnol Bioeng 36: 1151–1154.

Buléon A, Bizo H, Delage MM, Multon JL (1982) Evolution of crystallinity and specific gravity of potato starch versus water ad- and desorption. Starch/Stärke 11: 361–366.

Buléon A, Colonna P, Planchot V, Ball S (1998) Starch granules: structure and biosynthesis. Int J Biol Macromol 23: 85–112.

Bulik S, Grimbs S, Huthmacher C, Selbig J, Holzhütter HG (2009) Kinetic hybrid models composed of mechanistic and simplified enzymatic rate laws–a promising method for speeding up the kinetic modelling of complex metabolic networks. FEBS J 276: 410–424.

Burns RAJ, El-Sayed MY, Roberts MF (1982) Kinetic model for surface-active enzymes based on the Langmuir adsorption isotherm: Phospholipase C (*Bacillus cereus*) activity toward dimyristoyl phosphatidylcholine/detergent micelles. Proc Natl Acad Sci U S A 79: 4902–4906.

Callen HB (1985) Thermodynamics and an Introduction to Thermostatistics. 2nd ed., John Wiley & Sons.

Cantarel BL, Coutinho PM, Rancurel C, Bernard T, Lombard V, et al. (2009) The Carbohydrate-Active EnZymes database (CAZy): an expert resource for Glycogenomics. Nucleic Acids Res 37: D233–D238.

Caspi R, Altman T, Dale JM, Dreher K, Fulcher CA, et al. (2007) The MetaCyc database of metabolic pathways and enzymes and the BioCyc collection of pathway/genome databases. Nucleic Acids Res 38: D473–D479.

Cha S (1968) A simple method for derivation of rate equations for enzyme-catalyzed reactions under the rapid equilibrium assumption or combined assumptions of equilibrium and steady state. J Biol Chem 243: 820–825.

Chetkarov ML, Kolev DN (1984) The *Michaelis-Menten* equation in the case of enzyme-catalyzed hydrolysis of linear homopolymer substrates with different degrees of polymerization. Monatshefte für Chemie / Chemical Monthly 115: 1405–1412, 10.1007/BF00816339.

Christiansen C, Hachem MA, Glaring MA, Nielsen AV, Sigurskjold BW, et al. (2009) A CBM20 low-affinity starch-binding domain from glucan, water dikinase. FEBS Lett 583: 1159–1163.

Chu KT, Bazant MZ (2007) Surface conservation laws at microscopically diffuse interfaces. J Colloid Interface Sci 315: 319 – 329.

Ciliberto A, Capuani F, Tyson JJ (2007) Modeling networks of coupled enzymatic reactions using the total quasi-steady state approximation. PLoS Comput Biol 3: e45.

Clé C, Martin C, Field RA, Kuzmič P, Bornemann S (2010) Detection of enzyme-catalyzed polysaccharide synthesis on surfaces. Biocatal Biotransform 28: 64–71.

Colleoni C, Dauvillée D, Mouille G, Buléon A, Gallant D, et al. (1999a) Genetic and biochemical evidence for the involvement of α-1,4 glucanotransferases in amylopectin synthesis. Plant Physiol 120: 993–1004.

Colleoni C, Dauvillée D, Mouille G, Morell M, Samuel M, et al. (1999b) Biochemical characterization of the *Chlamydomonas reinhardtii* α-1,4 glucanotransferase supports a direct function in amylopectin biosynthesis. Plant Physiol 120: 1005–1014.

Converse AO, Optekar JD (1993) A synergistic kinetics model for enzymatic cellulose hydrolysis compared to degree-of-synergism experimental results. Biotechnol Bioeng 42: 145–148.

Corre DL, Bras J, Dufresne A (2010) Starch nanoparticles: a review. Biomacromolecules 11: 1139–1153.

Cosgrove DJ (2005) Growth of the plant cell wall. Nat Rev Mol Cell Biol 6: 850–861.

Coutinho PM, Deleury E, Davies GJ, Henrissat B (2003) An evolving hierarchical family classification for glycosyltransferases. J Mol Biol 328: 307–317.

Craig NC (1992) Entropy Analysis: An Introduction to Chemical Thermodynamics. VCH Publishers.

Creagh AL, Ong E, Jervis E, Kilburn DG, Haynes CA (1996) Binding of the cellulose-binding domain of exoglucanase Cex from Cellulomonas fimi to insoluble microcrystalline cellulose is entropically driven. Proc Natl Acad Sci U S A 93: 12229–12234.

Critchley JH, Zeeman SC, Takaha T, Smith AM, Smith SM (2001) A critical role for disproportionating enzyme in starch breakdown is revealed by a knock-out mutation in Arabidopsis. Plant J 26: 89–100.

Damager I, Engelsen SB, Blennow A, Møller BL, Motawia MS (2010) First principles insight into the alpha-glucan structures of starch: their synthesis, conformation, and hydration. Chem Rev 110: 2049–2080.

Damme EJV, Hu J, Barre A, Hause B, Baggerman G, et al. (2001) Purification, characterization, immunolocalization and structural analysis of the abundant cytoplasmic β-amylase from *Calystegia sepium* (hedge bindweed) rhizomes. Eur J Biochem 268: 6263–6273.

Davies GJ, Henrissat B (2002) Structural enzymology of carbohydrate-active enzymes: implications for the post-genomic era. Biochem Soc Trans 30: 291–297.

Deems RA (2000) Interfacial enzyme kinetics at the phospholipid/water interface: practical considerations. Anal Biochem 287: 1–16.

Delatte T, Umhang M, Trevisan M, Eicke S, Thorneycroft D, et al. (2006) Evidence for distinct mechanisms of starch granule breakdown in plants. J Biol Chem 281: 12050–12059.

Eaton BR, Dennis EA (1976) Analysis of phospholipase C (Bacillus cereus) action toward mixed micelles of phospholipid and surfactant. Arch Biochem Biophys 176: 604–609.

Edner C, Li J, Albrecht T, Mahlow S, Hejazi M, et al. (2007) Glucan, water dikinase activity stimulates breakdown of starch granules by plastidial β-Amylases. Plant Physiol 145: 17–18.

Esposito M, Van den Broeck C (2010) Three faces of the second law. I. Master equation formulation. Phys Rev E 82: 011143.

Evans JW (1993) Random and cooperative sequential adsorption. Rev Mod Phys 65: 1281–1330.

Fang F, Szleifer I (2001) Kinetics and thermodynamics of protein adsorption: a generalized molecular theoretical approach. Biophys J 80: 2568–2589.

Fell DA (1992) Metabolic control analysis: a survey of its theoretical and experimental development. Biochem J 286 (Pt 2): 313–330.

Feret J, Danos V, Krivine J, Harmer R, Fontana W (2009) Internal coarse-graining of molecular systems. Proc Natl Acad Sci U S A 106: 6453–6458.

Fettke J, Albrecht T, Hejazi M, Mahlow S, Nakamura Y, et al. (2010) Glucose 1-phosphate is efficiently taken up by potato (*Solanum tuberosum*) tuber parenchyma cells and converted to reserve starch granules. New Phytol 185: 663–675.

Fettke J, Chia T, Eckermann N, Smith A, Steup M (2006) A transglucosidase necessary for starch degradation and maltose metabolism in leaves at night acts on cytosolic heteroglycans (SHG). Plant J 46: 668–684.

Fettke J, Hejazi M, Smirnova J, Höchel E, Stage M, et al. (2009a) Eukaryotic starch degradation: integration of plastidial and cytosolic pathways. J Exp Bot 60: 2907–2922.

Fettke J, Malinova I, Eckermann N, Steup M (2009b) Cytosolic heteroglycans in photoautotrophic and heterotrophic plant cells. Phytochemistry 70: 696–702.

Flory PJ (1944) Thermodynamics of Heterogeneous Polymers and Their Solutions. J Chem Phys 12: 425–438.

Fulton DC, Stettler M, Mettler T, Vaughan CK, Li J, et al. (2008) β-AMYLASE4, a noncatalytic protein required for starch breakdown, acts upstream of three active β-amylases in *Arabidopsis* chloroplasts. Plant Cell 20: 1040–1058.

Gallant DJ, Bouchet B, Baldwin PM (1997) Microscopy of starch: evidence of a new level of granule organization. Carbohydr Polym 32: 177–191.

Gan Q, Allen SJ, Taylor G (2003) Kinetic dynamics in heterogeneous enzymatic hydrolysis of cellulose: an overview, an experimental study and mathematical modelling. Process Biochemistry 38: 1003–1018.

Garfinkel D, Rutledge JD, Higgins JJ (1961) Simulation and analysis of biochemical systems: I. representation of chemical kinetics. Commun ACM 4: 559–562.

Gentry MS, Dowen RH, Worby CA, Mattoo S, Ecker JR, et al. (2007) The phosphatase laforin crosses evolutionary boundaries and links carbohydrate metabolism to neuronal disease. J Cell Biol 178: 477–488.

Ghosh K, Dill KA, Inamdar MM, Seitaridou E, Phillips R (2006) Teaching the principles of statistical dynamics. American Journal of Physics 74: 123–133.

Gibon Y, Usadel B, Blaesing OE, Kamlage B, Hoehne M, et al. (2006) Integration of metabolite with transcript and enzyme activity profiling during diurnal cycles in *Arabidopsis* rosettes. Genome Biol 7: R76.

Gidley M, Hanashiro I, Hani N, Hill S, Huber A, et al. (2010) Reliable measurements of the size distributions of starch molecules in solution: Current dilemmas and recommendations. Carbohydr Polym 79: 255–261.

Gillespie D (1977) Exact stochastic simulation of coupled chemical reactions. J Phys Chem 8: 2340–2354.

Glaser R (1996) Biophysik. Gustav Fischer Verlag.

Gnedenko BV (2005) The Theory of Probability. 5th ed., AMS Chelsea Publishing.

Goldberg RN, Bell D, Tewari YB, McLaughlin MA (1991) Thermodynamics of hydrolysis of oligosaccharides. Biophys Chem 40: 69–76.

Goldenberg NM, Steinberg BE (2010) Surface Charge: A Key Determinant of Protein Localization and Function. Cancer Res 70: 1277–1280.

Graf A, Schlereth A, Stitt M, Smith AM (2010) Circadian control of carbohydrate availability for growth in *Arabidopsis* plants at night. Proc Natl Acad Sci U S A 107: 9458–9463.

Grimbs S, Selbig J, Bulik S, Holzhütter HG, Steuer R (2007) The stability and robustness of metabolic states: identifying stabilizing sites in metabolic networks. Mol Syst Biol 3: 146.

Guillén D, Sánchez S, Rodríguez-Sanoja R (2010) Carbohydrate-binding domains: multiplicity of biological roles. Appl Microbiol Biotechnol 85: 1241–1249.

Guillén D, Santiago M, Linares L, Pérez R, Morlon J, et al. (2007) Alpha-amylase starch binding domains: cooperative effects of binding to starch granules of multiple tandemly arranged domains. Appl Environ Microbiol 73: 3833–3837.

Hänggi P, Talkner P, Borkovec M (1990) Reaction rate theory: fifty years after Kramers. Rev Mod Phys 62: 251–342.

Hansen PI, Spraul M, Dvortsak P, Larsen FH, Blennow A, et al. (2009) Starch phosphorylation - maltosidic restrains upon 3'- and 6'-phosphorylation investigated by chemical synthesis, molecular dynamics and NMR spectroscopy. Biopolymers 91: 179–193.

Hanson KR (1962) Enzyme kinetics of short-chain polymer cleavage. Biochemistry 1: 723–734.

Harmer R, Danos V, Feret J, Krivine J, Fontana W (2010) Intrinsic information carriers in combinatorial dynamical systems. Chaos 20: 037108.

Heinrich R, Rapoport TA (1974) A linear steady-state treatment of enzymatic chains. General properties, control and effector strength. Eur J Biochem 42: 89–95.

Heinrich R, Schuster S (1996) The Regulation of Cellular Systems. Chapman & Hall.

Hejazi M, Fettke J, Kötting O, Zeeman SC, Steup M (2010) The Laforin-like dual-specificity phosphatase SEX4 from Arabidopsis hydrolyzes both C6- and C3-phosphate esters introduced by starch-related dikinases and thereby affects phase transition of α-glucans. Plant Physiol 152: 711–722.

Hejazi M, Fettke J, Paris O, Steup M (2009) The two plastidial starch-related dikinases sequentially phosphorylate glucosyl residues at the surface of both the A- and B-type allomorphs of crystallized maltodextrins but the mode of action differs. Plant Physiol 150: 962–976.

Hertz H (1894) Die Prinzipien der Mechanik. Johann Ambrosius Barth.

Himmel ME, Ding SY, Johnson DK, Adney WS, Nimlos MR, et al. (2007) Biomass recalcitrance: engineering plants and enzymes for biofuels production. Science 315: 804–807.

Holtzapple MT, Caram HS, Humphrey AE (1984) The HCH-1 model of enzymatic cellulose hydrolysis. Biotechnol Bioeng 26: 775–780.

Holzhütter HG (2004) Mathematische Zellmodelle - Fiktion oder greifbare Wirklichkeit. Bioforum .

Horn RA, Johnson CR (1985) Matrix Analysis. Cambridge University Press.

Horn RA, Johnson CR (1991) Topics in Matrix Analysis. Cambridge University Press.

Ishikawa K, Nakatani H, Katsuya Y, Fukazawa C (2007) Kinetic and structural analysis of enzyme sliding on a substrate: multiple attack in β-amylase. Biochemistry 46: 792–798.

Jaynes ET (1980) The minimum entropy production principle. Annu Rev Phys Chem 31: 579–601.

Jones G, Whelan WJ (1969) The action pattern of D-enzyme, a transmaltodextrinylase from potato. Carbohydr Res 9: 483–490.

Kacser H, Burns JA (1995) The control of flux. Biochem Soc Trans 23: 341–366 (Commented reprint of the 1973 original).

Kakefuda G, Duke SH (1989) Characterization of Pea Chloroplast D-Enzyme (4-α-D-Glucanotransferase). Plant Physiol 91: 136–143.

Kartal O, Ebenhöh O (2008) The Glucan, water dikinase - a kinetic model to understand the initial step in starch mobilization in plant leaves. In: Hansmann UHE, Meinke JH, Mohanty S, Nadler W, Zimmermann O, editors, From computational biophysics to systems biology (CBSB08), vol. 40 of NIC Series, pp. 245–248, John von Neumann Institute for Computing, Jülich.

Kolasinski KW (2008) Surface Science. Foundations of Catalysis and Nanoscience. 2nd ed., John Wiley & Sons.

Kooi CWV, Taylor AO, Pace RM, Meekins DA, Guo HF, et al. (2010) Structural basis for the glucan phosphatase activity of Starch Excess4. Proc Natl Acad Sci U S A 107: 15379–15384.

Kötting O, Kossmann J, Zeeman SC, Lloyd JR (2010) Regulation of starch metabolism: the age of enlightenment? Curr Opin Plant Biol 13: 321–329.

Kötting O, Santelia D, Edner C, Eicke S, Marthaler T, et al. (2009) STARCH-EXCESS4 is a Laforin-like phosphoglucan phosphatase required for starch degradation in *Arabidopsis thaliana*. Plant Cell 21: 334–346.

Kozlov SS, Blennow A, Krivandin AV, Yuryev VP (2007) Structural and thermodynamic properties of starches extracted from GBSS and GWD suppressed potato lines. Int J Biol Macromol 40: 449–460.

Landau LD, Lifschitz EM (1979) Lehrbuch der Theoretischen Physik V: Statistische Physik, Teil I. Akademie-Verlag.

Langmuir I (1918) The adsorption of gases on plane surfaces of glass, mica and platinum. J Am Chem Soc 40: 1361–1403.

Leloup V, Colonna P, Ring S (1991) α-Amylase adsorption on starch crystallites. Biotechnol Bioeng 38: 127–134.

Levine SE, Fox JM, Blanch HW, Clark DS (2010) A mechanistic model of the enzymatic hydrolysis of cellulose. Biotechnol Bioeng 107: 37–51.

Lieb EH, Yngvason J (1999) The physics and mathematics of the second law of thermodynamics. Physics Reports 310: 1–96.

Liebermeister W, Klipp E (2006) Bringing metabolic networks to life: convenience rate law and thermodynamic constraints. Theoretical Biology and Medical Modelling 3:41.

Limpert E, Stahel WA, Abbt M (2001) Log-normal distributions across the sciences: keys and clues. BioScience 51: 341–352.

Lin TP, Preiss J (1988) Characterization of D-enzyme (4-α-Glucanotransferase) in *Arabidopsis* leaf. Plant Physiol 86: 260–265.

Lizotte PA, Henson CA, Duke SH (1990) Purification and Characterization of Pea Epicotyl β-Amylase. Plant Physiol 92: 615–621.

Lorberth R, Ritte G, Willmitzer L, Kossmann J (1998) Inhibition of a starch-granule-bound protein leads to modified starch and repression of cold sweetening. Nat Biotechnol 16: 473–477.

Lu Y, Sharkey TD (2004) The role of amylomaltase on maltose metabolism in the cytosol of photosynthetic cells. Planta 218: 466–473.

Lu Y, Steichen JM, Yao J, Sharkey TD (2006) The role of cytosolic α-glucan phosphorylase in maltose metabolism and the comparison of amylomaltase in Arabidopsis and *Escherichia coli*. Plant Physiol 142: 878–889.

Lüttge U, Kluge M, Bauer G (2005) Botanik. Wiley-VCH.

Mackey MC (1989) The dynamic origin of increasing entropy. Rev Mod Phys 61: 981.

Marangoni AG (2003) Enzyme Kinetics: A Modern Approach. Wiley.

Marchal LM, Ulijn RV, Gooijer CDD, Franke GT, Tramper J (2003) Monte Carlo simulation of the α-amylolysis of amylopectin potato starch. 2. α-amylolysis of amylopectin. Bioprocess Biosyst Eng 26: 123–132.

Marchal LM, Zondervan J, Bergsma J, Beeftink HH, Tramper J (2001) Monte Carlo simulation of the α-amylolysis of amylopectin potato starch. Part I: modeling of the structure of amylopectin. Bioprocess Biosyst Eng 24: 163–170, 10.1007/s004490100247.

Marx K (1983) MEW 42: Grundrisse der Kritik der politischen Ökonomie. Dietz Verlag.

Masel RI (1996) Principles of Adsorption and Reaction on Solid Surfaces. John Wiley & Sons.

Medve J, Karlsson J, Lee D, Tjerneld F (1998) Hydrolysis of microcrystalline cellulose by cellobiohydrolase I and endoglucanase II from *Trichoderma reesei*: adsorption, sugar production pattern, and synergism of the enzymes. Biotechnol Bioeng 59: 621–634.

Medve J, Ståhlberg J, Tjerneld F (1994) Adsorption and synergism of cellobiohydrolase I and II of *Trichoderma reesei* during hydrolysis of microcrystalline cellulose. Biotechnol Bioeng 44: 1064–1073.

Medve J, Ståhlberg J, Tjerneld F (1997) Isotherms for adsorption of cellobiohydrolase I and II from *Trichoderma reesei* on microcrystalline cellulose. Appl Biochem Biotechnol 66: 39–56.

Meléndez-Hevia E, Waddell TG, Shelton ED (1993) Optimization of molecular design in the evolution of metabolism: the glycogen molecule. Biochem J 295 (Pt 2): 477–483.

Mikkelsen R, Baunsgaard L, Blennow A (2004) Functional characterization of α-glucan,water dikinase, the starch phosphorylating enzyme. Biochem J 377: 525–532.

Mikkelsen R, Suszkiewicz K, Blennow A (2006) A novel type carbohydrate-binding module identified in α-Glucan, water dikinases is specific for regulated plastidial starch metabolism. Biochemistry 45: 4674–4682.

Morgan JA, Rhodes D (2002) Mathematical modeling of plant metabolic pathways. Metab Eng 4: 80–89.

Murray JD (2008) Mathematical Biology. 3rd ed., Springer.

Nägele T, Henkel S, Hörmiller I, Sauter T, Sawodny O, et al. (2010) Mathematical modeling of the central carbohydrate metabolism in Arabidopsis reveals a substantial regulatory influence of vacuolar invertase on whole plant carbon metabolism. Plant Physiol 153: 260–272.

Nakatani H (1997) Monte Carlo simulation of multiple attack mechanism of β-amylase-catalyzed reaction. Biopolymers 42: 831–836.

Nakatani H (1999) Monte Carlo simulation of 4-α-glucanotransferase reaction. Biopolymers 50: 145–151.

Nakatani H (2001) Analysis of glycosidase-catalyzed transglycosylation reaction using probabilistic model. Arch Biochem Biophys 385: 387–391.

Nakatani H (2002) Monte Carlo simulation of hyaluronidase reaction involving hydrolysis, transglycosylation and condensation. Biochem J 365: 701–705.

Niittylä T, Comparot-Moss S, Lue WL, Messerli G, Trevisan M, et al. (2006) Similar protein phosphatases control starch metabolism in plants and glycogen metabolism in mammals. J Biol Chem 281: 11815–11818.

Niittylä T, Messerli G, Trevisan M, Chen J, Smith AM, et al. (2004) A previously unknown maltose transporter essential for starch degradation in leaves. Science 303: 87–89.

Ogata H, Goto S, Sato K, Fujibuchi W, Bono H, et al. (1999) KEGG: Kyoto Encyclopedia of Genes and Genomes. Nucleic Acids Res 27: 29–34.

Okazaki M, Moo-Young M (1978) Kinetics of enzymatic hydrolysis of cellulose: Analytical description of a mechanistic model. Biotechnol Bioeng 20: 637–663.

Olson CB, Talbot J (2000) Equilibria and kinetics of polydisperse mixture adsorption. J Chem Phys 112: 3868–3874.

Onsager L (1931) Reciprocal relations in irreversible processes. I. Physical Review 37: 405–426.

O'Sullivan AC, Perez S (1999) The relationship between internal chain length of amylopectin and crystallinity in starch. Biopolymers 50: 381–390.

Papin JA, Stelling J, Price ND, Klamt S, Schuster S, et al. (2004) Comparison of network-based pathway analysis methods. Trends Biotechnol 22: 400–405.

Peat S, Whelan WJ, Jones G (1957) The enzymic synthesis and degradation of starch. Part XXIII. Structural requirements of D-enzyme with respect to acceptors. J Chem Soc pp. 2490–2495.

Peat S, Whelan WJ, Rees WR (1953) D-enzyme: a disproportionating enzyme in potato juice. Nature 172: 158.

Peat S, Whelan WJ, Rees WR (1956) The enzymic synthesis and degradation of starch. Part XX. The disproportionating enzyme (D-enzyme) of the potato. J Chem Soc 44: 44–53.

Polanyi M (1968) Life's irreducible structure. Science 160: 1308–1312.

Poolman MG, Fell DA, Thomas S (2000) Modelling photosynthesis and its control. J Exp Bot 51 Spec No: 319–328.

Raines CA (2010) Overexpression of transketolase reveals a link between photosynthetic carbon metabolism, thiamine metabolism and isoprenoid biosynthesis. In: Abstracts of papers, 4th International Symposium of the SFB 429 "Signals, Sensing and Plant Primary Metabolism", Potsdam, Germany.

Ral JP, Derelle E, Ferraz C, Wattebled F, Farinas B, et al. (2004) Starch division and partitioning. A mechanism for granule propagation and maintenance in the picophytoplanktonic green alga *Ostreococcus tauri*. Plant Physiol 136: 3333–3340.

Ramsden (1993) Concentration scaling of protein deposition kinetics. Phys Rev Lett 71: 295–298.

Ramsden JJ (2002) Adsorption kinetics of proteins. In: Hubbard AT, editor, Encyclopedia of surface and colloid science, vol. 1, pp. 240–261, Marcel Dekker.

Rapoport TA, Heinrich R, Rapoport SM (1976) The regulatory principles of glycolysis in erythrocytes *in vivo* and *in vitro*. A minimal comprehensive model describing steady states, quasi-steady states and time-dependent processes. Biochem J 154: 449–469.

Reich JG, Sel'kov EE (1981) Energy Metabolism of the Cell. Academic Press.

Rios-Estepa R, Lange BM (2007) Experimental and mathematical approaches to modeling plant metabolic networks. Phytochemistry 68: 2351–2374.

Ritte G, Lloyd JR, Eckermann N, Rottmann A, Kossmann J, et al. (2002) The starch-related R1 protein is an α-glucan, water dikinase. Proc Natl Acad Sci U S A 99: 7166–7171.

Ritte G, Scharf A, Eckermann N, Haebel S, Steup M (2004) Phosphorylation of transitory starch is increased during degradation. Plant Physiol 135: 2068–2077.

Roberts GS, Kozak D, Anderson W, Broom MF, Vogel R, et al. (2010) Tunable Nano/Micropores for Particle Detection and Discrimination: Scanning Ion Occlusion Spectroscopy. Small 6: 2653–2658.

Rosen R (1985) Anticipatory Systems: Philosophical, Mathematical & Methodological Foundations. Pergamon Press.

Rusanov A (2005) Surface thermodynamics revisited. Surf Sci Rep 58: 111 – 239.

Schaaf P, Talbot J (1989) Kinetics of random sequential adsorption. Phys Rev Lett 62: 175–178.

Schmidt J, John M (1979) Starch metabolism in *Pseudomonas stutzeri*. II. Purification and properties of a dextrin glycosyl-transferase (D-enzyme) and amylomaltase. Biochim Biophys Acta 566: 100–114.

Schnell S, Maini PK (2003) A century of enzyme kinetics: reliability of the K M and v max estimates. Comments on Theoretical Biology 8: 169–187.

Seeberger PH (2005) Exploring life's sweet spot. Nature 437: 1239.

Segel IH (1993) Enzyme Kinetics: Behavior and Analysis of Rapid Equilibrium and Steady-State Enzyme Systems. John Wiley & Sons.

Shoseyov O, Shani Z, Levy I (2006) Carbohydrate binding modules: biochemical properties and novel applications. Microbiol Mol Biol Rev 70: 283–295.

Smith AM, Stitt M (2007) Coordination of carbon supply and plant growth. Plant, Cell and Environment 30: 1126–1149.

Smith AM, Zeeman SC, Smith SM (2005) Starch degradation. Annu Rev Plant Biol 56: 73–98.

Steichen JM, Petty RV, Sharkey TD (2008) Domain characterization of a 4-α-glucanotransferase essential for maltose metabolism in photosynthetic leaves. J Biol Chem 283: 20797–20804.

Steup M, Schächtele C (1981) Mode of glucan degradation by purified phosphorylase forms from spinach leaves. Planta 153: 351–361, 10.1007/BF00384254.

Stitt M, Lunn J, Usadel B (2010) Arabidopsis and primary photosynthetic metabolism - more than the icing on the cake. Plant J 61: 1067–1091.

Stitt M, Wirtz W, Gerhardt R, Heldt HW, Spencer C, et al. (1985) A comparative study of metabolite levels in plant leaf material in the dark. Planta 166: 354–364, 10.1007/BF00401173.

Suga K, Dedem GV, Moo-Young M (1975) Enzymatic breakdown of water insoluble substrates. Biotechnol Bioeng 17: 185–201.

Suganuma T, Setoguchi S, Fujimoto S, Nagahama T (1991) Analysis of the characteristic action of D-enzyme from sweet potato in terms of subsite theory. Carbohydr Res 212: 201–212.

Sulpice R, Pyl ET, Ishihara H, Trenkamp S, Steinfath M, et al. (2009) Starch as a major integrator in the regulation of plant growth. Proc Natl Acad Sci U S A 106: 10348–10353.

Tagliabracci VS, Turnbull J, Wang W, Girard JM, Zhao X, et al. (2007) Laforin is a glycogen phosphatase, deficiency of which leads to elevated phosphorylation of glycogen *in vivo*. Proc Natl Acad Sci U S A 104: 19262–19266.

Takaha T, Smith SM (1999) The functions of 4-α-glucanotransferases and their use for the production of cyclic glucans. Biotechnology and Genetic Engineering Reviews 16: 257–280.

Talbot J, Tarjus G, Tassel PRV, Viot P (2000) From car parking to protein adsorption: an overview of sequential adsorption processes. Colloids and Surfaces A: Physicochemical and Engineering Aspects 165: 287 – 324.

Tatsumi H, Katano H (2005) Kinetics of the surface hydrolysis of raw starch by glucoamylase. J Agric Food Chem 53: 8123–8127.

Tatsumi H, Katano H, Ikeda T (2007) Kinetic analysis of glucoamylase-catalyzed hydrolysis of starch granules from various botanical sources. Biosci Biotechnol Biochem 71: 946–950.

Tewari YB, Goldberg RN, Sato M (1997) Thermodynamics of the hydrolysis and cyclization reactions of α-, β-, and γ-cyclodextrin. Carbohydr Res 301: 11–22.

Thoma JA (1976) Models for depolymerizing enzymes. Application to α-Amylases. Biopolymers 15: 729–746.

Thoma JA, Rao GV, Brothers C, Spradlin J, Li LH (1971) Subsite mapping of enzymes. Correlation of product patterns with Michaelis parameters and substrate-induced strain. J Biol Chem 246: 5621–5635.

Trurnit HJ (1954) Studies on enzyme systems at a solid-liquid interface. II. The kinetics of adsorption and reaction. Arch Biochem Biophys 51: 176 – 199.

Tzafriri AR, Bercovier M, Parnas H (2002) Reaction diffusion model of the enzymatic erosion of insoluble fibrillar matrices. Biophys J 83: 776–793.

Uffink J (2001) Bluff your way in the second law of thermodynamics. Studies in History and Philosophy of Science Part B 32: 305–394.

Varki A (2007) Glycan-based interactions involving vertebrate sialic-acid-recognizing proteins. Nature 446: 1023–1029.

Verger R (1976) Interfacial enzyme kinetics of lipolysis. Annu Rev Biophys Bioeng 5: 77–117.

Waigh TA, Gidley MJ, Komanshek BU, Donald AM (2000a) The phase transformations in starch during gelatinisation: a liquid crystalline approach. Carbohydr Res 328: 165–176.

Waigh TA, Kato KL, Donald AM, Gidley MJ, Clarke CJ, et al. (2000b) Side-chain liquid-crystalline model for starch. Starch/Stärke 52: 450–460.

Walker GJ, Whelan WJ (1957) The mechanism of carbohydrase action. 4. The mechanism of D-enzyme action. Biochem J 67: 548–551.

Walker GJ, Whelan WJ (1959) Synthesis of amylose by potato D-enzyme. Nature 183: 46.

Wayllace NZ, Valdez HA, Ugalde RA, Busi MV, Gomez-Casati DF (2010) The starch-binding capacity of the noncatalytic SBD2 region and the interaction between the N- and C-terminal domains are involved in the modulation of the activity of starch synthase III from *Arabidopsis thaliana*. FEBS J 277: 428–440.

Wegner GJ, Wark AW, Lee HJ, Codner E, Saeki T, et al. (2004) Real-Time Surface Plasmon Resonance Imaging Measurements for the Multiplexed Determination of Protein Adsorption/Desorption Kinetics and Surface Enzymatic Reactions on Peptide Microarrays. Analytical Chemistry 76: 5677–5684, pMID: 15456285.

Wicken JS (1978) Entropy gradient: A heuristic approach to chemical equilibrium. J Chem Educ 55: 701–703.

Witt T, Gidley MJ, Gilbert RG (2010) Starch digestion mechanistic information from the time evolution of molecular size distributions. J Agric Food Chem 58: 8444–8452.

Wojciechowski PM, Koziol A, Noworyta A (2001) Iteration model of starch hydrolysis by amylolytic enzymes. Biotechnol Bioeng 75: 530–539.

Worby CA, Gentry MS, Dixon JE (2006) Laforin, a dual specificity phosphatase that dephosphorylates complex carbohydrates. J Biol Chem 281: 30412–30418.

Yoshida Y, Kuroiwa H, Misumi O, Yoshida M, Ohnuma M, et al. (2010) Chloroplasts divide by contraction of a bundle of nanofilaments consisting of polyglucan. Science 329: 949–953.

Yu TS, Kofler H, Häusler RE, Hille D, Flügge UI, et al. (2001) The Arabidopsis *sex1* mutant is defective in the R1 protein, a general regulator of starch degradation in plants, and not in the chloroplast hexose transporter. Plant Cell 13: 1907–1918.

Zeeman SC, Kossmann J, Smith AM (2010) Starch: its metabolism, evolution, and biotechnological modification in plants. Annu Rev Plant Biol 61: 209–234.

Zeeman SC, Smith SM, Smith AM (2007) The diurnal metabolism of leaf starch. Biochem J 401: 13–28.

Zeeman SC, Tiessen A, Pilling E, Kato KL, Donald AM, et al. (2002) Starch synthesis in Arabidopsis. Granule synthesis, composition, and structure. Plant Physiol 129: 516–529.

Zhang YHP, Lynd LR (2004) Toward an aggregated understanding of enzymatic hydrolysis of cellulose: noncomplexed cellulase systems. Biotechnol Bioeng 88: 797–824.

Zhang YHP, Lynd LR (2006) A functionally based model for hydrolysis of cellulose by fungal cellulase. Biotechnol Bioeng 94: 888–898.